Aerial-Terrestrial Network NOMA for Cellular-Connected UAVs

Journal:	*IEEE Transactions on Vehicular Technology*
Manuscript ID	VT-2021-00985.R1
Suggested Category:	Regular Paper
Date Submitted by the Author:	19-Aug-2021
Complete List of Authors:	New, Wee Kiat; Universiti Teknologi Malaysia, Electrical Engineering Leow, Chee Yen ; Universiti Teknologi Malaysia, Wireless Communication Centre Navaie, Keivan; Lancaster University, Computing and Communications Ding, Zhiguo; University of Manchester,
Keywords:	Index Terms--- Non-Orthogonal Multiple Access, Cellular-Connected UAV, Inter-cell Interference, Coordinated Multi-Point Transmission

Aerial-Terrestrial Network NOMA for Cellular-Connected UAVs

Wee Kiat New, Chee Yen Leow, Keivan Navaie, and Zhiguo Ding

(Manuscript ID: Paper-VT-2021-00985.R1)

Dear Prof. Hung-Yun Hsieh and the reviewers,

We thank you for the time and effort spent on reviewing our manuscript. We have carefully addressed the comments and revised our manuscript according to your comments. We believe the revision has significantly improved the quality of this manuscript. The responses made in the revised manuscript are detailed point-by-point to the comments.

In this response letter, the pages and references made are based on the double-column version of the revised manuscript. To facilitate the editor and reviewers, the text are colored in blue to highlight our amendments corresponding to those comments. Notations and grammar are also fixed to further improve the quality of this paper.

Sincerely,

Wee Kiat New, Chee Yen Leow, Keivan Navaie, and Zhiguo Ding

RESPONSE TO THE EDITOR'S COMMENTS

Comment 1:

"Reviewers have concerns about the system model, including the NOMA SIC setup, ICI of the TU, and beamforming of coordinated BSs. In addition, it is suggested that the presentation of the paper on theoretic analysis and performance evaluation be improved to provide more insights on the results. Please address reviewers' comments in making the revision."

Response 1 (i):

We thank the editor for the insightful comment. In this paper, we assume that the cell-center TUs perform SIC and the AU treats co-channel interference as noise to ensure reliable communications to the AU. The reverse SIC order, where the cell-center TUs treat co-channel interference as noise and the AU performs SIC, has been considered. Nevertheless, such a SIC order is not promising to the AU's performance due to strong AU's ICI. An in-depth discussion regarding the SIC setup is provided to the reviewers. The editor may refer to response 8 to reviewer 1, or response 2 to reviewer 2. To clarify our assumption, we added a footnote in the revised manuscript as follows:

> Section II, page 5, footnote 3,
>
> The reverse SIC order, where the AU performs SIC and cell-center TUs treat AU's message as noise, has been considered. Nevertheless, such a SIC order is not promising in ATN-NOMA because the SIC at the AU might fail due to strong ICI. To ensure reliable communications to the AU, we assume the AU treats cell-center TUs' messages as noise and the cell-center TUs perform SIC.

Response 1 (ii):

As advised, we revised our system model by further considering the ICI of TUs. We also revised our optimization problem accordingly and solved it by exploiting the structure of the problem and applying successive convex approximation (SCA). Compared to the previous version of this paper, our results showed similar behavior except that the TU's sum-rate of all schemes are degraded by about 20-30% due to the ICI of TUs. The AU's outage probability remains similar since the AU's ICI has been previously considered. The corresponding amendments can be found in several parts of the paper as follows:

Abstract, page 1,

... The corresponding optimization problem is non-convex in which we exploit the structure of the problem and apply successive convex approximation (SCA) to obtain a local optimal solution. ...

... Extensive simulation results show that our proposed ATN-NOMA scheme outperforms existing schemes by 52-91% in terms of the sum-rate, and its analytical outage probability can be as low as the order of 10^{-17}. ...

Section I, page 2,

We then formulate an optimization problem to maximize the sum-rate of the TUs by optimal beamwidth and power allocation subject to the AU's QoS requirement. A local optimal solution is also obtained for the non-convex optimization problem by exploiting the structure of the problem and applying successive convex approximation (SCA).

Section I, page 3,

... In this paper, we further consider the ICI of the TUs. By exploiting the structure of the problem and applying SCA, we also obtain a local optimal solution of the corresponding non-convex optimization problem. ...

Section II, page 5,

At the terrestrial platform, the signal observed by the cell-center TU t is:

$$y_t^{\mathrm{rx}} = \tilde{h}_{b,t}^H \tilde{S}_b + \sum_{\forall b' \in \mathcal{B} \setminus b} \tilde{h}_{b',t}^H \tilde{S}_{b'} + \sum_{\forall b'' \in \mathcal{I}} \tilde{h}_{b'',t}^H \tilde{S}_{b''} + \sigma_t, \qquad (13)$$

where $\tilde{h}_{b,t}$ is the complex channel tap from its associated BS b to the cell-center TU t such that $b = t$, $\tilde{h}_{b',t}$ and $\tilde{h}_{b'',t}$ are the complex channel tap from non-associated BS b' and b'', respectively, to the cell-center TU t such that $b' \neq t$ and $b'' \neq t$, and $\sigma_t \sim \mathcal{CN}(0, \sigma_{\mathrm{n}}^2)$ is the AWGN observed at t. ...

$$\vdots$$

$$\mathrm{SINR}_t^{(u)} = \frac{\sum\limits_{\forall b \in \mathcal{B}} \rho_{b,u} N \left| h_{b,t} \right|^2}{\sum\limits_{\forall b \in \mathcal{B}} \rho_b N \left| h_{b,t} \right|^2 + \sum\limits_{\forall b'' \in \mathcal{I}} N \left| h_{b'',t} \right|^2 + 1}. \qquad (14)$$

$$\vdots$$

$$\text{SINR}_t = \frac{\rho_b N \left|h_{b,t}\right|^2}{\sum\limits_{\forall b' \in \mathcal{B} \setminus b} \rho_{b'} N \left|h_{b',t}\right|^2 + \sum\limits_{\forall b'' \in \mathcal{I}} N \left|h_{b'',t}\right|^2 + 1}. \quad (15)$$

Section III, page 5,

where $\boldsymbol{\rho_{b,u}} = [\rho_{1,u}, \ldots, \rho_{B,u}]^T$ and $\boldsymbol{\rho_b} = [\rho_1, \ldots, \rho_B]^T$. ...

Section III, page 6,

Problem (17) is a non-convex optimization problem due to (17a), (17b), and (17c). ...

Section III, page 6-7,

Using proposition 2, (17) is then reduced to the following problem:

$$\vdots$$

(Due to its lengthy discussion, we kindly refer the editor to the revised manuscript.)

$$\vdots$$

Since (26) is a convex optimization problem, it can be solved efficiently [52].

Section V, page 11-13, Figs. 5-8.

(As there are many figures, we kindly refer the editor to the revised manuscript.)

Section V-F, page 13,

... In particular, the proposed ATN-NOMA scheme achieves an average of 91% and 52% sum-rate improvement as compared to schemes based on OMA and FNOMA, respectively. As compared to TN-NOMA, the sum-rate improvement is marginal although the AU gain is 30-60 dB higher than the cell-edge TU. ...

Specifically, the outage probability of TN-NOMA is 2.5×10^{-3} whereas the outage probability of the proposed ATN-NOMA scheme is 6.25×10^{-8} to 7.3×10^{-17}. ...

Section VI, page 13,

... The optimal beamwidth was then obtained in closed-form expression while the optimal power allocation was obtained via SCA. ...

Response 1 (iii):

In the revised manuscript, we also added clarification for the beamforming of coordinated

BSs. In this paper, we assume that the coordinated BSs jointly form maximum ratio transmission (MRT) beamforming to the AU. The MRT beamforming is suboptimal in a multi-cell setting, however, we choose this beamforming because its closed-form expression allows us to characterize the AU's outage probability. As discussed in Section V-B, if the data rate requirement is low and the AU experiences zero ICI, the outage probabilities of OB-OMA, OB-FNOMA, and ATN-NOMA are extremely low. In such cases, an exorbitant number of samples are required to accurately observe the numerical outage probability (e.g., 10^{20} samples are required if $R_{\min}$ = 100 Kbps). This is computationally challenging, if not infeasible. Thus, we use the tractable expressions provided by the MRT beamforming to examine the analytical outage probability. Using the analytical outage probability, we are able to verify that the AU's outage probability can be as low as the order of 10^{-17}. The corresponding amendments can be found as follows:

> Section II, page 4-5,
>
> Hence, each coordinated terrestrial BS, $b \in \mathcal{B}$, transmits the following signal to jointly form maximum ratio transmission (MRT) beamforming to the AU[2]:
>
> Section II, page 5, footnote 2
>
> The MRT beamforming is suboptimal in a multi-cell setting, however, we choose this beamforming because its closed-form expression allows us to characterize the AU's outage probability.

Response 1 (iv):

As suggested, we also included useful insights of the analytical forms for some special cases. These details can be found in Section IV as follows:

> Section IV, page 8,
>
> In proposition 4, it is observed that I_{tot} follows exactly a gamma distribution in cases where the probabilities of LOS/NLOS are one.
>
> Section IV, page 9,
>
> Furthermore, in cases where $\text{card}\,(\mathcal{D}) = 1$ and the probabilities of LOS/NLOS are one, the outage probability can be approximated using a gamma distribution.

Nevertheless, we believe the reviewer misunderstands our analysis a little bit. The theoretical analysis such as the aggregated ICI and outage probability were given in analytical forms. To highlight this matter, we made the expressions more explicitly as follows:

Section IV, page 8, proposition 4,

The pdf of the aggregated ICI, I_{tot}, in ATN-NOMA is approximated as:

$$\begin{aligned} & f_{I_{\text{tot}}}\left(\tau,\tilde{I},p_{b,u}^{\text{L}}\left(\hat{d}_{b,u},z_u\right),\hat{m},\hat{\theta}\right) \\ \approx & \sum_{0\le i\le\tilde{I}} f\left(i,\tilde{I},p_{b,u}^{\text{L}}\left(\hat{d}_{b,u},z_u\right)\right) f_{H^{(i)}}\left(\tau,\hat{m},\hat{\theta}\right),\tau>0 \qquad (36) \\ = & \sum_{0\le i\le\tilde{I}}\left[\binom{\tilde{I}}{i} p_{b,u}^{\text{L}}\left(\hat{d}_{b,u},z_u\right)^{i} p_{b,u}^{\text{N}}\left(\hat{d}_{b,u},z_u\right)^{(\tilde{I}-i)} \frac{\tau^{\hat{m}-1}\exp\left(-\frac{\tau}{\hat{\theta}}\right)}{\hat{\theta}^{\hat{m}}\Gamma\left(\hat{m}\right)}\right]. \end{aligned}$$

The CDF of the aggregated ICI, I_{tot}, in ATN-NOMA is approximated as:

$$\begin{aligned} & F_{I_{\text{tot}}}\left(\tau,\tilde{I},p_{b,u}^{\text{L}}\left(\hat{d}_{b,u},z_u\right),\hat{m},\hat{\theta}\right) \\ \approx & \sum_{0\le i\le\tilde{I}} f\left(i,\tilde{I},p_{b,u}^{\text{L}}\left(\hat{d}_{b,u},z_u\right)\right) F_{H^{(i)}}\left(\tau,\hat{m},\hat{\theta}\right),\tau>0 \qquad (37) \\ = & \sum_{0\le i\le\tilde{I}}\left[\binom{\tilde{I}}{i} p_{b,u}^{\text{L}}\left(\hat{d}_{b,u},z_u\right)^{i} p_{b,u}^{\text{N}}\left(\hat{d}_{b,u},z_u\right)^{(\tilde{I}-i)} \int_0^{\tau}\frac{\tau'^{\hat{m}-1}\exp\left(-\frac{\tau'}{\hat{\theta}}\right)}{\hat{\theta}^{\hat{m}}\Gamma\left(\hat{m}\right)}d\tau'\right]. \end{aligned}$$

Section IV, page 8-9, proposition 5,

If no interfering BSs $b\in\mathcal{I}$ have the same elevation-angle as the coordinated BS b', the AU's outage probability is approximately:

$$\begin{aligned} P^{\text{out}} \approx & F_{\beta_{\text{tot}}}\left(r,\tilde{B}_{d_1},\ldots,\tilde{B}_{d_{\bar{\beta}}},p_{b,u}^{\text{L}}\left(d_1,z_u\right),\ldots,p_{b,u}^{\text{L}}\left(d_{\bar{\beta}},z_u\right)\right), \qquad (41) \\ = & \sum_{\forall b_d\in\mathcal{L}}\left[\prod_{\tilde{L}_{d_\beta}=b_{d_\beta},\forall\beta}\binom{\tilde{B}_{d_\beta}}{b_{d_\beta}} p_{b,u}^{\text{L}}\left(d_\beta,z_u\right)^{b_{d_\beta}}\times\right. \\ & \left. p_{b,u}^{\text{N}}\left(d_\beta,z_u\right)^{\left(\tilde{B}_{d_\beta}-b_{d_\beta}\right)}\int_0^{r}\frac{\tau'^{\hat{m}-1}\exp\left(-\frac{\tau'}{\hat{\theta}}\right)}{\hat{\theta}^{\hat{m}}\Gamma\left(\hat{m}\right)}d\tau'\right]. \end{aligned}$$

Section IV, page 9, proof of proposition 5,

... The CDF of the β_{tot} is approximated as:

$$
\begin{aligned}
& F_{\beta_{\text{tot}}}\left(r, \tilde{B}_{d_1}, \ldots, \tilde{B}_{d_{\bar{\beta}}}, p_{b,u}^{\mathrm{L}}\left(d_1, z_u\right), \ldots, p_{b,u}^{\mathrm{L}}\left(d_{\bar{\beta}}, z_u\right)\right) \quad (44) \\
\approx & \sum_{\forall b_d \in \mathcal{L}} \mathbb{P}\left(\tilde{L}_{d_1}=b_{d_1}, \ldots, \tilde{L}_{d_{\bar{\beta}}}=b_{d_{\bar{\beta}}}\right) F_{H^{(b_d)}}\left(r, \hat{m}, \hat{\theta}\right) \\
= & \sum_{\forall b_d \in \mathcal{L}}\left[\prod_{\tilde{L}_{d_\beta}=b_{d_\beta}, \forall \beta}\binom{\tilde{B}_{d_\beta}}{b_{d_\beta}} p_{b,u}^{\mathrm{L}}\left(d_\beta, z_u\right)^{b_{d_\beta}} \times\right. \\
& \left. p_{b,u}^{\mathrm{N}}\left(d_\beta, z_u\right)^{\left(\tilde{B}_{d_\beta}-b_{d_\beta}\right)} \int_0^r \frac{\tau'^{\hat{m}-1} \exp\left(-\frac{\tau'}{\hat{\theta}}\right)}{\hat{\theta}^{\hat{m}} \Gamma\left(\hat{m}\right)} d\tau'\right].
\end{aligned}
$$

Response 1 (v):

To further improve the quality of this revised manuscript, we carefully addressed the reviewers' comments. Our amendments and responses are detailed point-by-point to the reviewers.

RESPONSE TO REVIEWER 1'S COMMENTS

Comment 1:

"In this paper, the authors proposed an aerial-ground CoMP-NOMA strategy, where multiple BSs cooperatively serve an AU and a cell-edge TU via NOMA, and in the meanwhile, individually serve their respective cell-center TUs. The authors first formulated an optimization problem to maximize the sum rate of cell-center TUs, by jointly optimizing the BSs' power allocations and the UAV's beamwidth. Then, the authors also analyzed the aggregated ICI suffered by the UAV. Finally, via simulation, the authors revealed some interesting observations and drove essential insights. Overall, this paper considers a timely and interesting topic. The paper is generally well organized and written. However, the reviewer still has some critical issues about its system setup, novelty, and clarity. Detailed comments are given below."

Response 1:

We thank the reviewer for the nice words and constructive comments. To improve the revised manuscript, we made amendments according to your suggestions. Please find them below.

Comment 2:

"Most of the results in this paper are only valid under a specific system setup (see below). This limits the generality and contributions of this paper.

1) The authors assumed a homogeneous network with hexagonal cells, which may result in ICI even if the UAV employs a tunable directional antenna. However, in future heterogeneous networks, due to the irregular deployment of the small BSs, the ICI hardly exists if the UAV applies a directional antenna, as it is difficult to find two BSs having the same elevation angle with the UAV. The considered problem may become non-existent in the future.

2) The authors proposed an elevation-angle based UAV-BS association strategy. First, this is in fact equivalent to the traditional nearest-distance association strategy, where the UAV is associated with the B nearest BSs, since all BSs have the same height. Second, although its performance looks good, it is due to the assumption that each BS is equipped with an omnidirectional antenna. However, in the case that each BS employs a fixed beam pattern with a downtilt angle, the nearest association strategy (or elevation angle-based strategy) may fail, since the UAV would easily fall into the antenna null of its nearby BSs."

Response 2:

The reviewer has several concerns in this comment. To carefully address each concern, we separate our responses into three parts. Please see below.

Comment 2 (i):

"Most of the results in this paper are only valid under a specific system setup (see below). This limits the generality and contributions of this paper.

1) The authors assumed a homogeneous network with hexagonal cells, which may result in ICI even if the UAV employs a tunable directional antenna. However, in future heterogeneous networks, due to the irregular deployment of the small BSs, the ICI hardly exists if the UAV applies a directional antenna, as it is difficult to find two BSs having the same elevation angle with the UAV. The considered problem may become non-existent in the future."

Response 2 (i):

We agree with the reviewer that the deployment of the BSs in future heterogeneous network are irregular. As a result, the ICI of the AU might be fully mitigated if our proposed scheme is being employed. Nevertheless, we see this as an advantage because this generalization doesn't make the performance of our proposed scheme worse. Instead, as pointed out by the reviewer, using our proposed scheme in an irregular cellular network might provide zero ICI performance to the AU, and such performance has been considered in our paper.

We believe a more important consideration is when the ICI of the AU cannot be fully mitigated in our proposed scheme, i.e., if multiple interfering BSs having the same elevation angle as the coordinated BSs. It is very important to know how well our proposed scheme performs in such cases too. Nonetheless, it is very challenging to use a stochastic or irregular network deployment to create this setting. Specifically, it is very hard to find three or more BSs having the same elevation angle to a 3-dimensional location in a stochastic process setup (i.e., a ring centered at a location with a fixed radius intersecting three or more points at a time). This motivates our assumption of considering a hexagonal cellular structure, where multiple BSs can easily have the same elevation angle to the AU.

Using this setup, not only are we able to provide quantitative insight on the effects of the AU's interference but we are also able to identify the key factors that determine the performance of our proposed scheme at a fundamental level. For example, in Section V-D, we observe that increasing the number of coordinated BSs is the only solution to fully mitigate the ICI of the AU if multiple interfering BSs have the same elevation angle as the coordinated BSs. In Section V-E, Fig. 7(c), we see that the existence of the AU's interference has an enormous effect on the AU's outage probability where the outage probability may increase from the order of 10^{-14} to 10^{-2}. These findings cannot be easily discovered in a stochastic process setup. Furthermore, our

ICI approximation can be extended to other settings as well (e.g., interfering BSs with different heights).

To further highlight the generality and contributions of our paper, we revised our paper in several parts as follows:

Section I, major contributions, page 3,

Extensive simulation results with different network parameters and settings are presented. Our simulation results provide quantitative insights on the effects of AU's interference, and also reveal the key factors that determine the performance of our proposed scheme at a fundamental level.

Section IV, page 7, footnote 5,

Corollary 1 suggests that in irregular cellular networks the AU in our proposed scheme is likely to experience zero ICI. This is because it is difficult to find multiple BSs having the same elevation angle to the AU in such settings.

Section IV, page 7,

For ease of exposition, we assume the interfering BSs have the same height here, and thus the same probability of LOS. In Appendix A, we generalize our analysis to cases where the interfering BSs have different heights.

Section V, page 9,

Thus, we consider multiple schemes based on different combinations to identify their corresponding gains and effects at a fundamental level.

Section V-D, page 12,

To fully mitigate the ICI of the AU, these results also suggest that increasing the number of coordinated BSs is the only solution.

Section V-E, page 12,

Specifically, the AU's outage probability may increase from the order of 10^{-14} to 10^{-2}.

Appendix A, page 13-14,

If the interfering BSs have different heights, we can approximate I_{tot} using the same method as approximating β_{tot}. Specifically, ...

Comment 2 (ii):

"*2) The authors proposed an elevation-angle based UAV-BS association strategy. First, this is in fact equivalent to the traditional nearest-distance association strategy, where the UAV is associated with the B nearest BSs, since all BSs have the same height.*"

Response 2 (ii):

We agree with the reviewer that our proposed elevation-angle based user association looks similar to the existing nearest distance (or minimum-distance) based user association. However, our analysis shows that the key parameter is the elevation-angle. To address this issue, we revised the simulation in Fig. 5 by further assuming the BSs have different heights. In addition, we consider both minimum-distance and maximum-SINR based user associations. Our simulation results show that our proposed elevation-angle based user association is different from existing user associations. More importantly, it provides the least probability of experiencing ICI, the highest sum-rate, and the lowest outage probability. Below is a copy of the amendments. These details can be found in Section V-C, page 10-11.

Fig. 5 compares the performance of the proposed elevation-angle based user association, minimum-distance based user association, and maximum-SINR based user association along with adjustable beamwidth directional antenna and network NOMA. Here, the AU is randomly located inside a disk centered at the origin with a radius of 500m, the BSs' height are uniformly distributed between 15m and 45m, and $R_{\min} = 2.8$ Mbps. As shown in Fig. 5(a), the minimum-distance and maximum-SINR based user associations are more likely to experience ICI. In the minimum-distance based user association, the nearest BSs might have a smaller elevation-angle to the AU. In the maximum-SINR based user association, the strongest BSs might be located farther away from the AU. In both cases, the optimal beamwidth might need to cover a larger area inclusive of the interfering BSs. This leads to a performance degradation in terms of sum-rate and outage probability as shown in Fig. 5(b) and Fig. 5(c), respectively. Nevertheless, if the proposed elevation-angle based user association is employed, the AU is more likely to experience zero ICI. This is because the optimal beamwidth typically covers a smaller area exclusive of the interfering BSs. Furthermore, using the smaller beamwidth increases the channel gain between the AU and the coordinated BSs. As a result, the proposed elevation-angle based user association outperforms existing user associations in both sum-rate and outage probability.

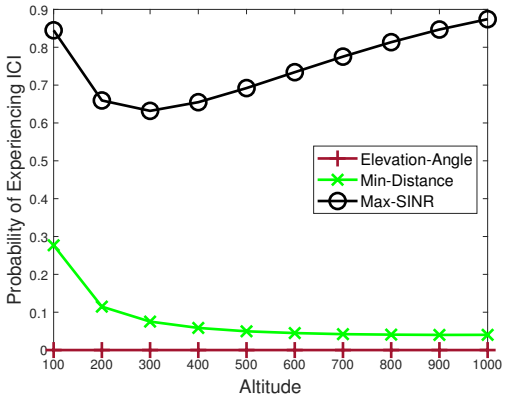

(a)

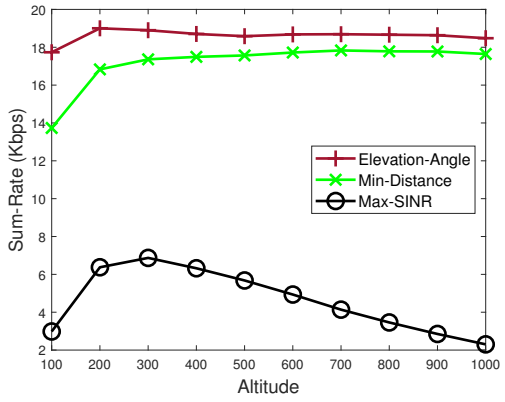

(b)

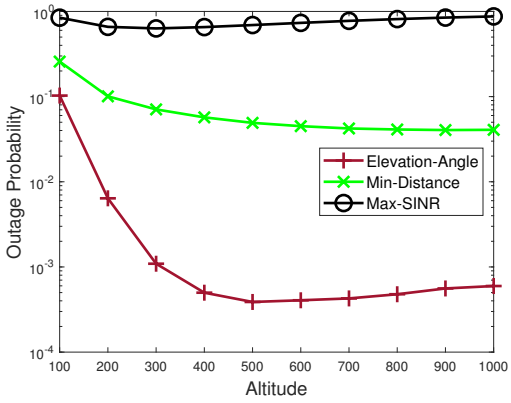

(c)

Figure 5: Performance of different user association policies: (a) probability of experiencing ICI; (b) sum-rate; (c) outage probability.

Comment 2 (iii):

"Second, although its performance looks good, it is due to the assumption that each BS is equipped with an omnidirectional antenna. However, in the case that each BS employs a fixed beam pattern with a downtilt angle, the nearest association strategy (or elevation angle-based strategy) may fail, since the UAV would easily fall into the antenna null of its nearby BSs."

Response 2 (iii):

We appreciate the reviewer's comment regarding the null issue. This is an interesting issue and we are aware that the existing works have pointed out that radio link failure might occur if the AU is located at the null of the associated BS. However, the existing works (e.g., [5],

[9], [14], [39]) assume that the AU is associated to a single BS only, whereas in our proposed scheme, the AU is associated to multiple BSs. Therefore, a larger macro diversity gain can be obtained to address this issue.

In this paper, we focus on the AU's interference issue. Thus, we use the ground-to-air probabilistic LOS/NLOS channel model which has been widely used in the literature for interference performance analysis (e.g., [15], [38], [42], [50]). In this channel model, the antenna radiation pattern of the BSs is assumed to be vertically directional and horizontally omnidirectional (implemented using multiple sector antennas). The AU is assumed to be served via the sidelobe and the TU is served via the mainlobe. We acknowledge that this channel modeling is unable to capture the null issue but it allows us to analyze the network performance (e.g., the ICI statistical properties and the AU's outage probability) in a tractable way and thus provide useful insights.

Regarding the robustness of our proposed scheme, the reviewer may refer to Section V-D. The reviewer may treat these results as a lower bound performance to the null issue. In particular, if the AU is located at the null of some coordinated BSs, the desired links are expected to decrease due to radio link failure. In Section V-D, as we decrease the number of coordinated BSs from four to two, not only do the desired links decrease but the interference links also increase. Thus, these results roughly provide a lower bound performance to the null issue.

Interestingly, our simulation results show that our proposed scheme provides a good performance to the AU and TUs. Specifically, as seen in Fig. 6, our proposed ATN-NOMA-P scheme with *two* coordinated BSs provides a comparable sum-rate and outage probability performance to FB-NOMA with *four* coordinated BSs. Furthermore, it is more superior than OMA based and FNOMA based schemes with *four* coordinated BSs in terms of sum-rate and outage probability.

Comment 3:

"There are many unclear portions in the proposed CoMP-NOMA. First, how many cell-edge users are paired with the UAV? Does each coordinated BS serve a CoMP cell-edge user, a CoMP UAV user and a non-CoMP cell-center user at the same time? If so, why there are only two users' signals superposed in (9)?"

Response 3:

We apologize for the confusion. In our proposed scheme, each coordinated BS only pairs a cell-center TU and an AU. The cell-center TU and the AU are referred to as the non-CoMP user and CoMP user, respectively. No cell-edge TU is considered in our proposed scheme. Thus, in eq. (9), there are only two user signals (i.e., cell-center TU and AU) being superimposed. To

further provide clarity on this matter, we revised our manuscript in several parts as follows:

> Section II, page 3,
>
> In this paper, we focus on the performance of a set of non-CoMP users and a CoMP user over an orthogonal RB as in [27], [28], [47], [48]. In our proposed scheme, the non-CoMP users are the cell-center TUs who are not significantly affected by ICI, and the CoMP user is the AU who suffers strong ICI. No cell-edge TU is considered in our proposed scheme.
>
> Section II, page 4,
>
> In addition, we adopt network NOMA that is promising to the pairing of cell-center TUs and AU. In the context of ATN-NOMA, each coordinated BS, $b \in \mathcal{B}$, pairs its associated cell-center TU t (i.e., the non-CoMP user) and the AU (i.e., the CoMP user) over the same RB. In each cell, the pairing consists of only two users to ensure low co-channel interference, hardware complexity, and processing delay [35].

Note that cell-edge TU is not considered in our proposed scheme because cell-edge TU also encounters ICI issue. For the pairing of cell-edge TU and AU, we suggest to employ other NOMA techniques such as CB-NOMA where both users can obtain beamforming gain. This is, however, beyond the scope of this paper. In this paper, we focus on network NOMA which is primarily designed to pair non-CoMP users and CoMP users [27], [28], [47], [48], where the former are those who are not significantly affected by ICI (e.g. cell-center TUs), and the latter are those who suffer strong ICI (e.g., AUs).

Comment 4:

"It is not reasonable to ignore the terrestrial ICI in (13), as other coordinated BSs are adjacent to BS b. You can only ignore the ICI from farther BSs."

Response 4:

As advised, we revised our system model by further considering the ICI of TUs. We also revised our optimization problem accordingly and solved it by exploiting the structure of the problem and applying successive convex approximation (SCA). Compared to the previous version of this paper, our results showed similar behavior except that the TU's sum-rate of all schemes are degraded by about 20-30% due to the ICI of TUs. The AU's outage probability remains similar since the AU's ICI has been previously considered. The corresponding amendments can be found in several parts of the paper as follows:

Abstract, page 1,

... The corresponding optimization problem is non-convex in which we exploit the structure of the problem and apply successive convex approximation (SCA) to obtain a local optimal solution. ...

... Extensive simulation results show that our proposed ATN-NOMA scheme outperforms existing schemes by 52-91% in terms of the sum-rate, and its analytical outage probability can be as low as the order of 10^{-17}. ...

Section I, page 2,

We then formulate an optimization problem to maximize the sum-rate of the TUs by optimal beamwidth and power allocation subject to the AU's QoS requirement. A local optimal solution is also obtained for the non-convex optimization problem by exploiting the structure of the problem and applying successive convex approximation (SCA).

Section I, page 3,

... In this paper, we further consider the ICI of the TUs. By exploiting the structure of the problem and applying SCA, we also obtain a local optimal solution of the corresponding non-convex optimization problem. ...

Section II, page 5,

At the terrestrial platform, the signal observed by the cell-center TU t is:

$$y_t^{\mathrm{rx}} = \tilde{h}_{b,t}^H \tilde{S}_b + \sum_{\forall b' \in \mathcal{B} \setminus b} \tilde{h}_{b',t}^H \tilde{S}_{b'} + \sum_{\forall b'' \in \mathcal{I}} \tilde{h}_{b'',t}^H \tilde{S}_{b''} + \sigma_t, \qquad (13)$$

where $\tilde{h}_{b,t}$ is the complex channel tap from its associated BS b to the cell-center TU t such that $b = t$, $\tilde{h}_{b',t}$ and $\tilde{h}_{b'',t}$ are the complex channel tap from non-associated BS b' and b'', respectively, to the cell-center TU t such that $b' \neq t$ and $b'' \neq t$, and $\sigma_t \sim \mathcal{CN}(0, \sigma_{\mathrm{n}}^2)$ is the AWGN observed at t. ...

$$\vdots$$

$$\mathrm{SINR}_t^{(u)} = \frac{\sum\limits_{\forall b \in \mathcal{B}} \rho_{b,u} N |h_{b,t}|^2}{\sum\limits_{\forall b \in \mathcal{B}} \rho_b N |h_{b,t}|^2 + \sum\limits_{\forall b'' \in \mathcal{I}} N |h_{b'',t}|^2 + 1}. \qquad (14)$$

$$\vdots$$

$$\text{SINR}_t = \frac{\rho_b N \left|h_{b,t}\right|^2}{\sum\limits_{\forall b' \in \mathcal{B} \setminus b} \rho_{b'} N \left|h_{b',t}\right|^2 + \sum\limits_{\forall b'' \in \mathcal{I}} N \left|h_{b'',t}\right|^2 + 1}. \quad (15)$$

Section III, page 5,

where $\boldsymbol{\rho_{b,u}} = [\rho_{1,u}, \ldots, \rho_{B,u}]^T$ and $\boldsymbol{\rho_b} = [\rho_1, \ldots, \rho_B]^T$. ...

Section III, page 6,

Problem (17) is a non-convex optimization problem due to (17a), (17b), and (17c). ...

Section III, page 6-7,

Using proposition 2, (17) is then reduced to the following problem:

$\vdots$

(Due to its lengthy discussion, we kindly refer the reviewer to the revised manuscript.)

$\vdots$

Since (26) is a convex optimization problem, it can be solved efficiently [52].

Section V, page 11-13, Figs. 5-8.

(As there are many figures, we kindly refer the reviewer to the revised manuscript.)

Section V-F, page 13,

... In particular, the proposed ATN-NOMA scheme achieves an average of 91% and 52% sum-rate improvement as compared to schemes based on OMA and FNOMA, respectively. As compared to TN-NOMA, the sum-rate improvement is marginal although the AU gain is 30-60 dB higher than the cell-edge TU. ...

Specifically, the outage probability of TN-NOMA is 2.5×10^{-3} whereas the outage probability of the proposed ATN-NOMA scheme is 6.25×10^{-8} to 7.3×10^{-17}. ...

Section VI, page 13,

... The optimal beamwidth was then obtained in closed-form expression while the optimal power allocation was obtained via SCA. ...

Comment 5:

"It is not practical to assume only a single AU. As the authors considered CoMP, why not

consider multiple AUs?"

Response 5:

We understand the reviewer's concern. Nevertheless, similar to existing network NOMA schemes, our proposed scheme can be used to serve multiple CoMP users (e.g., AUs) and non-CoMP users (e.g., cell-center TUs) in cellular networks by using a multi-carrier NOMA system. Specifically, one AU and multiple cell-center TUs are paired over a single orthogonal RB using NOMA. Different pairs of AUs and cell-center TUs are then served by using different orthogonal RBs. Thus, in this paper, we focus on the performance of a CoMP user (e.g., AU) as in [27], [28], [47], [48] because the key factors that determine the performance of our proposed scheme at a fundamental level can be more easily highlighted.

Furthermore, in our proposed scheme, each coordinated BS only pairs a cell-center TU and an AU. In each cell, the pairing consists of only two users to ensure low co-channel interference, hardware complexity, and processing delay [35]. To further provide these insights, we revised our manuscript as follows:

Section II, page 3,

Similar to existing network NOMA schemes, our proposed scheme can be used to serve multiple CoMP users (e.g., AUs) and non-CoMP users (e.g., cell-center TUs) by using a multi-carrier NOMA system. Specifically, a CoMP user and multiple non-CoMP users can be paired over a single orthogonal RB. Different pairs of CoMP users and non-CoMP users can then be served by using different orthogonal RBs.

Section II, page 4,

In addition, we adopt network NOMA that is promising to the pairing of cell-center TUs and AU. In the context of ATN-NOMA, each coordinated BS, $b \in \mathcal{B}$, pairs its associated cell-center TU t (i.e., the non-CoMP user) and the AU (i.e., the CoMP user) over the same RB. In each cell, the pairing consists of only two users to ensure low co-channel interference, hardware complexity, and processing delay [35].

Comment 6:

"In the formulated problem (17), why the performance of the cell-edge users is not considered?"

Response 6:

In our proposed scheme, each coordinated BS only pairs a cell-center TU and an AU. The cell-center TU and the AU are referred to as the non-CoMP user and CoMP user, respectively. No cell-edge TU is considered in our proposed scheme. Thus, in eq. (17), the performance of the cell-edge TU is not included. To further provide clarity, we revised our manuscript in several parts as follows:

> Section II, page 3,
>
> In this paper, we focus on the performance of a set of non-CoMP users and a CoMP user over an orthogonal RB as in [27], [28], [47], [48]. In our proposed scheme, the non-CoMP users are the cell-center TUs who are not significantly affected by ICI, and the CoMP user is the AU who suffers strong ICI. No cell-edge TU is considered in our proposed scheme.
>
> Section II, page 4,
>
> In addition, we adopt network NOMA that is promising to the pairing of cell-center TUs and AU. In the context of ATN-NOMA, each coordinated BS, $b \in \mathcal{B}$, pairs its associated cell-center TU t (i.e., the non-CoMP user) and the AU (i.e., the CoMP user) over the same RB. In each cell, the pairing consists of only two users to ensure low co-channel interference, hardware complexity, and processing delay [35].

Note that cell-edge TU is not considered in our proposed scheme because cell-edge TU also encounters ICI issue. For the pairing of cell-edge TU and AU, we suggest to employ other NOMA techniques such as CB-NOMA where both users can obtain beamforming gain. This is, however, beyond the scope of this paper. In this paper, we focus on network NOMA which is primarily designed to pair non-CoMP users and CoMP users [27], [28], [47], [48], where the former are those who are not significantly affected by ICI (e.g. cell-center TUs), and the latter are those who suffer strong ICI (e.g., AUs).

Comment 7:

It is not clear what beamforming technique is used by the coordinated BSs. It seems that the authors did not optimize the beamforming vector at all. Please explain the reason.

Response 7:

We thank the reviewer for bringing this up. In this paper, we assume that the coordinated BSs jointly form maximum ratio transmission (MRT) beamforming to the AU. The MRT beamforming is suboptimal in a multi-cell setting, however, we choose this beamforming because its closed-

form expression allows us to characterize the AU's outage probability. As discussed in Section V-B, if the data rate requirement is low and the AU experiences zero ICI, the outage probabilities of OB-OMA, OB-FNOMA, and ATN-NOMA are extremely low. In such cases, an exorbitant number of samples are required to accurately observe the numerical outage probability (e.g., 10^{20} samples are required if $R_{\min}$ = 100 Kbps). This is computationally challenging, if not infeasible. Thus, we use the tractable expressions provided by the MRT beamforming to examine the analytical outage probability. Using the analytical outage probability, we are able to verify that the AU's outage probability can be as low as the order of 10^{-17}. Based on the reviewer's point, we revised our paper as follows:

> Section II, page 4-5,
>
> Hence, each coordinated terrestrial BS, $b \in \mathcal{B}$, transmits the following signal to jointly form maximum ratio transmission (MRT) beamforming to the AU[2]:
>
> Section II, page 5, footnote 2
>
> The MRT beamforming is suboptimal in a multi-cell setting, however, we choose this beamforming because its closed-form expression allows us to characterize the AU's outage probability.

Comment 8:

"In (14), why did you assume that the cell-center TU (instead of the UAV) performs SIC? The effective channel condition of the UAV may be better than that of the cell-center TU thanks to the cooperative beamforming gain."

Response 8:

In this paper, we assume that the cell-center TUs perform SIC and the AU treats co-channel interference as noise to ensure reliable communications to the AU. The reverse SIC order, where the cell-center TUs treat co-channel interference as noise and the AU performs SIC, has been considered. Nevertheless, such a SIC order is not promising to the AU's performance due to strong AU's ICI. To fully understand this, we provide an in-depth discussion in the following.

For ease of exposition, let us refer to the co-channel interference induced by superposition coding as NOMA interference. In a downlink single-input-single-output NOMA system, it is well-known that weaker users should treat the NOMA interference as noise and stronger users should perform SIC. This strategy is optimal in terms of rate region [35]. Nevertheless, this

principle cannot be directly extended to network NOMA due to non-degraded channel and interference channel (i.e., ICI).

To see this, let's consider a network NOMA system with B coordinated BSs. In some cases, the AU might have a stronger channel gain than k cell-center TUs and a weaker channel gain than $(B-k)$ cell-center TUs, where $0<k<B$. Since AU is a CoMP user (or a common user) among the B coordinated BSs, the AU cannot simultaneously treat the NOMA interference as noise and perform SIC. More precisely, the AU can only treat the NOMA interference as noise or perform SIC.

In this paper, we choose the former. To understand the underlying reason, let's again consider a network NOMA with B coordinated BSs. Let us further assume that the cell-center TUs treat the NOMA interference as noise and the AU performs SIC (i.e., the reverse SIC order). Since the cell-center TUs treat the NOMA interference as noise, the rate of the cell-center TUs is:

$$R_t = B_{\mathrm{w}} \log\left(1+\frac{\rho_b N\left|h_{b,t}\right|^2}{\rho_{b,u} N\left|h_{b,t}\right|^2+\sum\limits_{\forall b'\in\mathcal{B}\setminus b} N\left|h_{b',t}\right|^2+K_t}\right), \tag{R.1}$$

where $b=t$ and $K_t=\sum\limits_{\forall b''\in\mathcal{I}} N\left|h_{b'',t}\right|^2+1$.

Since AU performs SIC, it has to independently remove each of the cell-center TUs' messages before decoding its own message. Note that the messages of cell-center TUs belong to different coordinated BSs. Thus, the ICI between cell-center TUs' messages cannot be cancelled at the AU via SIC. Consequently, the SINR of AU decoding the cell-center TU t's message is:

$$R_u^{(t)} = B_{\mathrm{w}} \log\left(1+\frac{\rho_b N\left|h_{b,u}^{v}\left(\Psi\right)\right|^2}{\rho_{b,u} N\left|h_{b,u}^{v}\left(\Psi\right)\right|^2+\sum\limits_{\forall b'\in\mathcal{B}\setminus b} N\left|h_{b',u}^{v}\left(\Psi\right)\right|^2+K_u}\right), \tag{R.2}$$

where $b=t$ and $K_u=\sum\limits_{\forall b''\in\mathcal{I}} N\left|h_{b'',u}^{v}\left(\Psi\right)\right|^2+1$. After successfully removing all the cell-center TUs' messages (i.e., a successful SIC), the AU then decodes its own message with the following SINR:

$$R_u = B_{\mathrm{w}} \log\left(1+\frac{\sum\limits_{\forall b\in\mathcal{B}} \rho_{b,u} N\left|h_{b,u}^{v}\left(\Psi\right)\right|^2}{K_u}\right). \tag{R.3}$$

The AU's QoS requirement is satisfied if and only if:

$$\sum_{\forall b\in\mathcal{B}} \rho_{b,u} N\left|h_{b,u}^{v}\left(\Psi\right)\right|^2 \geq \left(2^{\frac{R_{\min}}{B_{\mathrm{w}}}}-1\right) K_u, \tag{R.4}$$

which is very promising. Nevertheless, to ensure a successful SIC (i.e., R.3), (R.2) must be greater than or equal to (R.1) for $\forall t$. Simplifying the inequality, we have:

$$\frac{\left|h_{b,u}^{v}\left(\Psi\right)\right|^{2}}{\sum\limits_{\forall b'\in\mathcal{B}\setminus b}N\left|h_{b',u}^{v}\left(\Psi\right)\right|^{2}+K_{u}}\geq\frac{\left|h_{b,t}\right|^{2}}{\sum\limits_{\forall b'\in\mathcal{B}\setminus b}N\left|h_{b',t}\right|^{2}+K_{t}},\text{for }\forall t, \tag{R.5}$$

In aerial-terrestrial networks, $\left|h_{b,u}^{v}\left(\Psi\right)\right|^{2}$ is usually greater than $\left|h_{b,t}\right|^{2}$. Nevertheless, the ICI of AU is also much stronger than that of TU. Thus, we often have:

$$\left(\sum_{\forall b'\in\mathcal{B}\setminus b}N\left|h_{b',u}^{v}\left(\Psi\right)\right|^{2}+K_{u}\right)\gg\left(\sum_{\forall b'\in\mathcal{B}\setminus b}N\left|h_{b',t}\right|^{2}+K_{t}\right).$$

This is true even in cases where $K_u = 1$. Consequently, it is very hard to satisfy (R.5).

As the AU's SIC might not be successful at all times, the reliable communications to the AU cannot be guaranteed. To address this limitation, we therefore assume that the AU treats NOMA interference as noise and the cell-center TUs perform SIC. Using this SIC order, the reliable communications to the AU is always guaranteed unless outage occurs. Interestingly, the outage probability of our proposed scheme is extremely low. To clarify our assumption, we added a footnote in the revised manuscript as follows:

> Section II, page 5, footnote 3,
>
> The reverse SIC order, where the AU performs SIC and cell-center TUs treat AU's message as noise, has been considered. Nevertheless, such a SIC order is not promising in ATN-NOMA because the SIC at the AU might fail due to strong ICI. To ensure reliable communications to the AU, we assume the AU treats cell-center TUs' messages as noise and the cell-center TUs perform SIC.

Comment 9:

"Limited insights can be driven from the theoretical analysis in Section IV, as all results are not given in an analytical form. The authors should attempt to simplify them by considering some special cases, so that they become more useful and enlightening, thus proving more useful than simulations alone. "

Response 9:

As suggested, we provided useful insights of the analytical forms for some special cases. These details can be found in Section IV as follows:

Section IV, page 8,

In proposition 4, it is observed that I_{tot} follows exactly a gamma distribution in cases where the probabilities of LOS/NLOS are one.

Section IV, page 9,

Furthermore, in cases where $\text{card}\left(\mathcal{D}\right) = 1$ and the probabilities of LOS/NLOS are one, the outage probability can be approximated using a gamma distribution.

In addition, we notice there is a bit of misunderstanding. The theoretical analysis such as the aggregated ICI and outage probability are given in analytical forms. To highlight this matter, we made the expressions more explicitly as follows:

Section IV, page 8, proposition 4,

The pdf of the aggregated ICI, I_{tot}, in ATN-NOMA is approximated as:

$$\begin{aligned} & f_{I_{\text{tot}}}\left(\tau, \tilde{I}, p_{b,u}^{\text{L}}\left(\hat{d}_{b,u}, z_u\right), \hat{m}, \hat{\theta}\right) \\ \approx & \sum_{0\le i\le \tilde{I}} f\left(i, \tilde{I}, p_{b,u}^{\text{L}}\left(\hat{d}_{b,u}, z_u\right)\right) f_{H^{(i)}}\left(\tau, \hat{m}, \hat{\theta}\right), \tau > 0 \qquad (36) \\ = & \sum_{0\le i\le \tilde{I}} \left[\binom{\tilde{I}}{i} p_{b,u}^{\text{L}}\left(\hat{d}_{b,u}, z_u\right)^{i} p_{b,u}^{\text{N}}\left(\hat{d}_{b,u}, z_u\right)^{(\tilde{I}-i)} \frac{\tau^{\hat{m}-1}\exp\left(-\frac{\tau}{\hat{\theta}}\right)}{\hat{\theta}^{\hat{m}}\Gamma\left(\hat{m}\right)} \right]. \end{aligned}$$

The CDF of the aggregated ICI, I_{tot}, in ATN-NOMA is approximated as:

$$\begin{aligned} & F_{I_{\text{tot}}}\left(\tau, \tilde{I}, p_{b,u}^{\text{L}}\left(\hat{d}_{b,u}, z_u\right), \hat{m}, \hat{\theta}\right) \\ \approx & \sum_{0\le i\le \tilde{I}} f\left(i, \tilde{I}, p_{b,u}^{\text{L}}\left(\hat{d}_{b,u}, z_u\right)\right) F_{H^{(i)}}\left(\tau, \hat{m}, \hat{\theta}\right), \tau > 0 \qquad (37) \\ = & \sum_{0\le i\le \tilde{I}} \left[\binom{\tilde{I}}{i} p_{b,u}^{\text{L}}\left(\hat{d}_{b,u}, z_u\right)^{i} p_{b,u}^{\text{N}}\left(\hat{d}_{b,u}, z_u\right)^{(\tilde{I}-i)} \int_0^{\tau} \frac{\tau'^{\hat{m}-1}\exp\left(-\frac{\tau'}{\hat{\theta}}\right)}{\hat{\theta}^{\hat{m}}\Gamma\left(\hat{m}\right)} d\tau' \right]. \end{aligned}$$

Section IV, page 8-9, proposition 5,

If no interfering BSs $b \in \mathcal{I}$ have the same elevation-angle as the coordinated BS b', the AU's outage probability is approximately:

$$P^{\text{out}} \approx F_{\beta_{\text{tot}}}\left(r, \tilde{B}_{d_1}, \ldots, \tilde{B}_{d_{\bar{\beta}}}, p^{\text{L}}_{b,u}\left(d_1, z_u\right), \ldots, p^{\text{L}}_{b,u}\left(d_{\bar{\beta}}, z_u\right)\right), \tag{41}$$

$$= \sum_{\forall b_d \in \mathcal{L}} \left[\prod_{\tilde{L}_{d_\beta} = b_{d_\beta}, \forall \beta} \begin{pmatrix} \tilde{B}_{d_\beta} \\ b_{d_\beta} \end{pmatrix} p^{\text{L}}_{b,u}\left(d_\beta, z_u\right)^{b_{d_\beta}} \times \right.$$

$$\left. p^{\text{N}}_{b,u}\left(d_\beta, z_u\right)^{\left(\tilde{B}_{d_\beta} - b_{d_\beta}\right)} \int_0^r \frac{\tau'^{\hat{m}-1} \exp\left(-\frac{\tau'}{\hat{\theta}}\right)}{\hat{\theta}^{\hat{m}} \Gamma\left(\hat{m}\right)} d\tau' \right].$$

Section IV, page 9, proof of proposition 5,

... The CDF of the β_{tot} is approximated as:

$$F_{\beta_{\text{tot}}}\left(r, \tilde{B}_{d_1}, \ldots, \tilde{B}_{d_{\bar{\beta}}}, p^{\text{L}}_{b,u}\left(d_1, z_u\right), \ldots, p^{\text{L}}_{b,u}\left(d_{\bar{\beta}}, z_u\right)\right) \tag{44}$$

$$\approx \sum_{\forall b_d \in \mathcal{L}} \mathbb{P}\left(\tilde{L}_{d_1} = b_{d_1}, \ldots, \tilde{L}_{d_{\bar{\beta}}} = b_{d_{\bar{\beta}}}\right) F_{H^{(b_d)}}\left(r, \hat{m}, \hat{\theta}\right)$$

$$= \sum_{\forall b_d \in \mathcal{L}} \left[\prod_{\tilde{L}_{d_\beta} = b_{d_\beta}, \forall \beta} \begin{pmatrix} \tilde{B}_{d_\beta} \\ b_{d_\beta} \end{pmatrix} p^{\text{L}}_{b,u}\left(d_\beta, z_u\right)^{b_{d_\beta}} \times \right.$$

$$\left. p^{\text{N}}_{b,u}\left(d_\beta, z_u\right)^{\left(\tilde{B}_{d_\beta} - b_{d_\beta}\right)} \int_0^r \frac{\tau'^{\hat{m}-1} \exp\left(-\frac{\tau'}{\hat{\theta}}\right)}{\hat{\theta}^{\hat{m}} \Gamma\left(\hat{m}\right)} d\tau' \right].$$

Comment 10:

"The trend in Fig.4 is counterintuitive. Why can increasing the UAV height reduce the outage probability? This decreases the effective channel power since the UAV-BS distance is enlarged."

Response 10:

We thank the reviewer for bringing this up. The trend in Fig. 4 is anticipated because increasing the AU's altitude leads to a higher probability of LOS. In cases where the AU's experiences zero ICI, the LOS links are beneficial. Thus, the AU's outage probability first decreases as the AU's altitude increases. After the LOS gain is substantially obtained at a certain altitude, the outage probability then increases due to a higher path loss. To clarify this matter, we revised the simulation in Fig. 4 by considering a wider range of altitudes and also added more discussions.

Section V, page 10,

... Furthermore, in cases where the AU experiences zero ICI, we notice that the outage probability first decreases as the AU's altitude increases. This is due to the LOS gain. After the LOS gain is substantially obtained at a certain altitude, the outage probability then

increases due to higher path loss.

Section V, page 10,

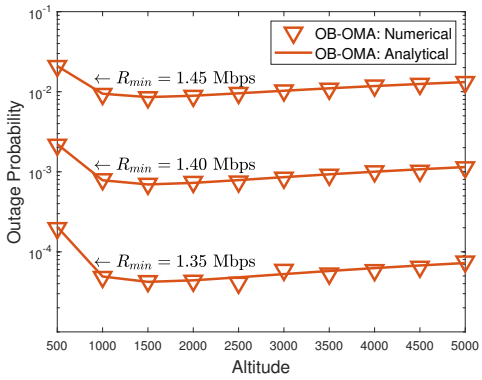

(a)

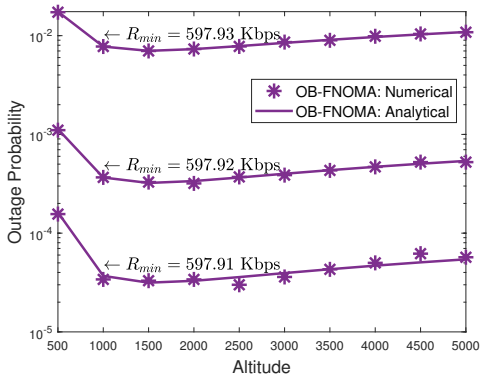

(b)

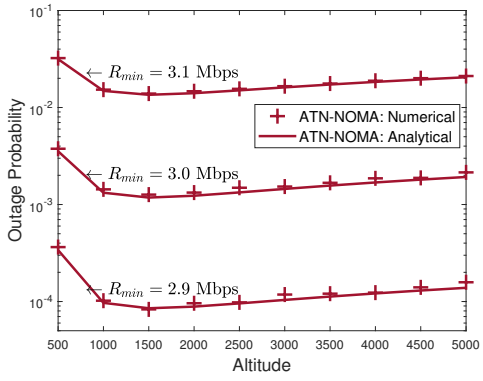

(c)

Figure 4: Numerical outage probability vs. analytical outage probability: (a) OB-OMA; (b) OB-FNOMA; (c) ATN-NOMA.

Comment 11:

"In Section V-F, the authors compared the proposal with the benchmark of pairing two TUs. Does the UAV exist in this benchmark? It is more interesting to consider cell-center TU, cell-edge TU, and the AU simultaneously. Then, you compare the two pairing strategies, i.e., pairing the first two or the last two users."

Response 11:

We thank the reviewer for the helpful suggestion. In each cell, the pairing consists of only two users. In our proposed scheme, each coordinated BS only pairs a cell-center TU and an AU. No cell-edge TU is considered in our proposed scheme. In the comparison scheme, each coordinated BS only pairs a cell-center TU and a cell-edge TU (i.e., terrestrial network NOMA scheme). No AU is considered in the comparison scheme. Interestingly, our simulation results show the pairing of cell-center TU and AU (i.e., our proposed scheme) is more beneficial than that of cell-center TU and cell-edge TU (i.e. the comparison scheme).

Note that the pairing of cell-edge TU and AU is not considered in this paper because network NOMA is primarily designed to pair non-CoMP users and CoMP users [27], [28], [47], [48], where the former are those who are not significantly affected by ICI (e.g. cell-center TUs), and the latter are those who suffer strong ICI (e.g., AUs/cell-edge TUs).

Comment 12:

"In (9), why h_{b,u}^v can be both bold and normal at the same time?"

Response 12:

We thank the reviewer for bringing this up and we apologize for the notation's confusion. In this paper, $\boldsymbol{h}_{\boldsymbol{b,u}}^{\boldsymbol{v}}\left(\boldsymbol{\Psi}\right) = \left[h_{1,u}^{v}\left(\Psi\right),\ldots,h_{B,u}^{v}\left(\Psi\right)\right]$ is the complex channel vector among the coordinated BS $b \in \mathcal{B}$ and $h_{b,u}^{v}\left(\Psi\right)$ is the complex channel tap between BS b and the AU. To provide better clarity, we revised our manuscript as follows:

> Section II, page 5,
> where $\boldsymbol{h}_{\boldsymbol{b,u}}^{\boldsymbol{v}}\left(\boldsymbol{\Psi}\right) = \left[h_{1,u}^{v}\left(\Psi\right),\ldots,h_{B,u}^{v}\left(\Psi\right)\right]$ is the complex channel vector among the coordinated BS $b \in \mathcal{B}$, $h_{b,u}^{v}\left(\Psi\right)$ is the complex channel tap between BS b and the AU, $\frac{h_{b,u}^{v}(\Psi)}{\left\|\boldsymbol{h}_{\boldsymbol{b,u}}^{\boldsymbol{v}}(\boldsymbol{\Psi})\right\|}$ is the beamforming phase from the BS b to the AU and P_{tx} is the total transmit power at the BS.

Comment 13:

"The literature survey should be improved. See below:

1) Magazine papers on cellular-connected UAV communications:

[R1] "Mobile network-connected drones: Field trials, simulations, and design insights," IEEE Veh. Technol. Mag.

[R2] "Aerial-Ground Interference Mitigation for Cellular-Connected UAV," IEEE Wireless Communications.

[R3] "The Essential Guide to Realizing 5G-Connected UAVs with Massive MIMO," IEEE Communications Magazine.

2) UAV plus NOMA:

[R1] "Non-Orthogonal Multiple Access for Air-to-Ground Communication," IEEE Transactions on Communications.

[R2] "NOMA-Aided UAV Communications over Correlated Rician Shadowed Fading Channels," IEEE Transactions on Signal Processing.

[R3] "Exploiting NOMA for UAV Communications in Large-Scale Cellular Networks," in IEEE Transactions on Communications.

[R4] "Non-orthogonal multiple access for mmWave drone networks with limited feedback." IEEE Transactions on Communications."

Response 13:

As suggested, we revised the literature survey. The above references can be found in our revised manuscript as follows:

Section I, page 1,

Field trials and simulation studies have been conducted to verify the feasibility of cellular-connected UAVs in 4th generation (4G) [5] and 5th generation (5G) cellular networks [6]. Preliminary results show that the idea is feasible.

Section I, page 1,

Different types of aerial-ground interference mitigation techniques are also compared in [17] for evaluation purpose.

Section I, page 2,

Some existing studies on NOMA-enabled UAV communications have been conducted in recent years. On the one hand, existing works (e.g., [31]–[34]) have considered the applications of aerial base stations. On the other hand, existing works have focused on the applications of AUs. Pertaining to the latter, [35] has proposed a robust NOMA scheme to serve AUs and TUs for control and data links, respectively, and [36] has derived the outage probability and finite SINR diversity gain where multiple AUs are served by a terrestrial BS. Nevertheless, the ICI issue at the AUs is not considered in [35], [36]. Besides, [37] has proposed an optimal trajectory and user association that minimizes the AU's mission

completion time. In [37], the ICI of AU is considered but no ICI mitigation technique is proposed.

RESPONSE TO REVIEWER 2'S COMMENTS

Comment 1:

"The system model (including channel model, perfect knowledge of the location of UAV) in this manuscript is very simple so that some optimization techniques can be applied. It is doubtful whether those system model and assumptions are realistic in practical communication system. "

Response 1:

We thank the reviewer for the constructive feedback. We acknowledge that our system model is simpler than the actual process in the real world. However, our system model has captured important parts of the wireless communication process that are major players in our analysis. Besides, in this paper, we use the ground-to-air probabilistic LOS/NLOS channel model and gamma distribution (i.e., the channel amplitude follows the Nakagami-M fading model) for the aerial large-scale and small-scale fading effects. For the terrestrial large-scale and small-scale fading effects, we use the simplified path loss model and gamma distribution. These models are widely used in existing literature (e.g., [15], [38], [42], [48]).

Furthermore, we assume that the location of the UAV is perfectly known for three realistic reasons. Firstly, the AU's location must be known for safety and security purposes [L1-L3], [35]. Secondly, the AU's location can be obtained very accurately using state-of-the-art techniques [L4], [L5]. Thirdly, the command and control messages contain the AU's location, which have to be relayed to the BSs before transmitting to the AU [L2], [35].

To make our system model more realistic, we revised our system model by further considering the ICI of TUs. We also revised our optimization problem accordingly and solved it by exploiting the structure of the problem and applying successive convex approximation (SCA). Compared to the previous version of this paper, our results showed similar behavior except that the TU's sum-rate of all schemes are degraded by about 20-30% due to the ICI of TUs. The AU's outage probability remains similar since the AU's ICI has been previously considered. The corresponding amendments can be found in several parts of the paper as follows:

> Abstract, page 1,
>
> ... The corresponding optimization problem is non-convex in which we exploit the structure of the problem and apply successive convex approximation (SCA) to obtain a local optimal solution. ...

... Extensive simulation results show that our proposed ATN-NOMA scheme outperforms existing schemes by 52-91% in terms of the sum-rate, and its analytical outage probability can be as low as the order of 10^{-17}. ...

Section I, page 2,

We then formulate an optimization problem to maximize the sum-rate of the TUs by optimal beamwidth and power allocation subject to the AU's QoS requirement. A local optimal solution is also obtained for the non-convex optimization problem by exploiting the structure of the problem and applying successive convex approximation (SCA).

Section I, page 3,

... In this paper, we further consider the ICI of the TUs. By exploiting the structure of the problem and applying SCA, we also obtain a local optimal solution of the corresponding non-convex optimization problem. ...

Section II, page 5,

At the terrestrial platform, the signal observed by the cell-center TU t is:

$$y_t^{\text{rx}} = \tilde{h}_{b,t}^H \tilde{S}_b + \sum_{\forall b' \in \mathcal{B} \setminus b} \tilde{h}_{b',t}^H \tilde{S}_{b'} + \sum_{\forall b'' \in \mathcal{I}} \tilde{h}_{b'',t}^H \tilde{S}_{b''} + \sigma_t, \qquad (13)$$

where $\tilde{h}_{b,t}$ is the complex channel tap from its associated BS b to the cell-center TU t such that $b = t$, $\tilde{h}_{b',t}$ and $\tilde{h}_{b'',t}$ are the complex channel tap from non-associated BS b' and b'', respectively, to the cell-center TU t such that $b' \neq t$ and $b'' \neq t$, and $\sigma_t \sim \mathcal{CN}(0, \sigma_{\text{n}}^2)$ is the AWGN observed at t. ...

$$\vdots$$

$$\text{SINR}_t^{(u)} = \frac{\sum\limits_{\forall b \in \mathcal{B}} \rho_{b,u} N \left| h_{b,t} \right|^2}{\sum\limits_{\forall b \in \mathcal{B}} \rho_b N \left| h_{b,t} \right|^2 + \sum\limits_{\forall b'' \in \mathcal{I}} N \left| h_{b'',t} \right|^2 + 1}. \qquad (14)$$

$$\vdots$$

$$\text{SINR}_t = \frac{\rho_b N \left| h_{b,t} \right|^2}{\sum\limits_{\forall b' \in \mathcal{B} \setminus b} \rho_{b'} N \left| h_{b',t} \right|^2 + \sum\limits_{\forall b'' \in \mathcal{I}} N \left| h_{b'',t} \right|^2 + 1}. \qquad (15)$$

Section III, page 5,

where $\boldsymbol{\rho_{b,u}} = [\rho_{1,u}, \ldots, \rho_{B,u}]^T$ and $\boldsymbol{\rho_b} = [\rho_1, \ldots, \rho_B]^T$. ...

Section III, page 6,

Problem (17) is a non-convex optimization problem due to (17a), (17b), and (17c). ...

Section III, page 6-7,

Using proposition 2, (17) is then reduced to the following problem:

⋮

(Due to its lengthy discussion, we kindly refer the reviewer to the revised manuscript.)

⋮

Since (26) is a convex optimization problem, it can be solved efficiently [52].

Section V, page 11-13, Figs. 5-8.

(As there are many figures, we kindly refer the reviewer to the revised manuscript.)

Section V-F, page 13,

... In particular, the proposed ATN-NOMA scheme achieves an average of 91% and 52% sum-rate improvement as compared to schemes based on OMA and FNOMA, respectively. As compared to TN-NOMA, the sum-rate improvement is marginal although the AU gain is 30-60 dB higher than the cell-edge TU. ...

Specifically, the outage probability of TN-NOMA is 2.5×10^{-3} whereas the outage probability of the proposed ATN-NOMA scheme is 6.25×10^{-8} to 7.3×10^{-17}. ...

Section VI, page 13,

... The optimal beamwidth was then obtained in closed-form expression while the optimal power allocation was obtained via SCA. ...

[L1] 3rd Generation Partnership Project, "Study on supporting Unmanned Aerial Systems (UAS) connectivity, identification and tracking", TR. 23.754-Release 17, March 2021.

[L2] 3rd Generation Partnership Project, "Study on application layer support for Unmanned Aerial Systems (UAS)", TR. 23.755-Release 17, April 2021.

[L3] G. Ding, Q. Wu, L. Zhang, Y. Lin, T. A. Tsiftsis, and Y. Yao. An Amateur Drone Surveillance System Based on the Cognitive Internet of Things. IEEE Communications Magazine, 56(1):29–35, Jan 2018.

[L4] C. Laoudias, A. Moreira, S. Kim, S. Lee, L. Wirola, and C. Fischione. A Survey of Enabling Technologies for Network Localization, Tracking, and Navigation. IEEE Communications Surveys Tutorials, 20(4):3607– 3644, Fourthquarter 2018.

[L5] Will Hedgecock, Miklos Maroti, Janos Sallai, Peter Volgyesi, and Akos Ledeczi. High-Accuracy Differential Tracking of Low-cost GPS Receivers. In Proceedings of the 11th Annual International Conference on Mobile Systems, Applications, and Services, ACM MobiSys '13, pages 221– 234, New York, NY, USA, 2013.

Comment 2:

"Two type of users, AUs and TUs, with different QoS requirements are investigated. TUs perform SIC algorithm to boost the NOMA gain. On the other hand, AU, which has more stringent QoS requirement, does not apply any advanced receiving techniques as observed by equations (10)~(12). More justification about the system design and assumption should be explained."

Response 2:

By advanced receiving technique, we suppose the reviewer is referring to SIC. In this case, it is not promising for AU to apply SIC. For ease of exposition, let us refer to the co-channel interference induced by superposition coding as NOMA interference. In a downlink single-input-single-output NOMA system, it is well-known that weaker users should treat the NOMA interference as noise and stronger users should perform SIC. This strategy is optimal in terms of rate region [35]. Nevertheless, this principle cannot be directly extended to network NOMA due to non-degraded channel and interference channel (i.e., ICI).

To see this, let's consider a network NOMA system with B coordinated BSs. In some cases, the AU might have a stronger channel gain than k cell-center TUs and a weaker channel gain than $(B-k)$ cell-center TUs, where $0<k<B$. Since AU is a CoMP user (or a common user) among the B coordinated BSs, the AU cannot simultaneously treat the NOMA interference as noise and perform SIC. More precisely, the AU can only treat the NOMA interference as noise or perform SIC.

In this paper, we choose the former. To understand the underlying reason, let's again consider a network NOMA with B coordinated BSs. Let us further assume that the cell-center TUs treat the NOMA interference as noise and the AU performs SIC (i.e., the reverse SIC order). Since

the cell-center TUs treat the NOMA interference as noise, the rate of the cell-center TUs is:

$$R_t = B_{\mathrm{w}} \log \left(1 + \frac{\rho_b N \left| h_{b,t} \right|^2}{\rho_{b,u} N \left| h_{b,t} \right|^2 + \sum\limits_{\forall b' \in \mathcal{B} \setminus b} N \left| h_{b',t} \right|^2 + K_t} \right), \tag{R.6}$$

where $b = t$ and $K_t = \sum\limits_{\forall b'' \in \mathcal{I}} N \left| h_{b'',t} \right|^2 + 1$.

Since AU performs SIC, it has to independently remove each of the cell-center TUs' messages before decoding its own message. Note that the messages of cell-center TUs belong to different coordinated BSs. Thus, the ICI between cell-center TUs' messages cannot be cancelled at the AU via SIC. Consequently, the SINR of AU decoding the cell-center TU t's message is:

$$R_u^{(t)} = B_{\mathrm{w}} \log \left(1 + \frac{\rho_b N \left| h_{b,u}^{\upsilon} \left(\Psi \right) \right|^2}{\rho_{b,u} N \left| h_{b,u}^{\upsilon} \left(\Psi \right) \right|^2 + \sum\limits_{\forall b' \in \mathcal{B} \setminus b} N \left| h_{b',u}^{\upsilon} \left(\Psi \right) \right|^2 + K_u} \right), \tag{R.7}$$

where $b = t$ and $K_u = \sum\limits_{\forall b'' \in \mathcal{I}} N \left| h_{b'',u}^{\upsilon} \left(\Psi \right) \right|^2 + 1$. After successfully removing all the cell-center TUs' messages (i.e., a successful SIC), the AU then decodes its own message with the following SINR:

$$R_u = B_{\mathrm{w}} \log \left(1 + \frac{\sum\limits_{\forall b \in \mathcal{B}} \rho_{b,u} N \left| h_{b,u}^{\upsilon} \left(\Psi \right) \right|^2}{K_u} \right). \tag{R.8}$$

The AU's QoS requirement is satisfied if and only if:

$$\sum_{\forall b \in \mathcal{B}} \rho_{b,u} N \left| h_{b,u}^{\upsilon} \left(\Psi \right) \right|^2 \geq \left(2^{\frac{R_{\min}}{B_{\mathrm{w}}}} - 1 \right) K_u, \tag{R.9}$$

which is very promising. Nevertheless, to ensure a successful SIC (i.e., R.8), (R.7) must be greater than or equal to (R.6) for $\forall t$. Simplifying the inequality, we have:

$$\frac{\left| h_{b,u}^{\upsilon} \left(\Psi \right) \right|^2}{\sum\limits_{\forall b' \in \mathcal{B} \setminus b} N \left| h_{b',u}^{\upsilon} \left(\Psi \right) \right|^2 + K_u} \geq \frac{\left| h_{b,t} \right|^2}{\sum\limits_{\forall b' \in \mathcal{B} \setminus b} N \left| h_{b',t} \right|^2 + K_t}, \text{for } \forall t, \tag{R.10}$$

In aerial-terrestrial networks, $\left| h_{b,u}^{\upsilon} \left(\Psi \right) \right|^2$ is usually greater than $\left| h_{b,t} \right|^2$. Nevertheless, the ICI of AU is also much stronger than that of TU. Thus, we often have:

$$\left(\sum_{\forall b' \in \mathcal{B} \setminus b} N \left| h_{b',u}^{\upsilon} \left(\Psi \right) \right|^2 + K_u \right) \gg \left(\sum_{\forall b' \in \mathcal{B} \setminus b} N \left| h_{b',t} \right|^2 + K_t \right).$$

This is true even in cases where $K_u = 1$. Consequently, it is very hard to satisfy (R.10).

As the AU's SIC might not be successful at all times, the reliable communications to the AU cannot be guaranteed. To address this limitation, we therefore assume that the AU treats NOMA interference as noise and the cell-center TUs perform SIC. Using this SIC order, the reliable communications to the AU is always guaranteed unless outage occurs. Interestingly, the outage probability of our proposed scheme is extremely low. To clarify our assumption, we added a footnote in the revised manuscript as follows:

> Section II, page 5, footnote 3,
>
> The reverse SIC order, where the AU performs SIC and cell-center TUs treat AU's message as noise, has been considered. Nevertheless, such a SIC order is not promising in ATN-NOMA because the SIC at the AU might fail due to strong ICI. To ensure reliable communications to the AU, we assume the AU treats cell-center TUs' messages as noise and the cell-center TUs perform SIC.

Comment 3:

"Besides, it requires some clarification for "CoMP user" and "non-CoMP user" as defined in line 16 in page 2. For me, CoMP is a transmission scheme/technology involving coordination between BSs, pairing of users, BSs transmission and UE reception and processing. If two UEs are paired together, both of them are "CoMP Users". Some of the CoMP users may not perform advanced receiving algorithm (for example, SIC receiving). "non-CoMP user" refer to the user that is served by BS with single user transmission. non-CoMP user has no information about the appearance and/or statistics of the interference."

Response 3:

We understand the reviewer's definitions, however, the definitions of the CoMP and non-CoMP users are a little different in the literature of network NOMA. In NOMA, each BS has the capability to pair multiple users over an orthogonal RB in a single cell. Thus, each BS might pair a non-CoMP user and a CoMP user over the same RB using NOMA. In network NOMA, the non-CoMP user is referred to as a user who is independently served by its associated BS only, and the CoMP user is referred to as a user who is jointly served by a set of coordinated BSs. These definitions were introduced in [27, 29]. Based on the reviewer's comment, we revised Fig. 1 to provide better clarity. The definitions of the CoMP and non-CoMP users can be seen

in Fig. 1(b). Below is a copy of the amendment.

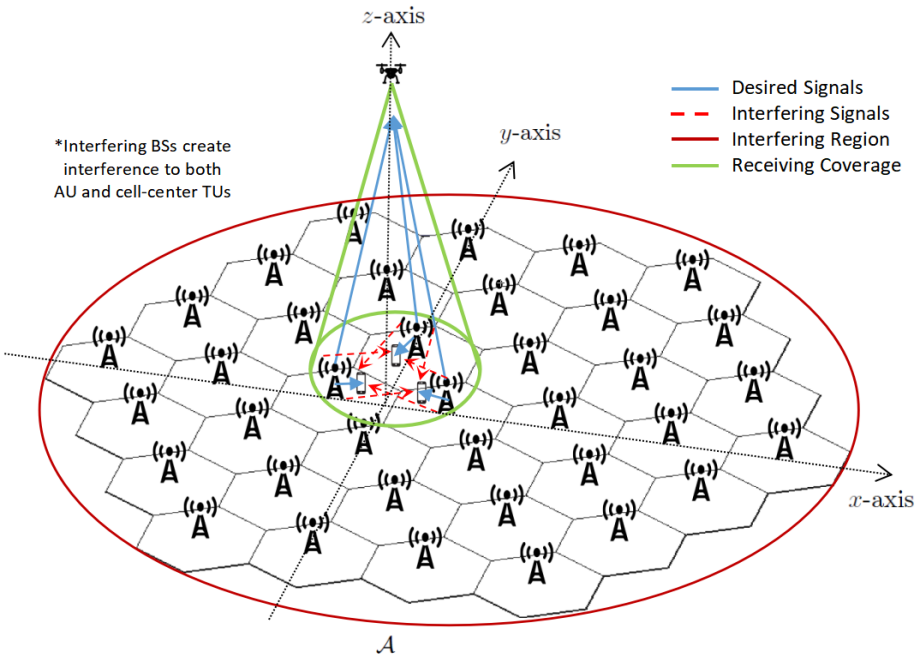

(d)

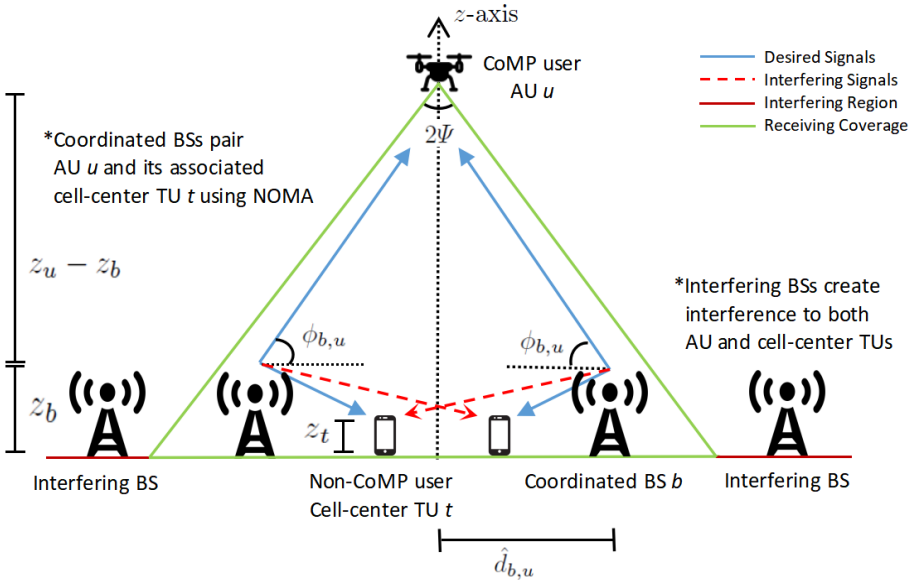

(e)

Figure 1: A schematic of downlink multi-cell networks with AU and TUs: (a) 3-dimensional; (b) 2-dimensional.

Aerial-Terrestrial Network NOMA for Cellular-Connected UAVs

Wee Kiat New, *Student Member*, IEEE, Chee Yen Leow, *Member*, IEEE, Keivan Navaie, *Senior Member*, IEEE, and Zhiguo Ding, *Fellow*, IEEE.

***Abstract*—Efficient connectivity in cellular-connected unmanned aerial vehicles (UAV)s is limited by scarcity of the radio spectrum and strong inter-cell interference (ICI). To address these issues, we propose an aerial-terrestrial network non-orthogonal multiple access (ATN-NOMA) scheme. In this proposed scheme, we pair the aerial user (AU) and terrestrial user (TU) in a NOMA setting to leverage their asymmetric channel gains and rate demands in downlink communications. In ATN-NOMA, the strong ICI issue at the AU receiver is further managed by an elevation-angle based user association, equipping the AU with an adjustable beamwidth directional antenna, and forming a beamforming among the coordinated terrestrial base stations (BS)s. We then obtain the optimal beamwidth and power allocation so that the TUs' sum-rate is maximized subject to the AU's Quality-of-Service (QoS) requirement. The corresponding optimization problem is non-convex in which we exploit the structure of the problem and apply successive convex approximation (SCA) to obtain a local optimal solution. We then derive the statistical properties, which consequently enable us to estimate the aggregated ICI. In cases where no interfering BSs have the same elevation angle as the coordinated BSs, we further approximate the AU's outage probability. We then compare the TUs' sum-rate and the outage probability of the ATN-NOMA with multiple existing schemes. Extensive simulation results show that our proposed ATN-NOMA scheme outperforms existing schemes by 52-91% in terms of the sum-rate, and its analytical outage probability can be as low as the order of 10^{-17}. Furthermore, we show that the pairing of AU and TU in multi-cell networks remains beneficial, subject to effective mitigation of ICI.**

***Index Terms*—Non-Orthogonal Multiple Access, Cellular-Connected UAV, Coordinated Multi-Point Transmission, Inter-cell Interference**

I. Introduction

Unmanned aerial vehicles (UAV)s have emerged as promising tools in civil applications such as agriculture, construction, delivery, inspection, and surveillance [2]. Serving UAVs as aerial users (AU)s in the existing cellular networks enables beyond visual line-of-sight operation. Such idea is referred to as cellular-connected UAVs [3], [4]. Field trials and simulation studies have been conducted to verify the feasibility of cellular-connected UAVs in 4th generation (4G) [5] and 5th generation (5G) cellular networks [6]. Preliminary results show that the idea is feasible.

Co-existence of AUs and terrestrial users (TU)s, however, introduces new challenges to the operation of cellular networks. One of the key issues is strong inter-cell interference (ICI) at the AUs. In general, AUs that are hovering at a high altitude establish line-of-sight (LOS) links with their associated terrestrial base stations (BS)s. Nevertheless, as analyzed in [7]–[10], AUs also establish LOS links with other terrestrial BSs. This causes strong ICI at the AUs, where other terrestrial BSs transmit to their associated users via the same resource block (RB). Due to high altitudes and LOS links, the ICI at the AUs is much stronger than that of the TUs located at the cell-edge.

To address this issue, [11], [12] have examined the applications of the conventional interference mitigation techniques, such as antenna beam selection and coordinated multi-point (CoMP) transmission. To ensure a reliable cell-acquisition for the AUs, [13] exploits the coverage extension feature of long-term evolution networks, which can achieve a higher maximum coupling loss and alleviate the ICI. Similarly, [14] shows that the coverage extension feature can better support the mobility of the AUs. Nevertheless, severe ICI issue remains unsolved by these conventional techniques.

In [15], the use of a tilted directional antenna with a fixed beamwidth is explored, and furthermore [16] proposes a new cooperative beamforming and interference cancellation (CB-ITC) technique. Nevertheless, the use of a tilted antenna with fixed beamwidth is only beneficial for a low or intermediate network density [15]. Moreover, CB-ITC can only be employed for low user density [16]. Different types of aerial-ground interference mitigation techniques are also compared in [17] for evaluation purpose. Many works (e.g., [7]–[17]) focus on orthogonal multiple access (OMA) to support both AUs and TUs. Although OMA avoids multi-user interference in a single-cell network, its spectral efficiency and number of concurrent connections are fundamentally limited as each orthogonal RB can only be assigned to a single user.

To overcome these limitations, non-orthogonal multiple access (NOMA) has been proposed for beyond 5th generation cellular networks [18]–[20]. By leveraging superposition coding (SC) at the transmitter and successive interference cancellation (SIC) at the receiver, NOMA allows multiple users to share the same RB. With the same amount of

This work was supported in part by the Ministry of Higher Education Malaysia and Universiti Teknologi Malaysia under Grant 4J416, Grant 08G83, Grant 19H58, and Grant 04G37, Grant 09G15, and Grant 00L27. Part of this paper has been presented in IEEE VTC2020-Fall [1].
Wee Kiat New (email: weekiat@graduate.utm.my) and Chee Yen Leow (email: bruceleow@fke.utm.my) are with the Wireless Communication Centre, School of Electrical Engineering, Faculty of Engineering, Universiti Teknologi Malaysia, 81310 Skudai, Johor, Malaysia; Keivan Navaie (e-mail: k.navaie@lancaster.ac.uk) is with the School of Computing and Communications, Lancaster University, Lancaster, LA1 4WA, United Kingdom; Zhiguo Ding (e-mail: zhiguo.ding@manchester.ac.uk) is with the School of Electrical and Electronic Engineering, the University of Manchester, Manchester, M13 9PL, United Kingdom.

radio resources, NOMA enhances the spectral efficiency and enables massive connectivity. Nevertheless, using NOMA in multi-cell networks is also challenged by the ICI problem, i.e., mainly for the cell-edge users. There are several promising solutions to this problem. For instance, [21] proposes an optimal coefficient and power allocation in a multi-cell NOMA system. It is further shown in [21] that utilization of power control technique is sufficient to reduce the ICI level resulting in outperforming an equivalent OMA system.

Several efficient coordinated multi-point (CoMP) techniques have also been proposed to enhance the NOMA performance in multi-cell networks [22]. For example, [23], [24] have proposed coordinated scheduling (CS)-NOMA to mitigate the ICI of the cell-edge users. To further improve the spectral efficiency, [25], [26] have proposed coordinated beamforming (CB)-NOMA to eliminate the ICI of the cell-edge users via precoding. CB-NOMA is, however, not applicable to all scenarios because the dimension of the user channels may be different, e.g., the cell-edge user experiences multiple channels from neighboring cell while a cell-center user experiences a single channel from its serving cell [27].

To address this issue, joint transmission (JT)-NOMA, also known as network NOMA [28], has been proposed. In network NOMA, each coordinated BS pairs a non-CoMP user and a CoMP user over the same RB. The non-CoMP user is referred to as a user who is independently served by its associated BS and the CoMP user is referred to as a user who is jointly served by a set of coordinated BSs [27], [29]. In [28], the analytical outage probability of network NOMA with fixed power allocation is derived and in [29], a distributed power allocation that maximizes the users' sum-rate is investigated. Later, an opportunistic network NOMA is proposed, where some users are served by network NOMA and some are served by basic NOMA [30]. Nevertheless, [21]–[30] do not consider the co-existence of AUs and TUs, and, therefore, strong ICI issue at the AUs in the multi-cell NOMA networks remains to be addressed.

Some existing studies on NOMA-enabled UAV communications have been conducted in recent years. On the one hand, existing works (e.g., [31]–[34]) have considered the applications of aerial base stations. On the other hand, existing works have focused on the applications of AUs. Pertaining to the latter, [35] has proposed a robust NOMA scheme to serve AUs and TUs for control and data links, respectively, and [36] has derived the outage probability and finite SINR diversity gain where multiple AUs are served by a terrestrial BS. Nevertheless, the ICI issue at the AUs is not considered in [35], [36]. Besides, [37] has proposed an optimal trajectory and user association that minimizes the AU's mission completion time. In [37], the ICI of AU is considered but no ICI mitigation technique is proposed.

Mitigating strong ICI of the AUs is a very challenging problem [38]. Several mechanisms need to be carefully designed. In particular, [39] shows that the AUs' user association plays an important role in determining the AUs' performance. [40] shows that using directional antenna with fixed beamwidth at the AUs leads to a tradeoff between the coverage and the ICI level. Also, [41] shows that the use of beamforming improves the performance of the AUs. Besides, [42] verifies that efficient usage of NOMA for aerial-terrestrial multi-cell networks requires a combination of an appropriate user association, receive antenna, and interference mitigation technique.

Due to the aforementioned motivations, we propose an aerial-terrestrial network NOMA (ATN-NOMA) scheme. In this scheme, we propose an elevation-angle based user association for the AUs. Specifically, the AUs are associated to a set of coordinated BSs that have the largest elevation angle to the AUs. This enables the AUs to have a higher probability of experiencing LOS to the coordinated BSs, and a lower probability of LOS with the interfering BSs. Inspired by [43], [44], we then propose the use of a directional antenna with adjustable beamwidth at the AU receivers. The use of a directional antenna with adjustable beamwidth has been applied in various applications such as satellite communication and remote sensing. There are at least two antenna designs to enable adjustable beamwidth such as the re-configurable parasitic element [45] or switchable partially reflective surface [46] that are placed in the vicinity of a single antenna source. In addition, we propose employing network NOMA, so that beamforming can be used as an extra tool to tackle the severe ICI at the AUs. As shown later in this paper, these combinations can result in zero ICI of the AUs with limited number of coordinated BSs.

In this paper, we consider the downlink multi-cell networks with the co-existence of an AU and TUs. We assume that the coordinated BSs are simultaneously serving the AU as well as their own associated TUs via NOMA. The objective of the proposed ATN-NOMA scheme is subject to efficient TUs' sum-rate and while AU's reliable connectivity is emphasized. Since the control link is directly related to the safe operation of the UAV, a corresponding QoS requirement is imposed. We then investigate the maximum sum-rate of the TUs subject to AU's QoS requirement. The major contributions of this paper are summarized as follows.

- We propose a novel ATN-NOMA scheme for the co-existence of AUs and TUs. Specifically, we pair the AU and TU in a NOMA setting to leverage their asymmetric channel and rate demand characteristics. In our proposed scheme, we employ the elevation-angle based user association, the use of a directional antenna with adjustable beamwidth at the AU, and network NOMA to address the strong ICI issue at the AU.
- We then formulate an optimization problem to maximize the sum-rate of the TUs by optimal beamwidth and power allocation subject to the AU's QoS requirement. A local optimal solution is also obtained for the non-convex optimization problem by exploiting the structure of the problem and applying successive convex approximation (SCA).
- By leveraging the unique properties of the proposed scheme and the statistical channel state information (CSI), we derive the probability density function (pdf) and cumulative distribution function (CDF) of the aggregated ICI experienced at the AU. Deriving the statistical properties is a challenging task because the aggregated ICI is generally the sum of independent non-identical

gamma random variables conditioned by the number of LOS/NLOS links. Utilizing the derived statistical properties, the aggregated ICI at the AU can be estimated reliably.

- Based on the techniques we have developed, we further outline a criterion where AU experiences zero ICI. Specifically, AU experiences zero ICI when there are no interfering BSs having the same elevation angle as the coordinated BSs. In such cases, we further approximate the AU's outage probability. This analytical result helps to verify the superiority of the proposed ATN-NOMA scheme in terms of outage probability, and confirms that the proposed ATN-NOMA scheme is able to support reliable communications for the AU's links.
- Extensive simulation results with different network parameters and settings are presented. Our simulation results provide quantitative insights on the effects of AU's interference, and also reveal the key factors that determine the performance of our proposed scheme at a fundamental level.

We note that this paper is a substantial extension of our previous work [1]. In this paper, we further consider the ICI of the TUs. By exploiting the structure of the problem and applying SCA, we also obtain a local optimal solution of the corresponding non-convex optimization problem. Besides, this paper considers an elevation-angle based user association, which subsequently allows us to outline the criterion where AU experiences zero ICI. Furthermore, the statistical properties of the aggregated ICI are derived and the AU's outage probability is approximated. Extensive simulation results over various network parameters and settings are also presented. In addition, in this paper, we demonstrate that the pairing of AU and TU in multi-cell networks remains beneficial as compared to the pairing of TU and TU, subject to effective mitigation of ICI.

The rest of the paper is organized as follows: Section II details the system model and the proposed scheme, and Section III presents the solution to maximize the sum-rate of the TUs subject to the AU's QoS requirement. Section IV then presents the statistical properties of the aggregated ICI in the proposed scheme as well as the analytical outage probability. The simulation results are provided in Section V followed by the conclusion drawn in Section VI.

Notations: In this paper, scalar parameters/variables are denoted by italic letters (e.g., c), vectors are denoted by boldface letters (e.g., $\boldsymbol{c}$), and card(C) denotes the cardinality of set C. Besides, $c \sim \text{Gamma}(m, \theta)$ denotes that c is a gamma distributed random variable with rate, m, and scale, θ, while $c \sim \text{Bino}(n, p)$ denotes that c is a binomial distributed random variable with n trials and probability of p. Furthermore, $\|\cdot\|$ denotes Euclidean norm, $\log(\cdot)$ denotes logarithm with base 2, $(\cdot)^T$ denotes transpose, and $(\cdot)^H$ denotes conjugate transpose.

II. System Model and The Proposed Scheme

As shown in Fig. 1, we consider a downlink wireless communication system with multiple terrestrial BSs in a subregion, $\mathcal{A}$. In this paper, we focus on the performance of a

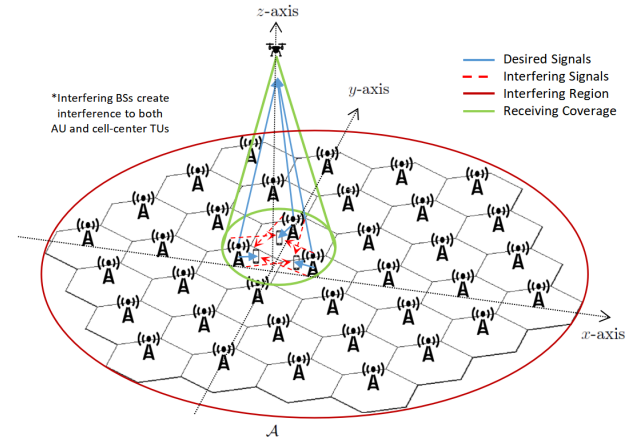

(a)

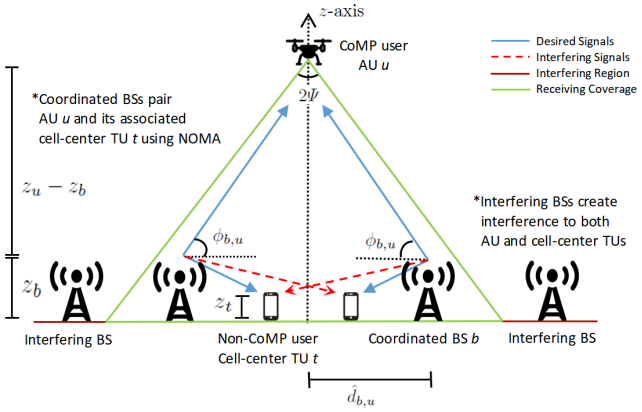

(b)

Figure 1: A schematic of downlink multi-cell networks with AU and TUs: (a) 3-dimensional; (b) 2-dimensional.

set of non-CoMP users and a CoMP user over an orthogonal RB as in [27], [28], [47], [48]. In our proposed scheme, the non-CoMP users are the cell-center TUs who are not significantly affected by ICI, and the CoMP user is the AU who suffers strong ICI. No cell-edge TU is considered in our proposed scheme.

Similar to existing network NOMA schemes, our proposed scheme can be used to serve multiple CoMP users (e.g., AUs) and non-CoMP users (e.g., cell-center TUs) by using a multi-carrier NOMA system. Specifically, a CoMP user and multiple non-CoMP users can be paired over a single orthogonal RB. Different pairs of CoMP users and non-CoMP users can then be served by using different orthogonal RBs.

We denote the subscript, u, as the AU, $t \in \mathcal{T} = \{1, \ldots, T\}$, as the associated cell-center TUs, $b \in \mathcal{B} = \{1, \ldots, B\}$, as the coordinated terrestrial BSs with $T = B > 1$, and $\mathcal{I} = \{B+1, B+2, \ldots, I\}$, as the set of interfering terrestrial BSs. The cell-centered TUs are TUs not located near to the cell-edge, and the interfering BSs are non-coordinated terrestrial BSs that transmit to their own users via the same RB. For brevity, we assume a fixed card$(\mathcal{B})$.

According to [16], [49], we assume that the locations of the terrestrial BSs are distributed according to the hexagonal

cellular structure with a radius of r_0 and a height of z_b within a subregion $\mathcal{A}$. The locations of the associated cell-center TUs are uniformly distributed around their associated BS with a maximum distance of $\frac{r_0}{2}$ and a fixed height of z_t.

Without loss of generality, we assume that the cell-center TU, $t \in \mathcal{T}$, is associated to the BS, $b \in \mathcal{B}$, if $t = b$, and the cell-center TU, $t \in \mathcal{T}$, is not associated to the BS, $b \in \mathcal{B}$, if $t \neq b$. We denote $\boldsymbol{w}^{\text{AU}} = [x_u, y_u, z_u]^T$, $\boldsymbol{w}_t^{\text{TU}} = \left[x_t^{\text{TU}}, y_t^{\text{TU}}, z_t^{\text{TU}}\right]^T$, and $\boldsymbol{w}_b^{\mathbf{BS}} = \left[x_b^{\mathbf{BS}}, y_b^{\mathbf{BS}}, z_b^{\mathbf{BS}}\right]^T$ as the 3D location of the AU, TU t, and BS b, respectively. The Euclidean distance between TU t and BS b is:

$$d_{b,t} = \left\| \boldsymbol{w}_t^{\text{TU}} - \boldsymbol{w}_b^{\text{BS}} \right\|, \tag{1}$$

and the Euclidean distance between the AU and BS b is:

$$d_{b,u} = \left\| \boldsymbol{w}^{\text{AU}} - \boldsymbol{w}_b^{\text{BS}} \right\|. \tag{2}$$

Let $\hat{\boldsymbol{w}}_b^{\text{BS}} \triangleq \left[x_b^{\text{BS}}, y_b^{\text{BS}}\right]^T$ and $\hat{\boldsymbol{w}}^{\text{AU}} \triangleq [x_u, y_u]^T$ be the 2D coordinates of the BS b and AU, respectively. We then denote the horizontal distance between AU and BS b as $\hat{d}_{b,u} = \left\| \hat{\boldsymbol{w}}^{\text{AU}} - \hat{\boldsymbol{w}}_b^{\text{BS}} \right\|$.

A. Aerial-Terrestrial Channel Model

According to [15], [50], the aerial communication link between the AU and the BS b follows the probabilistic LOS/NLOS model. Denote $\upsilon \in \{\text{L}, \text{N}\}$ as the types of links, where, L, and, N, represent the LOS and NLOS links, respectively. The probability of LOS between the AU and BS b is:

$$p_{b,u}^{\text{L}}\left(\hat{d}_{b,u}, z_u\right) = -\varphi \cdot \exp\left(-\xi \cdot \phi_{b,u}\right) + \zeta, \tag{3}$$

where $\phi_{b,u}$ is the elevation angle between the AU and BS b. In (3), φ, ξ, and ζ are constant coefficients related to the communication environment [50]. The probability of NLOS between the AU and BS b is $p_{b,u}^{\text{N}}\left(\hat{d}_{b,u}, z_u\right) = 1 - p_{b,u}^{\text{L}}\left(\hat{d}_{b,u}, z_u\right)$.

Given link type, υ, the channel gain between the AU and BS b is:

$$\left|h_{b,u}^{\upsilon}(\Psi)\right|^2 = \Xi_{b,u}^{\upsilon}(\Psi)\left|\Omega_{b,u}^{\upsilon}\right|^2, \upsilon \in \{\text{L}, \text{N}\}, \tag{4}$$

where $\Xi_{b,u}^{\upsilon}(\Psi) \triangleq \frac{E_u F G_u^{\text{rx}}(\Psi)}{{d_{b,u}}^{\alpha_\upsilon}}$, and $\left|\Omega_{b,u}^{\upsilon}\right|^2$ are the large and small-scale fading effects, respectively. In large-scale fading, $\Xi_{b,u}^{\upsilon}(\Psi)$, E_u is the BS's side lobe antenna gain, $F = \left(\frac{4\pi f_c}{c}\right)^{-2}$ is the attenuation loss at the operating frequency f_c, $G_u^{\text{rx}}(\Psi)$ is the receiving antenna gain at the AU with a beamwidth Ψ, and α_υ denotes the aerial pathloss exponents. In (4), $\left|\Omega_{b,u}^{\upsilon}\right|^2 \sim \text{Gamma}\left(m_u^{\upsilon}, \theta_u^{\upsilon}\right)$.

The channel gain between the TU t and BS b is:

$$|h_{b,t}|^2 = \Xi_{b,t}|\Omega_{b,t}|^2. \tag{5}$$

In (5), $\Xi_{b,t} \triangleq \frac{E_t F G_t^{\text{rx}}}{{d_{b,t}}^{\alpha}}$, and $|\Omega_{b,t}|^2$ are the large and small-scale fading effects, respectively. In the large-scale fading effect, $\Xi_{b,t}$, E_t is the BS's main lobe antenna gain, G_t^{rx} is the receiving antenna gain at the TU t, and α is the terrestrial pathloss exponent. Moreover, $|\Omega_{b,t}|^2 \sim \text{Gamma}\left(m_{\text{t}}, \theta_{\text{t}}\right)$. We assume that the TUs are equipped with omni-directional antenna and thus $G_t^{\text{rx}} = 1, \forall t$. In practice, we have $\alpha \geq \alpha_{\text{N}} \geq \alpha_{\text{L}}$, and $m_u^{\text{L}} \geq m_u^{\text{N}} \geq m_t$.

B. ATN-NOMA: Elevation-Angle Based User Association

The proposed ATN-NOMA scheme consists of three mechanisms: user association, receiving, and transmitting strategies. To enable AU to have a higher probability of LOS with the coordinated BSs, $b \in \mathcal{B}$, and a lower probability of LOS with the interfering BSs, $b \in \mathcal{I}$, we propose an elevation-angle based user association. The elevation angle between the AU and BS b is $\phi_{b,u} = \tan^{-1}\left(\frac{z_u - z_b}{\hat{d}_{b,u}}\right)$. In the elevation-angle based user association, the AU is served by the terrestrial BSs that have the B largest elevation-angle, so that:

$$\phi_{b,u} \geq \phi_{b'',u}, \quad \forall b \in \mathcal{B}, \forall b'' \in \mathcal{I}. \tag{6}$$

As seen later in this paper, the property in (6) is very useful in characterizing the ICI.

C. ATN-NOMA: Transmitting and Receiving Strategies

Based on the unique characteristics of the aerial-terrestrial networks, we design efficient receiving and transmitting strategies. In this scheme, a single directional antenna with adjustable beamwidth is implemented at the AU. The antenna is pointing directly below the AU (i.e., $\hat{\boldsymbol{w}}^{\text{AU}}$). We denote ψ_u^{a} and ψ_u^{e} as the azimuth and elevation angles at the AU, respectively. The azimuth and elevation half-power beamwidth are assumed equal and they are denoted by 2Ψ, where $\Psi \in \left(0, \frac{\pi}{2}\right)$. According to [51], (eq. 2.2-2.51), the antenna gain in the direction of $(\psi_u^{\text{a}}, \psi_u^{\text{e}})$ is:

$$G_u^{\text{rx}}(\Psi) = \begin{cases} \frac{G_{\text{ref}}}{\Psi^2}, & \text{if } 0 \leq \psi_u^{\text{a}} \leq \Psi, 0 \leq \psi_u^{\text{e}} \leq \Psi, \\ G_0 \approx 0, & \text{otherwise}, \end{cases} \tag{7}$$

where $G_{\text{ref}} \approx 2.2856$, and G_0 denotes the antenna gain outside the beamwidth of the directional antenna[1]. For any given $\boldsymbol{w}^{\text{AU}}$, the receiving coverage of the AU is:

$$\mathcal{K}(\Psi) = \left\{ \boldsymbol{w}_k \;\middle|\; \begin{array}{c} x = (z_u - c_u)\tan\Psi\cos\psi, \\ y = (z_u - c_u)\tan\Psi\sin\psi, \\ z = c_u\,,\; c_u \in [0, z_u]\,, \psi \in [0, 2\pi)\,, \end{array} \right\}, \tag{8}$$

where $\boldsymbol{w}_k = [x + x_u, y + y_u, z]^T$, $\mathcal{K}(\Psi)$ is a cone, $\boldsymbol{w}^{\text{AU}}$ is the apex of the cone, $z_u \tan\Psi$ is the radius of the cone base, and z_u is the height of the cone (see, Fig. 2).

In addition, we adopt network NOMA that is promising to the pairing of cell-center TUs and AU. In the context of ATN-NOMA, each coordinated BS, $b \in \mathcal{B}$, pairs its associated cell-center TU t (i.e., the non-CoMP user) and the AU (i.e., the CoMP user) over the same RB. In each cell, the pairing consists of only two users to ensure low co-channel interference, hardware complexity, and processing delay [35]. Due to the high-altitude, the AU is a common user among the coordinated BSs. Hence, each coordinated terrestrial BS,

[1]Similar to [15], [42]–[44], for brevity, we assume $G_o = 0$.

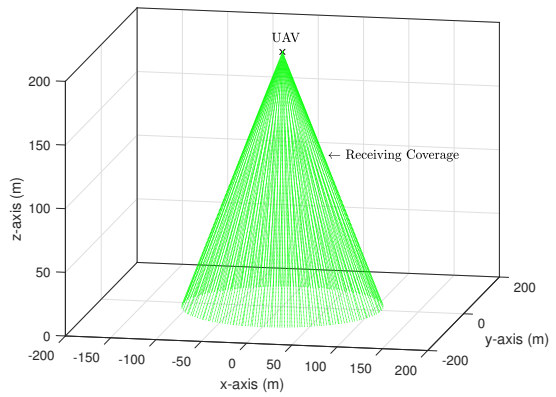

Figure 2: The AU receiving coverage, for $\boldsymbol{w}^{\mathrm{AU}} = [0, 0, 200]^T$, $\Psi = 0.5$.

$b \in \mathcal{B}$, transmits the following signal to jointly form maximum ratio transmission (MRT) beamforming to the AU[2]:

$$\tilde{S}_b = \frac{h^{\upsilon}_{b,u}(\Psi)}{\left\|\boldsymbol{h}^{\upsilon}_{\boldsymbol{b,u}}(\boldsymbol{\Psi})\right\|}\sqrt{\rho_{b,u}P_{\mathrm{tx}}}s_u + \frac{h^{\upsilon}_{b,u}(\Psi)}{\left\|\boldsymbol{h}^{\upsilon}_{\boldsymbol{b,u}}(\boldsymbol{\Psi})\right\|}\sqrt{\rho_b P_{\mathrm{tx}}}s_b, \quad (9)$$

where $\boldsymbol{h}^{\upsilon}_{\boldsymbol{b,u}}(\boldsymbol{\Psi}) = \left[h^{\upsilon}_{1,u}(\Psi), \ldots, h^{\upsilon}_{B,u}(\Psi)\right]$ is the complex channel vector among the coordinated BS $b \in \mathcal{B}$, $h^{\upsilon}_{b,u}(\Psi)$ is the complex channel tap between BS b and the AU, $\frac{h^{\upsilon}_{b,u}(\Psi)}{\left\|\boldsymbol{h}^{\upsilon}_{\boldsymbol{b,u}}(\boldsymbol{\Psi})\right\|}$ is the beamforming phase from the BS b to the AU and P_{tx} is the total transmit power at the BS. Note that, the cell-center TU t is associated to the BS b if $t = b$. Furthermore, s_u and s_b are random signals intended for AU and the associated cell-center TU b, respectively, with $\mathbb{E}\left[|s_u|^2\right] = \mathbb{E}\left[|s_b|^2\right] = 1$. Besides, $\rho_{b,u}$ and ρ_b are the power coefficients assigned to AU and the associated cell-center TU b, respectively, where $\rho_{b,u} + \rho_b \leq 1$.

Unlike terrestrial cell-edge user, AU experiences strong ICI from other BSs due to its high altitude. The received signal at the AU is:

$$y^{\mathrm{rx}}_u = \sum_{\forall b \in \mathcal{B}} h^{\upsilon}_{b,u}(\Psi)^H \tilde{S}_b + \underbrace{\sum_{\forall b'' \in \mathcal{I}} h^{\upsilon}_{b'',u}(\Psi)^H \tilde{S}_{b''}}_{\text{ICI term}} + \sigma_{\mathrm{u}}, \quad (10)$$

where $\sigma_u \sim \mathcal{CN}\left(0, \sigma^2_{\mathrm{n}}\right)$ is the additive white Gaussian noise (AWGN) observed at the AU and σ^2_{n} is the noise power level. In order to decode its own signal, AU has to treat $s_b, \forall b \in \mathcal{B}$, and $\tilde{S}_{b''}, \forall b'' \in \mathcal{I}$, as noise [3]. Hence, the signal-to-interference-plus-noise ratio (SINR) at the AU is:

$$\mathrm{SINR}_u = \frac{\sum\limits_{\forall b \in \mathcal{B}} \rho_{b,u} N \left|h^{\upsilon}_{b,u}(\Psi)\right|^2}{\sum\limits_{\forall b \in \mathcal{B}} \rho_b N \left|h^{\upsilon}_{b,u}(\Psi)\right|^2 + \sum\limits_{\forall b'' \in \mathcal{I}} N \left|h^{\upsilon}_{b'',u}(\Psi)\right|^2 + 1}, \quad (11)$$

where $N = \frac{P_{\mathrm{tx}}}{B_{\mathrm{w}} \cdot \sigma^2_{\mathrm{n}}}$ is the normalized transmit signal-to-noise ratio (SNR) and B_{w} is the system bandwidth. The achievable rate of AU is therefore:

$$R_u = B_{\mathrm{w}} \log\left(1 + \mathrm{SINR}_u\right). \quad (12)$$

At the terrestrial platform, the signal observed by the cell-center TU t is:

$$y^{\mathrm{rx}}_t = \tilde{h}^H_{b,t}\tilde{S}_b + \sum_{\forall b' \in \mathcal{B}\setminus b} \tilde{h}^H_{b',t}\tilde{S}_{b'} + \sum_{\forall b'' \in \mathcal{I}} \tilde{h}^H_{b'',t}\tilde{S}_{b''} + \sigma_t, \quad (13)$$

where $\tilde{h}_{b,t}$ is the complex channel tap from its associated BS b to the cell-center TU t such that $b = t$, $\tilde{h}_{b',t}$ and $\tilde{h}_{b'',t}$ are the complex channel tap from non-associated BS b' and b'', respectively, to the cell-center TU t such that $b' \neq t$ and $b'' \neq t$, and $\sigma_t \sim \mathcal{CN}\left(0, \sigma^2_{\mathrm{n}}\right)$ is the AWGN observed at t. We denote $h_{b,t} = \frac{\tilde{h}^H_{b,t} h^{\upsilon}_{b,u}(\Psi)}{\left\|\boldsymbol{h}^{\upsilon}_{\boldsymbol{b,u}}(\boldsymbol{\Psi})\right\|}$. To decode its own message, the associated cell-center TU t carries out SIC by first removing the message to AU, where:

$$\mathrm{SINR}^{(u)}_t = \frac{\sum\limits_{\forall b \in \mathcal{B}} \rho_{b,u} N \left|h_{b,t}\right|^2}{\sum\limits_{\forall b \in \mathcal{B}} \rho_b N \left|h_{b,t}\right|^2 + \sum\limits_{\forall b'' \in \mathcal{I}} N \left|h_{b'',t}\right|^2 + 1}. \quad (14)$$

Following the principle of NOMA, the associated cell-center TU t decodes its own message with the following SINR:

$$\mathrm{SINR}_t = \frac{\rho_b N \left|h_{b,t}\right|^2}{\sum\limits_{\forall b' \in \mathcal{B}\setminus b} \rho_{b'} N \left|h_{b',t}\right|^2 + \sum\limits_{\forall b'' \in \mathcal{I}} N \left|h_{b'',t}\right|^2 + 1}. \quad (15)$$

The achievable rate of TU t is therefore:

$$R_t = B_{\mathrm{w}} \log\left(1 + \mathrm{SINR}_t\right). \quad (16)$$

III. Optimal Beamwidth and Power Allocation

The objective of ATN-NOMA is to efficiently serve the TUs' link and reliably support the AU's link. For this reason, we maximize the sum-rate of the cell-center TUs by optimal beamwidth and power allocation subject to the AU's QoS requirement (i.e., reliability). The optimization problem can be formulated as follows:

$$\max_{\Psi, \boldsymbol{\rho_{b,u}}, \boldsymbol{\rho_b}} \quad \sum_{\forall b \in \mathcal{B}} R_b, \quad (17a)$$

$$\text{s.t.} \quad R_u \geq R_{\min}, \quad (17b)$$

$$B_{\mathrm{w}} \log(1 + \mathrm{SINR}^{(u)}_b) \geq R_{\min}, \forall b \in \mathcal{B}, \quad (17c)$$

$$0 \leq \rho_b\,,\ 0 \leq \rho_{b,u}, \forall b \in \mathcal{B}, \quad (17d)$$

$$\rho_b + \rho_{b,u} \leq 1, \forall b \in \mathcal{B}, \quad (17e)$$

$$\boldsymbol{w}^{\mathrm{BS}}_b \subseteq \mathcal{K}(\Psi), \forall b \in \mathcal{B}, \quad (17f)$$

where $\boldsymbol{\rho_{b,u}} = [\rho_{1,u}, \ldots, \rho_{B,u}]^T$ and $\boldsymbol{\rho_b} = [\rho_1, \ldots, \rho_B]^T$. (17a) is the sum-rate of the cell-center TUs, constraint (17b)

[2]The MRT beamforming is suboptimal in a multi-cell setting, however, we choose this beamforming because its closed-form expression allows us to characterize the AU's outage probability.

[3]The reverse SIC order, where the AU performs SIC and cell-center TUs treat AU's message as noise, has been considered. Nevertheless, such a SIC order is not promising in ATN-NOMA because the SIC at the AU might fail due to strong ICI. To ensure reliable communications to the AU, we assume the AU treats cell-center TUs' messages as noise and the cell-center TUs perform SIC.

ensures the AU's QoS requirement is satisfied, and (17c) ensures that each associated cell-center TU can decode the AU information successfully. In addition, (17d) ensures the power coefficients are non-negative, (17e) ensures the power allocation is feasible, and (17f) ensures the coordinated BSs are within the receiving coverage of the AU so that the ATN-NOMA can be performed. Note that, the formulation in (17) is expressed using the fact that the cell-center TU $t \in \mathcal{T}$ is associated to the BS $b \in \mathcal{B}$ if $t = b$.

Problem (17) is a non-convex optimization problem due to (17a), (17b), and (17c). Furthermore, the optimization variables are mutually coupled. To find the optimal solution, we exploit the structure of the problem (17). Note that (17a), (17c), (17d) and (17e) are independent of Ψ. To obtain the optimal beamwidth, we use the following propositions:

Proposition 1. *R_u is a non-increasing function of Ψ.*

Proof: Substituting (4) and (7) into (12), yields

$$R_u = B_{\mathrm{w}} \log \left(1 + \frac{\sum\limits_{\forall b \in \mathcal{B}} \frac{\Upsilon_b^v \rho_{b,u}}{\Psi^2}}{\sum\limits_{\forall b \in \mathcal{B}} \frac{\Upsilon_b^v \rho_b}{\Psi^2} + \sum\limits_{\forall b \in \mathcal{I}} \frac{\Upsilon_b^v}{\Psi^2} + 1} \right). \tag{18}$$

where $\Upsilon_b^v = \frac{N E_u F G_{ref} |\Omega_{u,v}|^2}{{d_{b,u}}^{\alpha_v}}$. Taking the derivative of R_u w.r.t. Ψ, yields:

$$\frac{\partial R_u}{\partial \Psi} = \frac{-2 B_{\mathrm{w}} \Psi \sum\limits_{\forall b \in \mathcal{B}} \Upsilon_b^v \rho_{b,u}}{\ln(2)\, c_1 \cdot c_2} \leq 0, \tag{19}$$

where $c_1 = \left(\Psi^2 + \sum\limits_{\forall b \in \mathcal{B}} \Upsilon_b^v (\rho_b + \rho_{b,u}) + \sum\limits_{\forall b \in \mathcal{I}} \Upsilon_b^v \right)$ and $c_2 = \left(\Psi^2 + \sum\limits_{\forall b \in \mathcal{B}} \Upsilon_b^v \rho_b + \sum\limits_{\forall b \in \mathcal{I}} \Upsilon_b^v \right)$. ■

Interestingly, this suggests that the desired signal of the AU always increases more than the ICI level if the beamwidth is reduced and it is independent of the number of coordinated BSs and interfering BSs.

Proposition 2. *The optimal bandwidth Ψ^* in (17) is* $\Psi^* = \tan^{-1}\left(\arg\max\limits_{b \in \mathcal{B}} \frac{\|\hat{\boldsymbol{w}}_b^{BS} - \hat{\boldsymbol{w}}^{AU}\|}{(z_u - z_b)} \right)$.

Proof: Since (17a), (17c), (17d) and (17e) are independent of Ψ, and according to proposition 1, R_u is a non-increasing function of Ψ, the optimal bandwidth Ψ in (17) can be equivalently obtained by solving the following convex optimization problem:

$$\min_{\Psi} \quad \Psi, \tag{20a}$$

$$\text{s.t.} \quad \hat{d}_{b,u} \leq (z_u - z_b) \tan \Psi, \quad \forall b \in \mathcal{B}. \tag{20b}$$

To obtain the closed form solution in (20), we denote $b' = \left\{ b \,|\, \arg\max\limits_{b \in \mathcal{B}} \frac{\|\hat{\boldsymbol{w}}_b^{\mathrm{BS}} - \hat{\boldsymbol{w}}^{\mathrm{AU}}\|}{(z_u - z_b)} \right\}$. The 3D location of the coordinated BS b' is $\boldsymbol{w}_{b'}^{\mathrm{BS}} = [x_{b'}, y_{b'}, z_{b'}]^T$. For $\boldsymbol{w}_{b'}^{\mathrm{BS}} \subseteq \mathcal{K}(\Psi)$, we must have $\boldsymbol{w}_{b'}^{\mathrm{BS}} \subseteq \mathcal{K}'(\Psi) \subseteq \mathcal{K}(\Psi)$, where $\mathcal{K}'(\Psi) = \{\boldsymbol{w}_{k'} | x = r' \cos\psi, y = r' \sin\psi, z = z_{b'}, r' = (z_u - z_{b'}) \tan\Psi\}$. This implies that $\boldsymbol{w}_{b'}^{\mathrm{BS}} \subseteq \mathcal{K}'(\Psi) \iff [x_{b'}, y_{b'}, z_{b'}]^T \subseteq [x + x_u, y + y_u, z_{b'}]^T$. By the rule of translation, we conclude that $[x_{b'} - x_u, y_{b'} - y_u, z_{b'}]^T \subseteq [r' \cos\psi, r' \sin\psi, z_{b'}]^T$. We then use Euclidean norm, and write:

$$\sqrt{(x_{b'} - x_u)^2 + (y_{b'} - y_u)^2} = \left\| \hat{\boldsymbol{w}}_{b'}^{\mathrm{BS}} - \hat{\boldsymbol{w}}^{\mathrm{AU}} \right\| = \hat{d}_{b',u}, \tag{21}$$

and

$$\sqrt{(r' \cos\psi)^2 + (r' \sin\psi)^2} = r' = (z_u - z_{b'}) \tan\Psi. \tag{22}$$

Thus, $[x_{b'} - x_u, y_{b'} - y_u, z_{b'}]^T \subseteq [r' \cos\psi, r' \sin\psi, z_{b'}]^T$, implies that:

$$\hat{d}_{b',u} \leq (z_u - z_{b'}) \tan\Psi. \tag{23}$$

According to proposition 1, Ψ should be minimized such that (23) is satisfied. Therefore, the closed-form solution is $\Psi^* = \tan^{-1}\left(\arg\max\limits_{b \in \mathcal{B}} \frac{\|\hat{\boldsymbol{w}}_b^{\mathrm{BS}} - \hat{\boldsymbol{w}}^{\mathrm{AU}}\|}{(z_u - z_b)} \right)$. ■

This suggests that the optimal beamwidth in (17) is unique and it is the smallest beamwidth that covers all the coordinated BSs. Using proposition 2, (17) is then reduced to the following problem:

$$\max_{\boldsymbol{\rho_{b,u}}, \boldsymbol{\rho_b}} \sum_{\forall b \in \mathcal{B}} B_{\mathrm{w}} \log \left(1 + \frac{\rho_b N |h_{b,b}|^2}{\sum\limits_{\forall b' \in \mathcal{B} \setminus b} \rho_{b'} N |h_{b,b}|^2 + I_{\mathrm{tot}}^{(b)} + 1} \right), \tag{24a}$$

$$\text{s.t.} \quad B_{\mathrm{w}} \log \left(1 + \frac{\boldsymbol{\rho_{b,u}}^T \boldsymbol{h}_u(\Psi^*)}{\boldsymbol{\rho_b}^T \boldsymbol{h}_u(\Psi^*) + I_{\mathrm{tot}}^{(u)} + 1} \right) \geq R_{\min}, \tag{24b}$$

$$B_{\mathrm{w}} \log \left(1 + \frac{\boldsymbol{\rho_{b,u}}^T \boldsymbol{h}_b}{\boldsymbol{\rho_b}^T \boldsymbol{h}_b + I_{\mathrm{tot}}^{(b)} + 1} \right) \geq R_{\min}, \forall b \in \mathcal{B}, \tag{24c}$$

$$0 \leq \boldsymbol{\rho_b}, 0 \leq \boldsymbol{\rho_{b,u}}, \boldsymbol{\rho_b} + \boldsymbol{\rho_{b,u}} \leq 1, \tag{24d}$$

where $\boldsymbol{h}_u(\Psi^*) = N \left[|h_{1,u}^v(\Psi^*)|^2, \ldots |h_{B,u}^v(\Psi^*)|^2 \right]^T$ and $\boldsymbol{h}_b = N \left[|h_{1,b}|^2, \ldots, |h_{B,b}|^2 \right]^T$. Besides, $I_{\mathrm{tot}}^{(u)} = N \sum\limits_{\forall b'' \in \mathcal{I}} \left| h_{b'',u}^v(\Psi^*) \right|^2$ and $I_{\mathrm{tot}}^{(b)} = N \sum\limits_{\forall b'' \in \mathcal{I}} |h_{b'',b}|^2$ are the aggregated ICI at the AU u and TU $t = b$, respectively.

The optimization problem in (24) is still a non-convex optimization problem. To address this issue, we introduce an auxiliary variable $\boldsymbol{q_b} = [q_1, \ldots, q_B]$, which can be interpreted as the SINR of the TUs. By rearranging the term, (24) is reformulated as follows:

$$\max_{\boldsymbol{q_b}, \boldsymbol{\rho_{b,u}}, \boldsymbol{\rho_b}} \quad \sum_{\forall b \in \mathcal{B}} B_{\mathrm{w}} \log(1 + q_b), \tag{25a}$$

$$\text{s.t.} \quad \frac{\rho_b N |h_{b,b}|^2}{\sum\limits_{\forall b' \in \mathcal{B} \setminus b} \rho_{b'} N |h_{b',b}|^2 + I_{\mathrm{tot}}^{(b)} + 1} \geq q_b, \forall b \in \mathcal{B}, \tag{25b}$$

$$\boldsymbol{\rho_{b,u}}^T \boldsymbol{h}_u(\Psi^*) \geq r \left(\boldsymbol{\rho_b}^T \boldsymbol{h}_u(\Psi^*) + I_{\mathrm{tot}}^{(u)} + 1 \right), \tag{25c}$$

$$\boldsymbol{\rho_{b,u}}^T \boldsymbol{h_b} \geq r \left(\boldsymbol{\rho_b}^T \boldsymbol{h_b} + I_{\mathrm{tot}}^{(b)} + 1 \right), \tag{25d}$$

(24d),

where $r = \left(2^{\frac{R_{\min}}{B_{\rm w}}} - 1\right)$.

In (25), only (25b) remains to be non-convex[4]. To address the non-convexity challenge, we employ SCA. Rearranging the term and applying first order Taylor approximation to (25b), (25) can be successively solved via the following convex optimization problem:

$$\begin{aligned}
\max_{\boldsymbol{q_b},\boldsymbol{\rho_{b,u}},\boldsymbol{\rho_b}} \quad & \sum_{\forall b\in\mathcal{B}} B_{\rm w}\log\left(1+q_b\right), && \text{(26a)}\\
\text{s.t.} \quad & \rho_b N\left|h_{b,b}\right|^2 \geq q_b^{(n)}\times && \text{(26b)}\\
& \left(\sum_{\forall b'\in\mathcal{B}\setminus b}\rho_{b'}^{(n)}N\left|h_{b',b}\right|^2 + I_{\rm tot}^{(b)}+1\right)\\
& + \left(q_b - q_b^{(n)}\right)\times\\
& \left(\sum_{\forall b'\in\mathcal{B}\setminus b}\rho_{b'}^{(n)}N\left|h_{b',b}\right|^2 + I_{\rm tot}^{(b)}+1\right)\\
& + \left(\rho_{b'} - \rho_{b'}^{(n)}\right)\times\\
& \sum_{\forall b'\in\mathcal{B}\setminus b} q_b^{(n)}N\left|h_{b',b}\right|^2, \forall b\in\mathcal{B},\\
& (25c),(25d),(24d),
\end{aligned}$$

where $q_b^{(n)}$ and $\rho_b^{(n)}$ are the optimal values of q_b and ρ_b, respectively, in the $(n-1)$th iterations. Note that, the initial values of $\rho_b^{(0)}, \forall b$, can be randomly initialized between $[0,1]$ while the initial values of $q_b^{(0)}, \forall b$, can be initialized by setting (25b) with equality. Since (26) is a convex optimization problem, it can be solved efficiently [52].

IV. Inter-Cell Interference and AU's Outage Probability

In this section, we estimate the aggregated ICI by leveraging the unique properties of the proposed ATN-NOMA scheme and the statistical CSI. Then, we use the derived statistical properties to approximate the AU's outage probability in cases where no interfering BSs have the same elevation angle as the coordinated BSs. To estimate the aggregated ICI, we utilize the following proposition and corollary:

Proposition 3. *The interfering BSs $b\in\mathcal{I}$ that impose ICI have the same elevation-angle as the coordinated BS b'.*

Proof: Let $b' = \left\{b \,|\, \arg\max_{b\in\mathcal{B}} \frac{\left\|\boldsymbol{w}_b^{\rm BS} - \boldsymbol{w}^{\rm AU}\right\|}{(z_u - z_{\rm b})}\right\}$ and $\Psi^* = \tan^{-1}\left(\frac{\left\|\hat{\boldsymbol{w}}_{b'}^{\rm BS} - \hat{\boldsymbol{w}}^{\rm AU}\right\|}{(z_u - z_{b'})}\right)$. Then, (6) ensures that $\phi_{b',u} \geq \phi_{b'',u}$ for $\forall b''\in\mathcal{I}$. Define $\Psi_{b''} = \tan^{-1}\left(\frac{\left\|\hat{\boldsymbol{w}}_{b''}^{\rm BS} - \hat{\boldsymbol{w}}^{\rm AU}\right\|}{(z_u - z_{b''})}\right)$ for $\forall b''\in\mathcal{I}$. It is then observed that $\Psi^*\leq\Psi_{b''}$ for $\forall b''\in\mathcal{I}$ since $\Psi_b + \phi_{b,u} = \frac{\pi}{2}$. Let $\mathcal{I}_0 = \left\{b'' \,|\, \Psi^* = \Psi_{b''}, \forall b''\in\mathcal{I}\right\}$, and $\mathcal{I}_1 = \left\{b'' \,|\, \Psi^* < \Psi_{b''}, \forall b''\in\mathcal{I}\right\}$. According to (4), (7) and Proposition 2, $\left|h_{b'',u}\left(\Psi^*\right)\right|^2 = 0$ for $\forall b''\in\mathcal{I}_1$. Since $\Psi^* = \Psi_b \iff \phi_{b',u} = \phi_{b,u}$, $\forall b\in\mathcal{I}_0$, the interfering BSs $b\in\mathcal{I}_0$ that causes ICI (e.g., $\left|h_{b,u}\left(\Psi^*\right)\right|^2 \neq 0$) have the same elevation-angle as the coordinated BS b'. ■

[4]Note that if the ICI of cell-center TUs is negligible, (25) can be reformulated as a convex optimization problem.

Corollary 1. *If no interfering BSs $b\in\mathcal{I}$ have the same elevation-angle as the coordinated BS b', the AU experiences zero ICI*[5].

Proof: When no interfering BSs $b\in\mathcal{I}$ have the same elevation-angle as the coordinated BS b', $\mathcal{I}_0 = \emptyset$. Thus, the AU experiences zero ICI. ■

Using (4), the aggregated ICI, $I_{\rm tot} = \sum_{\forall b\in\mathcal{I}} N\left|h_{b,u}^{\upsilon}\left(\Psi^*\right)\right|^2$, is then written as:

$$I_{\rm tot} = \sum_{\forall b\in\mathcal{I}} N\Xi_{b,u}^{\upsilon}\left(\Psi^*\right)\left|\Omega_{b,u}^{\upsilon}\right|^2. \tag{27}$$

Using proposition 3, the interfering BSs $b\in\mathcal{I}_0$ that impose the ICI have the same elevation-angle as the coordinated BS b'. For ease of exposition, we assume the interfering BSs have the same height here, and thus the same probability of LOS. In Appendix A, we generalize our analysis to cases where the interfering BSs have different heights. Let $\tilde{I} = \text{card}(\mathcal{I}_0)$ and $\tilde{L}$ be the number of LOS links among these $\tilde{I}$ interfering links. Further define $\mathcal{I}^{\rm L}$ as the set of interfering BSs that establishes LOS links to the AU, i.e., $\tilde{L} = \text{card}\left(\mathcal{I}^{\rm L}\right)$, and $\mathcal{I}^{\rm N}$ as the set of interfering BSs that establishes NLOS links to the AU, such that $\mathcal{I} = \mathcal{I}^{\rm L}\cup\mathcal{I}^{\rm N}$ and $\mathcal{I}^{\rm L}\cap\mathcal{I}^{\rm N} = \emptyset$.

Given above definitions, it is straightforward to see that $\tilde{L}$ is a binomial random variable with $\tilde{I}$ interfering links, and probability of $p_{b,u}^{\rm L}\left(\hat{d}_{b,u}, z_u\right)$, i.e., $\tilde{L}\sim\text{Bino}\left(\tilde{I}, p_{b,u}^{\rm L}\left(\hat{d}_{b,u}, z_u\right)\right)$. Therefore, its probability mass function (pmf) is:

$$f\left(i,\tilde{I},p_{b,u}^{\rm L}\left(\hat{d}_{b,u},z_u\right)\right) = \binom{\tilde{I}}{i} p_{b,u}^{\rm L}\left(\hat{d}_{b,u},z_u\right)^i \times p_{b,u}^{\rm N}\left(\hat{d}_{b,u},z_u\right)^{(\tilde{I}-i)}. \tag{28}$$

More concretely, (28) is the probability of getting exactly i LOS links and $\tilde{I}-i$ NLOS links with $\tilde{I}$ interfering links. Suppose there are i LOS links among $\tilde{I}$ interfering links, then $I_{\rm tot}^{(i)}$ is:

$$\begin{aligned}
I_{\rm tot}^{(i)} &= \sum_{\forall b\in\mathcal{I}_0} N\Xi_{b,u}^{\upsilon}\left(\Psi^*\right)\left|\Omega_{b,u}^{\upsilon}\right|^2,\\
&= \sum_{\forall b\in\mathcal{I}^L} N\Xi_{b,u}^{\rm L}\left(\Psi^*\right)\left|\Omega_{b,u}^{\rm L}\right|^2 + \sum_{\forall b\in\mathcal{I}^N} N\Xi_{b,u}^{\rm N}\left(\Psi^*\right)\left|\Omega_{b,u}^{\rm N}\right|^2,\\
&= H_i^{\rm L} + H_{(\tilde{I}-i)}^{\rm N}.
\end{aligned} \tag{29}$$

Given the number of LOS links, $H_i^{\rm L}$ and $H_{(\tilde{I}-i)}^{\rm N}$ are gamma distributed random variables. Suppose $H\sim\text{gamma}\left(m,\theta\right)$. The pdf of the gamma random variable H is given as:

$$f_H(h,m,\theta) = \frac{h^{m-1}\exp\left(-\frac{h}{\theta}\right)}{\theta^m\Gamma\left(m\right)}, h>0, \tag{30}$$

where $\Gamma\left(\cdot\right)$ is the gamma function. The CDF of the gamma random variable is:

$$F_H\left(\bar{h},m,\theta\right) = \int_0^{\bar{h}}\frac{h^{m-1}\exp\left(-\frac{h}{\theta}\right)}{\theta^m\Gamma\left(m\right)}dh, \bar{h}>0. \tag{31}$$

[5]Corollary 1 suggests that in irregular cellular networks the AU in our proposed scheme is likely to experience zero ICI. This is because it is difficult to find multiple BSs having the same elevation angle to the AU in such settings.

In the gamma distribution, there exists summation and scaling properties. That is, if $H_i \sim \text{gamma}(m_i, \theta)$, then $\sum_{\forall i} H_i \sim \text{gamma}\left(\sum_{\forall i} m_i, \theta\right)$. If $H \sim \text{gamma}(m, \theta)$, then $c \cdot H \sim \text{gamma}(m, c\theta)$. Thus, if $i = 0$, then $I_{\text{tot}}^{(0)} = H_{\tilde{I}}^{\text{N}} \sim \text{gamma}\left(\tilde{I} m_u^{\text{N}}, N\Xi_{b,u}^{\text{N}}(\Psi^*)\theta_u^{\text{N}}\right)$, and if $i = \tilde{I}$, then $I_{\text{tot}}^{(\tilde{I})} = H_{\tilde{I}}^{\text{L}} \sim \text{gamma}\left(\tilde{I} m_u^{\text{L}}, N\Xi_{b,u}^{\text{L}}(\Psi^*)\theta_u^{\text{L}}\right)$.

According to [53], if $0 < i < \tilde{I}$, then $I_{\text{tot}}^{(i)}$ is the summation of independent non-identical distributed (i.n.i.d.) gamma random variables, where $H_i^{\text{L}} \sim \text{gamma}\left(i m_u^{\text{L}}, N\Xi_{b,u}^{\text{L}}(\Psi^*)\theta_u^{\text{L}}\right)$ and $H_{(\tilde{I}-i)}^{\text{N}} \sim \text{gamma}\left(\left(\tilde{I}-i\right) m_u^{\text{N}}, N\Xi_{b,u}^{\text{N}}(\Psi^*)\theta_u^{\text{N}}\right)$. The exact pdf is:

$$f_{I_{\text{tot}}^{(i)}}(h) = C \sum_{j=0}^{\infty} \frac{\delta_j h^{k+j-1} \exp\left(-\frac{h}{\theta_{\min}}\right)}{\Gamma(k+j)\theta_{\min}^{k+j}}, \qquad h > 0, \quad (32)$$

where $\theta_{\min} = \arg\min_{\upsilon \in \{\text{L},\text{N}\}} \left\{N\Xi_{b,u}^{\upsilon}(\Psi^*)\theta_u^{\upsilon}\right\}$, $k = i m_u^{\text{L}} + \left(\tilde{I}-i\right) m_u^{\text{N}}$, $\delta_{j+1} = \frac{1}{j+1}\sum_{l=1}^{j+1} l\gamma_l \delta_{j+1-l}$ with $\delta_0 = 1$,

$$\gamma_j = \frac{i m_u^{\text{L}} \left(1 - \frac{\theta_{\min}}{N\Xi_{b,u}^{\text{L}}(\Psi^*)\theta_u^{\text{L}}}\right)^j}{j} + \frac{\left(\tilde{I}-i\right) m_u^{\text{N}} \left(1 - \frac{\theta_{\min}}{N\Xi_{b,u}^{\text{N}}(\Psi^*)\theta_u^{\text{N}}}\right)^j}{j},$$

and

$$C = \left(\frac{\theta_{\min}}{N\Xi_{b,u}^{\text{L}}(\Psi^*)\theta_u^{\text{L}}}\right)^{i m_u^{\text{L}}} \times \left(\frac{\theta_{\min}}{N\Xi_{b,u}^{\text{N}}(\Psi^*)\theta_u^{\text{N}}}\right)^{\left(\tilde{I}-i\right)m_u^{\text{N}}}.$$

The CDF is therefore:

$$F_{I_{\text{tot}}^{(i)}}\left(\bar{h}\right) = C \sum_{j=0}^{\infty} \delta_j \int_0^{\bar{h}} \left[\frac{h^{k+j-1} \exp\left(-\frac{h}{\theta_{\min}}\right)}{\Gamma(k+j)\theta_{\min}^{k+j}}\right] dh. \quad (33)$$

The exact pdf and CDF respectively shown in (32) and (33) are in fact theoretically important. However, they are not very useful in this application. This is because, although the infinite series in the expressions can be truncated to a finite series with a bounded error, the numerical value of $\theta_{\min}^{k+j}$ in the denominator of (32) and (33) may be zero due to the magnitude of the large-scale fading effect. Hence, an approximation is required for our purpose.

According to [54], $I_{\text{tot}}^{(i)}$ for $0 < i < \tilde{I}$, can be approximated by $H^{(i)} \sim \text{gamma}\left(\hat{m}, \hat{\theta}\right)$, where

$$\hat{m} = \frac{\mu^2}{\hat{m}_L \vartheta_L^2 + \hat{m}_N \vartheta_N^2}, \quad (34)$$

$$\hat{\theta} = \frac{\hat{m}_L \vartheta_L^2 + \hat{m}_N \vartheta_N^2}{\mu}, \quad (35)$$

In (34) and (35), $\hat{m}_L = i m_u^{\text{L}}$, $\vartheta_L = N\Xi_{b,u}^{\text{L}}(\Psi^*)\theta_u^{\text{L}}$, $\hat{m}_N = \left(\tilde{I}-i\right) m_u^{\text{N}}$, $\vartheta_N = N\Xi_{b,u}^{\text{N}}(\Psi^*)\theta_u^{\text{N}}$, and $\mu = \hat{m}_L \vartheta_L + \hat{m}_N \vartheta_N$. Based on the above, we present the following:

Proposition 4. *The pdf of the aggregated ICI, I_{tot}, in ATN-NOMA is approximated as:*

$$\begin{aligned} & f_{I_{tot}}\left(\tau, \tilde{I}, p_{b,u}^{L}\left(\hat{d}_{b,u}, z_u\right), \hat{m}, \hat{\theta}\right) \\ \approx & \sum_{0 \le i \le \tilde{I}} f\left(i, \tilde{I}, p_{b,u}^{L}\left(\hat{d}_{b,u}, z_u\right)\right) f_{H^{(i)}}\left(\tau, \hat{m}, \hat{\theta}\right), \tau > 0 \\ = & \sum_{0 \le i \le \tilde{I}} \left[\binom{\tilde{I}}{i} p_{b,u}^{L}\left(\hat{d}_{b,u}, z_u\right)^{i} \times p_{b,u}^{N}\left(\hat{d}_{b,u}, z_u\right)^{(\tilde{I}-i)} \frac{\tau^{\hat{m}-1}\exp\left(-\frac{\tau}{\hat{\theta}}\right)}{\hat{\theta}^{\hat{m}}\Gamma(\hat{m})}\right]. \end{aligned} \quad (36)$$

The CDF of the aggregated ICI, I_{tot}, in ATN-NOMA is approximated as:

$$\begin{aligned} & F_{I_{tot}}\left(\tau, \tilde{I}, p_{b,u}^{L}\left(\hat{d}_{b,u}, z_u\right), \hat{m}, \hat{\theta}\right) \\ \approx & \sum_{0 \le i \le \tilde{I}} f\left(i, \tilde{I}, p_{b,u}^{L}\left(\hat{d}_{b,u}, z_u\right)\right) F_{H^{(i)}}\left(\tau, \hat{m}, \hat{\theta}\right), \tau > 0 \\ = & \sum_{0 \le i \le \tilde{I}} \left[\binom{\tilde{I}}{i} p_{b,u}^{L}\left(\hat{d}_{b,u}, z_u\right)^{i} \times p_{b,u}^{N}\left(\hat{d}_{b,u}, z_u\right)^{(\tilde{I}-i)} \int_0^{\tau} \frac{\tau'^{\hat{m}-1}\exp\left(-\frac{\tau'}{\hat{\theta}}\right)}{\hat{\theta}^{\hat{m}}\Gamma(\hat{m})} d\tau'\right]. \end{aligned} \quad (37)$$

Proof: $f_{I_{\text{tot}}}$ and $F_{I_{\text{tot}}}$ in (36) and (37), respectively, follow immediately noting that I_{tot} is the sum of i.n.i.d. gamma random variables conditioned by the number of LOS/NLOS links. ■

In proposition 4, it is observed that I_{tot} follows exactly a gamma distribution in cases where the probabilities of LOS/NLOS are one. Using proposition 4, we can now estimate the aggregated ICI, I_{tot}, with $\hat{I}_{\text{tot}}$ for a given probability δ, as follows:

$$\mathbb{P}\left(I_{\text{tot}} \le \hat{I}_{tot}\right) = \delta, \quad (38)$$

where $\hat{I}_{\text{tot}}$ must satisfy the following equality:

$$F_{I_{\text{tot}}}\left(\hat{I}_{\text{tot}}, \tilde{I}, p_{b,u}^{\text{L}}\left(\hat{d}_{b,u}, z_u\right), \hat{m}, \hat{\theta}\right) = \delta. \quad (39)$$

Note that using (38), the proposed scheme only requires the CSI of the coordinated BSs to perform ATN-NOMA.

Due to zero ICI and low data rate requirement, the AU's outage probability is extremely low. Thus, it is useful to approximate the AU's outage probability if there are no interfering BSs having the same elevation-angle as the coordinated BS b'. Specifically, the outage probability can be written as follows:

$$P^{\text{out}} = \mathbb{P}\{R_u < R_{\min}\}. \quad (40)$$

Proposition 5. *If no interfering BSs $b \in \mathcal{I}$ have the same elevation-angle as the coordinated BS b', the AU's outage*

probability is approximately:

$$P^{out} \approx F_{\beta_{tot}}\left(r, \tilde{B}_{d_1}, \ldots, \tilde{B}_{d_{\bar{\beta}}}, p^{L}_{b,u}\left(d_1, z_u\right), \ldots, p^{L}_{b,u}\left(d_{\bar{\beta}}, z_u\right)\right), \tag{41}$$

$$= \sum_{\forall b_d \in \mathcal{L}} \left[\prod_{\tilde{L}_{d_\beta} = b_{d_\beta}, \forall \beta} \binom{\tilde{B}_{d_\beta}}{b_{d_\beta}} p^{L}_{b,u}\left(d_\beta, z_u\right)^{b_{d_\beta}} \times p^{N}_{b,u}\left(d_\beta, z_u\right)^{\left(\tilde{B}_{d_\beta} - b_{d_\beta}\right)} \int_0^r \frac{\tau'^{\hat{m}-1} \exp\left(-\frac{\tau'}{\hat{\theta}}\right)}{\hat{\theta}^{\hat{m}} \Gamma\left(\hat{m}\right)} d\tau' \right].$$

Proof: Using Corollary 1 and maximizing R_u, (40) is reduced to:

$$P^{\text{out}} = \mathbb{P}\left\{ \sum_{\forall b \in \mathcal{B}} N \left| h^{v}_{b,u}\left(\Psi^*\right) \right|^2 < 2^{\frac{R_{\min}}{B_w}} - 1 \right\}. \tag{42}$$

Denote $\beta_{\text{tot}} = \sum_{\forall b \in \mathcal{B}} N \left| h^{v}_{b,u}\left(\Psi^*\right) \right|^2$. Note that β_{tot} is the sum of i.n.i.d. gamma random variables conditioned by the number of LOS/NLOS links. Define $\mathcal{D} = \left\{d_1, \ldots, d_{\bar{\beta}}\right\}$ as the set of *distinctive* horizontal distance between the AU and the coordinated BS, $b \in \mathcal{B}$, where $\bar{\beta} \leq B$, and $\mathcal{B}_{d_\beta} = \left\{ b \,|\, \hat{d}_{b,u} = d_\beta, \forall b \in \mathcal{B} \right\}$ as the set of coordinated BSs with horizontal distance d_β from the AU. Let $\tilde{B}_{d_\beta} = \text{card}\left(\mathcal{B}_{d_\beta}\right)$ and $\tilde{L}_{d_\beta}$ be the number of LOS links among these $\tilde{B}_{d_\beta}$ connected links. Further define $\mathcal{L} = \left\{ \left(\tilde{L}_{d_1}, \ldots, \tilde{L}_{d_{\bar{\beta}}}\right) | 0 \leq \tilde{L}_{d_\beta} \leq \tilde{B}_{d_\beta}, \beta = 1, \ldots, \bar{\beta} \right\}$, and $b_d = \left(b_{d_1}, \ldots, b_{d_{\bar{\beta}}}\right)$. Note that, $\tilde{L}_{d_\beta} \sim \text{Bino}\left(\tilde{B}_{d_\beta}, p^{\text{L}}_{b,u}\left(d_\beta, z_u\right)\right)$. Since $\tilde{L}_{d_\beta}$ is independent of $\tilde{L}_{d_{\beta'}}$ for $\beta \neq \beta'$, we have:

$$\mathbb{P}\left(\tilde{L}_{d_1} = b_{d_1}, \ldots, \tilde{L}_{d_{\bar{\beta}}} = b_{d_{\bar{\beta}}}\right) = \prod_{\tilde{L}_{d_\beta} = b_{d_\beta}, \forall \beta} f_{\tilde{L}_{d_\beta}}\left(b_{d_\beta}, \tilde{B}_{d_\beta}, p^{\text{L}}_{b,u}\left(d_\beta, z_u\right)\right). \tag{43}$$

Denote $H^{(b_d)} = \sum_{\forall \beta} H^{\left(b_{d_\beta}\right)}$, and $r = 2^{\frac{R_{\min}}{B_w}} - 1$. The CDF of the β_{tot} is approximated as:

$$\begin{aligned} & F_{\beta_{\text{tot}}}\left(r, \tilde{B}_{d_1}, \ldots, \tilde{B}_{d_{\bar{\beta}}}, p^{\text{L}}_{b,u}\left(d_1, z_u\right), \ldots, p^{\text{L}}_{b,u}\left(d_{\bar{\beta}}, z_u\right)\right) \\ \approx & \sum_{\forall b_d \in \mathcal{L}} \mathbb{P}\left(\tilde{L}_{d_1} = b_{d_1}, \ldots, \tilde{L}_{d_{\bar{\beta}}} = b_{d_{\bar{\beta}}}\right) F_{H^{(b_d)}}\left(r, \hat{m}, \hat{\theta}\right) \\ = & \sum_{\forall b_d \in \mathcal{L}} \left[\prod_{\tilde{L}_{d_\beta} = b_{d_\beta}, \forall \beta} \binom{\tilde{B}_{d_\beta}}{b_{d_\beta}} p^{\text{L}}_{b,u}\left(d_\beta, z_u\right)^{b_{d_\beta}} \times p^{\text{N}}_{b,u}\left(d_\beta, z_u\right)^{\left(\tilde{B}_{d_\beta} - b_{d_\beta}\right)} \int_0^r \frac{\tau'^{\hat{m}-1} \exp\left(-\frac{\tau'}{\hat{\theta}}\right)}{\hat{\theta}^{\hat{m}} \Gamma\left(\hat{m}\right)} d\tau' \right]. \end{aligned} \tag{44}$$

■

We note that the outage probability of CoMP-OMA with optimal beamwidth, and network NOMA with fixed power allocation and optimal beamwidth can similarly be obtained using (41) by replacing r with $r_{\text{OMA}} = 2\left(2^{\frac{2R_{\min}}{B_w}} - 1\right)$ and $r_{\text{FNOMA}} = \frac{r}{[\rho_{b,u} - \rho_b r]^+}$, respectively. Furthermore, in cases where $\text{card}\left(\mathcal{D}\right) = 1$ and the probabilities of LOS/NLOS are one, the outage probability can be approximated using a gamma distribution.

Table I: Parameter Settings

Parameter	Value	Parameter	Value
P_{tx}	26 dBm	f_{c}	2 GHz
B_{w}	180 KHz	r_0	500 m
σ^2_{n}	-174 dBm/Hz	(E_u, E_t)	(-3, 10) dB
$R_{\min}$	100 Kbps	(φ, ξ, ζ)	(1, .151, 1)
$\text{card}\left(\mathcal{B} \cup \mathcal{I}\right) \subseteq \mathcal{A}$	37	$(\alpha_{\text{L}}, \alpha_{\text{N}}, \alpha)$	(2.1, 3.7, 4)
$\text{card}\left(\mathcal{B}\right)$	3	$\left(m^{\text{L}}_u, m^{\text{N}}_u, m_t\right)$	(3, 2, 1)
z_b, z_t	(19, 1.5) m	$\left(\theta^{\text{L}}_u, \theta^{\text{N}}_u, \theta_t\right)$	$(\frac{1}{3}, \frac{1}{2}, 1)$

V. Simulation Results

In this section, we provide the simulation results to evaluate the performance of our proposed ATN-NOMA scheme. Since multiple techniques are jointly employed in the proposed scheme, the contributions of each technique are unclear. Thus, we consider multiple schemes based on different combinations to identify their corresponding gains and effects at a fundamental level. In this paper, we consider the following schemes:

- CoMP-OMA [11] with fixed beamwidth (FB-OMA),
- CoMP-OMA [11] with optimal beamwidth (OB-OMA),
- Network NOMA with fixed power allocation [28] and fixed beamwidth (FB-FNOMA),
- Network NOMA with fixed power allocation [28] and optimal beamwidth (OB-FNOMA),
- Network NOMA with fixed beamwidth and optimal power allocation (FB-NOMA),
- The proposed ATN-NOMA with optimal beamwidth, power allocation, and statistical CSI (ATN-NOMA-S),
- The proposed ATN-NOMA with optimal beamwidth, power allocation, and perfect CSI (ATN-NOMA-P).

For CoMP-OMA, we consider FDMA with equal bandwidth allocation to the AU and TUs. For fixed beamwidth, we set $\Psi_f = \tan\left(\frac{2r_o}{81}\right)$ to ensure $\text{card}\left(\mathcal{B}\right) = 3$. For network NOMA with fixed power allocation, we set $\rho_{b,\text{u}} = 0.9$ and $\rho_b = 0.1$ to compensate the ICI at the AU. For the proposed ATN-NOMA-S scheme, we set $\delta = 0.999$ to guarantee reliable communications to the AU. Unless stated otherwise, the parameters used in the simulation are as shown in Table I.

A. Statistical Properties of Aggregated ICI

Fig. 3 shows the statistical properties of the aggregated ICI in the proposed ATN-NOMA scheme, where we consider the AU at the origin. We also consider two altitudes: 100m and 500m. Fig. 3(a) and Fig. 3(b) show the pdf and CDF of the aggregated ICI, respectively. As observed, the numerical results match the analytical results given in (36) and (37). Hence, by leveraging the derived statistical properties, the aggregated ICI in the proposed ATN-NOMA scheme can be reliably estimated for any given δ.

B. Accuracy of the Analytical Outage Probability

In cases where the data rate requirement is low and the AU experiences zero ICI, the outage probabilities of OB-OMA, OB-FNOMA, and ATN-NOMA are extremely low. In such cases, an exorbitant number of samples might be required

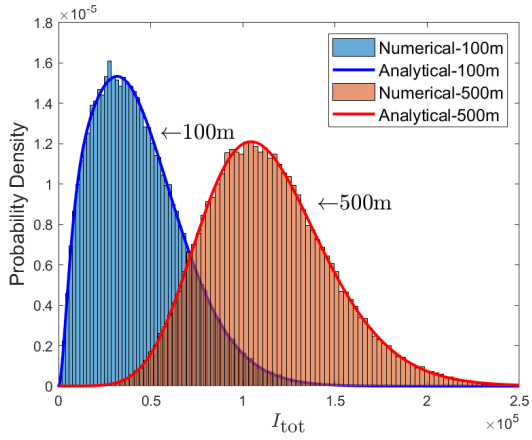

(a)

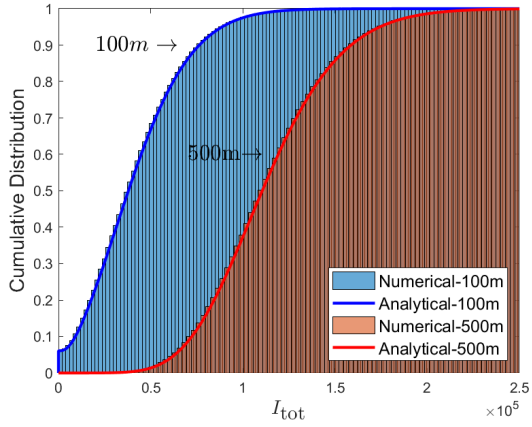

(b)

Figure 3: The statistical properties of the aggregated ICI: (a) pdf; (b) CDF.

to accurately observe the numerical outage probability (e.g., 10^{20} samples are required if $R_{\min} = 100$ Kbps). This is computationally challenging. Thus, as an alternative, we examine the analytical outage probability. Fig. 4 compares the numerical and analytical outage probabilities of OB-OMA, OB-FNOMA, and ATN-NOMA schemes. As seen in Fig. 4(a)-(c), the numerical results closely match the analytical results given in (41). This suggests that we may efficiently measure the analytical outage probability of OB-OMA, OB-FNOMA, and ATN-NOMA using (41) in cases where the AU experiences zero ICI and the data rate requirement is low. Furthermore, in cases where the AU experiences zero ICI, we notice that the outage probability first decreases as the AU's altitude increases. This is due to the LOS gain. After the LOS gain is substantially obtained at a certain altitude, the outage probability then increases due to higher path loss.

C. Types of User Association Policies

Fig. 5 compares the performance of the proposed elevation-angle based user association, minimum-distance based user association, and maximum-SINR based user association along with adjustable beamwidth directional antenna and network

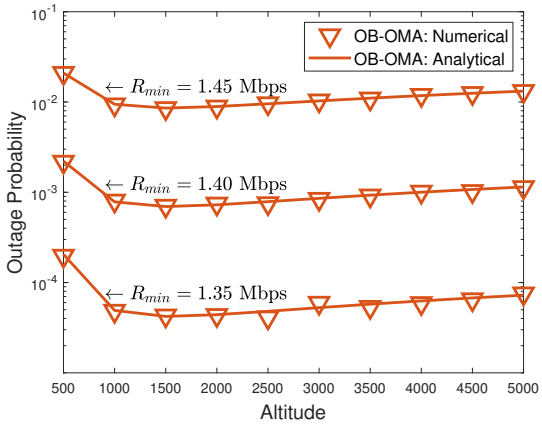

(a)

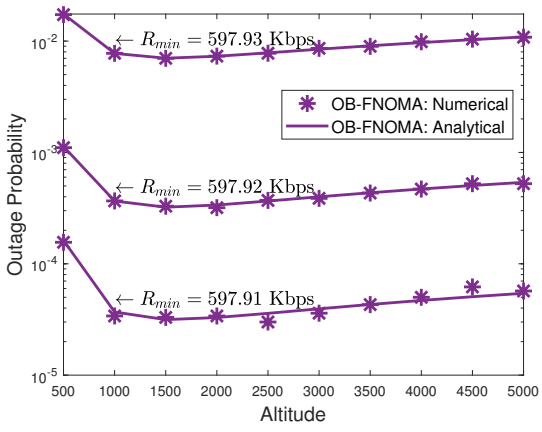

(b)

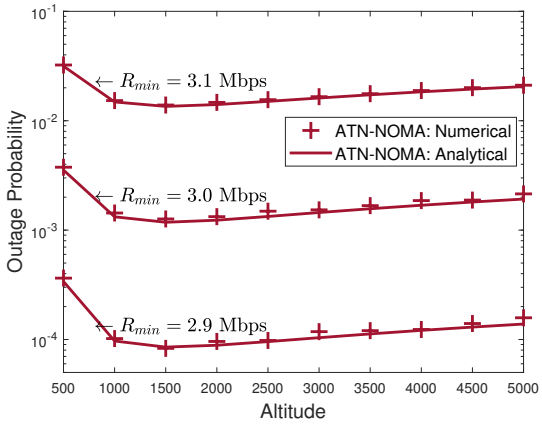

(c)

Figure 4: Numerical outage probability vs. analytical outage probability: (a) OB-OMA; (b) OB-FNOMA; (c) ATN-NOMA.

NOMA. Here, the AU is randomly located inside a disk centered at the origin with a radius of 500m, the BSs' height are uniformly distributed between 15m and 45m, and $R_{\min} = 2.8$ Mbps. As shown in Fig. 5(a), the minimum-distance and maximum-SINR based user associations are more likely to experience ICI. In the minimum-distance

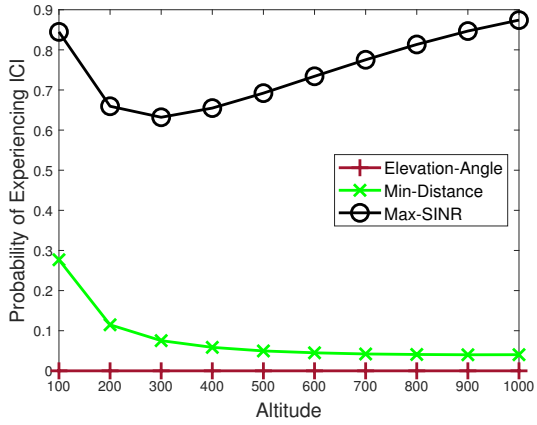

(a)

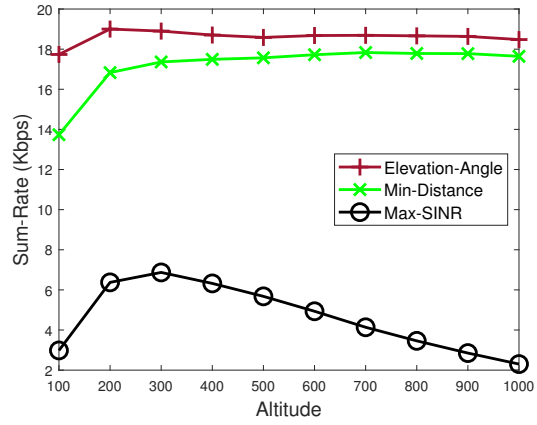

(b)

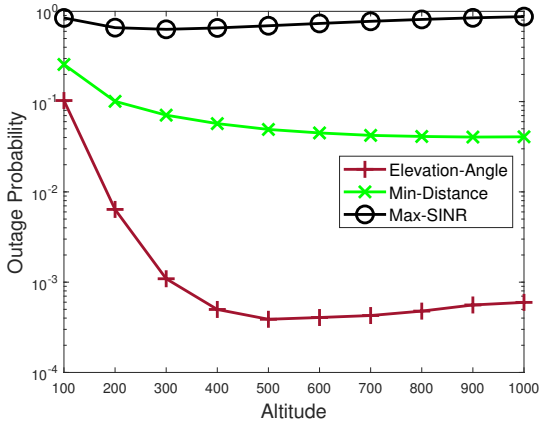

(c)

Figure 5: Performance of different user association policies: (a) probability of experiencing ICI; (b) sum-rate; (c) outage probability.

based user association, the nearest BSs might have a smaller elevation-angle to the AU. In the maximum-SINR based user association, the strongest BSs might be located farther away from the AU. In both cases, the optimal beamwidth might need to cover a larger area inclusive of the interfering BSs.

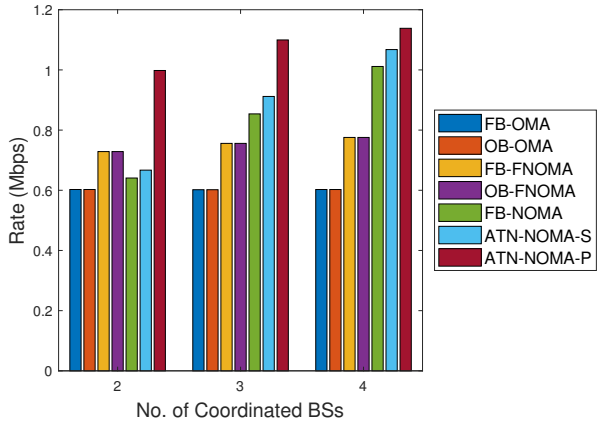

(a)

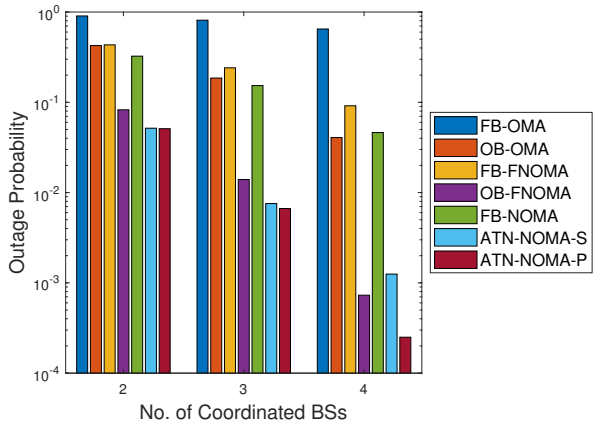

(b)

Figure 6: The effects on the number of coordinated BSs: (a) average TU rate; (b) outage probability.

This leads to a performance degradation in terms of sum-rate and outage probability as shown in Fig. 5(b) and Fig. 5(c), respectively. Nevertheless, if the proposed elevation-angle based user association is employed, the AU is more likely to experience zero ICI. This is because the optimal beamwidth typically covers a smaller area exclusive of the interfering BSs. Furthermore, using the smaller beamwidth increases the channel gain between the AU and the coordinated BSs. As a result, the proposed elevation-angle based user association outperforms existing user associations in both sum-rate and outage probability.

D. Transmitting Strategy: Effects on the Number of Coordinated BSs

Fig. 6 depicts the effects of increasing the number of coordinated BSs, i.e., card $(\mathcal{B})$. Here, the AU is located at the origin with an altitude of 500m. As seen in Fig. 6(a), the average TU rate of the proposed ATN-NOMA schemes improves by increasing the number of coordinated BSs. The outage probability of the AU also decreases as shown in Fig. 6(b).

These improvements are contributed by two factors. Firstly, the increase number of coordinated BSs leads to an increase in the beamforming gain. We note that the beamforming gain is only obtained if optimal power allocation is used. Secondly, an increase in the number of coordinated BSs reduces the number of interfering BSs and hence the aggregated ICI experienced at the AU is reduced. Due to the latter factor, the performance of the ATN-NOMA-S also approaches the ATN-NOMA-P by increasing the number of coordinated BSs.

Due to the ICI estimation, the outage probabilities of ATN-NOMA-S is bounded by $(1-\delta)$. However, if there are no interfering BSs having the same elevation-angle as the coordinated BSs, the bound vanishes and ATN-NOMA-S would achieve the same performance as ATN-NOMA-P. To fully mitigate the ICI of the AU, these results also suggest that increasing the number of coordinated BSs is the only solution.

In Fig. 6(a), it is observed that the average TU rates of FB-FNOMA and OB-FNOMA outperform FB-NOMA and ATN-NOMA-S, where card $(\mathcal{B}) = 2$. This is because a fixed power is allocated to the TUs in FNOMA regardless of the AU's QoS requirement. Without prioritizing the AU's QoS requirement, the outage probabilities of FB-FNOMA and OB-FNOMA are higher than that of the FB-NOMA and ATN-NOMA-S, respectively. Moreover, schemes based on NOMA generally outperform schemes based on OMA in terms of the average TU rate and outage probability, thanks to the spectrum sharing technique.

In addition, FB-OMA and OB-OMA achieve the same TU rate because fixed resource allocation is given to the TUs regardless of the AU's performance. For the same reason, FB-FNOMA and OB-FNOMA achieve the same TU rate. Nevertheless, the benefit of optimal beamwidth (OB) over fixed beamwidth (FB) can be observed in Fig. 6(b). Specifically, schemes based on OB have a lower outage probability than that of schemes based on FB as the ICI of the AU is minimized.

E. Receiving Strategy: Effects on the AU's Position

Fig. 7 presents the effects of the AU's position. As shown in Fig. 7(a), we investigate three important locations to understand the effects of AU's position. These locations are: (A) on top of one of the coordinated BSs, (B) on the cell-edge of two coordinated BSs, and (C) on the cell-edge of three coordinated BSs. In these locations, we assume that the AU is hovering at an altitude of 500m.

Since card $(\mathcal{B}) = 3$, both the sum-rate and outage probability perform the best where the AU is located at position C (i.e., the cell-edge of the three coordinated BSs). This is anticipated because position C is the central region of the three coordinated BSs. Therefore, a higher level of macro diversity can be obtained at this location. With *optimal beamwidth*, the AU also experiences zero ICI at this position, as guaranteed by Corollary 1, because the receiving coverage only covers the coordinated BS and there are no interfering BSs in the receiving coverage.

In cases where the AU is located at position A and B, it experiences ICI from interfering BSs. The performance degradation in terms of outage probability is enormous, see Fig. 7(c). Specifically, the AU's outage probability may increase from the order of 10^{-14} to 10^{-2}. Nevertheless, the ICI issue can be addressed by designing an opportunistic ATN-NOMA scheme, where card $(\mathcal{B})$ is adaptively varied. When card $(\mathcal{B})$ is adaptive, the AU can still experience zero ICI (see, section V-D and Corollary 1).

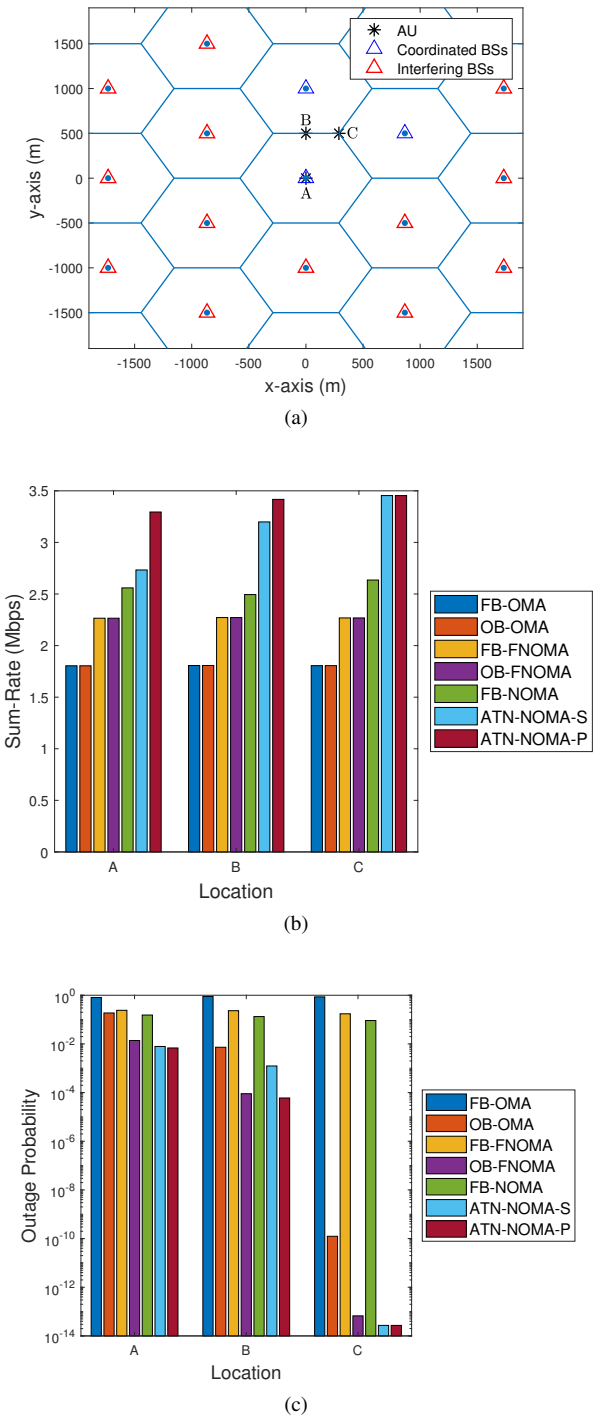

Figure 7: The effects on the 3D location of the AU: (a) locations of the AU; (b) sum-rate of the TUs; (c) outage probability.

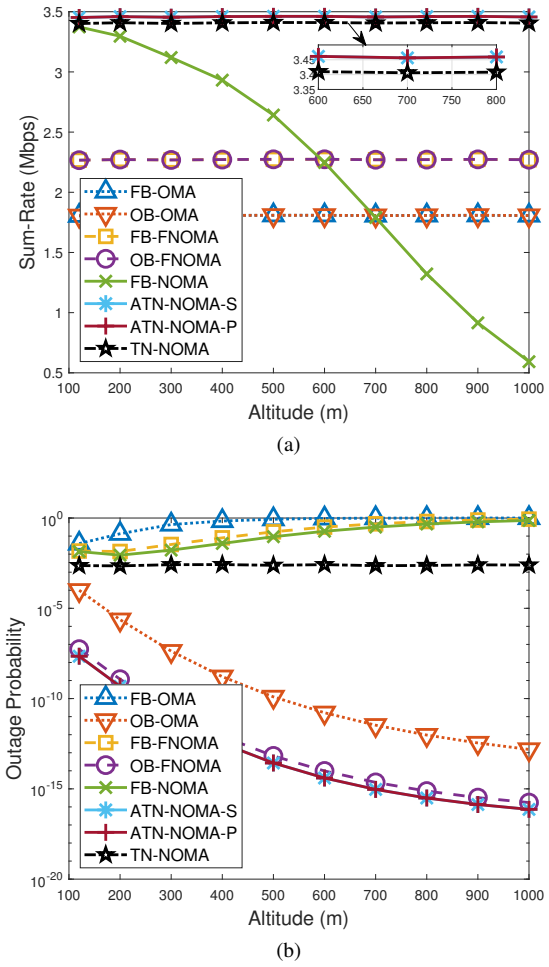

Figure 8: The performance of different pairing schemes versus AU's altitude: (a) sum-rate of the TUs; (b) outage probability.

F. AU/TUs vs. TU/TUs Pairing

The above results have shown that each of the proposed techniques is important in achieving an outstanding performance. However, it remains unclear whether the pairing of AU and TU in multi-cell networks remains beneficial as compared to the pairing of TU and TU. Thus, Fig. 8 further compares the performance of two different pairing schemes. On the one hand, we consider the pairing of the AU and the cell-center TUs (ATN-NOMA). On the other hand, we consider the pairing of the cell-edge TU and the cell-center TUs, also referred as TN-NOMA. We assume the AU and the cell-edge TU are located at position C while only the AU can vary its altitude.

Figs. 8(a) and 8(b) show that, among all of the considered schemes, only the newly proposed ATN-NOMA schemes outperform TN-NOMA in both sum-rate and outage probability. In particular, the proposed ATN-NOMA scheme achieves an average of 91% and 52% sum-rate improvement as compared to schemes based on OMA and FNOMA, respectively. As compared to TN-NOMA, the sum-rate improvement is marginal although the AU gain is 30-60 dB higher than the cell-edge TU. This phenomenon occurs because the beamforming is performed on the AU and the cell-edge TU, while the objective of the schemes is to maximize the sum-rate of the cell-center TUs subject to the minimum rate requirement of the AU or the cell-edge TU. Thus, the advantage of the beamforming actually lies on the outage probability rather than the sum-rate of the cell-center TUs.

Specifically, the outage probability of TN-NOMA is 2.5×10^{-3} whereas the outage probability of the proposed ATN-NOMA scheme is 6.25×10^{-8} to 7.3×10^{-17}. Such an outstanding performance is anticipated because aerial links are stronger. This suggests that the proposed ATN-NOMA scheme is able to support reliable communications for the AU links. Furthermore, the pairing of AU and TU in multi-cell networks remains beneficial, subject to effective mitigation of ICI.

VI. Conclusion

In this paper, we considered the downlink multi-cell networks with the co-existence of an AU and TUs. To ensure high spectral efficiency and massive connectivity, we proposed the ATN-NOMA scheme to support both AU and TUs for control and data links, respectively. In the proposed ATN-NOMA scheme, an elevation-angle based user association was employed, a directional antenna with adjustable beamwidth was implemented at the AU, and beamforming was performed by the coordinated BSs to mitigate the strong ICI issue at the AU. To guarantee the optimality of the proposed ATN-NOMA scheme, we maximized the sum-rate of the TUs by optimal beamwidth and power allocation subject to the AU's QoS requirement. The optimal beamwidth was then obtained in closed-form expression while the optimal power allocation was obtained via SCA. Furthermore, we derived the pdf, CDF, and consequently estimated the aggregated ICI in the proposed ATN-NOMA scheme. In cases where there are no interfering BSs having the same elevation-angle as the coordinated BSs, the AU experiences zero ICI, and, in such cases, we approximated the AU's outage probability analytically. Our simulation results showed that the proposed ATN-NOMA scheme significantly outperforms existing schemes in terms of the TUs' sum-rate and the AU's outage probability. When compared to the pairing of the cell-edge TU and the cell-center TUs, the proposed ATN-NOMA scheme also provided a much lower outage probability and some improvements in the sum-rate of the TUs.

Appendix A: Inter-Cell Interference with Different Interfering BS Heights

If the interfering BSs have different heights, we can approximate I_{tot} using the same method as approximating β_{tot}. Specifically, define $\mathcal{D} = \{d_1, \ldots, d_{\bar{I}}\}$ as the set of *distinctive* horizontal distance between AU and interfering BSs, and $\mathcal{I}_{d_\iota} = \left\{b \,|\, \hat{d}_{b,u} = d_\iota, \forall b \in \mathcal{I}\right\}$ as the set of interfering BSs with horizontal distance d_ι from the AU. Let $\tilde{I}_{d_\iota} = \text{card}(\mathcal{I}_{d_\iota})$ and $\tilde{L}_{d_\iota}$ be the number of LOS links among these $\tilde{I}_{d_\iota}$ interfering links. Also, define $\mathcal{L} = \left\{\left(\tilde{L}_{d_1}, \ldots, \tilde{L}_{d_{\bar{I}}}\right) | 0 \le \tilde{L}_{d_\iota} \le \tilde{I}_{d_\iota}, \iota = 1, \ldots, \bar{I}\right\}$ and $i_\iota = \left(i_{d_1}, \ldots, i_{d_{\bar{I}}}\right)$.

As discussed, $\tilde{L}_{d_\iota} \sim \text{Bino}\left(\tilde{I}_{d_\iota}, p^{\text{L}}_{b,u}\left(d_\iota, z_u\right)\right)$. Since $\tilde{L}_{d_\iota}$ is independent of $\tilde{L}_{d_{\iota'}}$ for $\iota \neq \iota'$, we have:

$$\mathbb{P}\left(\tilde{L}_{d_1} = i_{d_1}, \ldots, \tilde{L}_{d_{\bar{\iota}}} = i_{d_{\bar{\iota}}}\right) = \prod_{\tilde{L}_{d_\iota} = i_{d_\iota}, \forall \iota} f_{\tilde{L}_{d_\iota}}\left(i_{d_\iota}, \tilde{I}_{d_\iota}, p^{\text{L}}_{b,u}\left(d_\iota, z_u\right)\right).$$

Following the same line of argument in Section IV, the pdf of the generalized aggregated ICI can be approximated as:

$$\begin{aligned} & f_{I_{\text{tot}}}\left(\tau, \tilde{I}_{d_1}, \ldots, \tilde{I}_{d_{\bar{I}}}, p^{\text{L}}_{b,u}\left(d_1, z_u\right), \ldots, p^{\text{L}}_{b,u}\left(d_{\bar{I}}, z_u\right)\right) \\ \approx & \sum_{\forall i_\iota \in \mathcal{L}} \mathbb{P}\left(\tilde{L}_{d_1} = i_{d_1}, \ldots, \tilde{L}_{d_{\bar{I}}} = i_{d_{\bar{I}}}\right) f_{H^{(i_\iota)}}\left(\tau, \hat{m}, \hat{\theta}\right) \\ = & \sum_{\forall i_\iota \in \mathcal{L}} \left[\prod_{\tilde{L}_{d_\iota} = i_{d_\iota}, \forall \iota} \binom{\tilde{I}_{d_\iota}}{i_{d_\iota}} p^{\text{L}}_{b,u}\left(d_\iota, z_u\right)^{i_{d_\iota}} \times \right. \\ & \left. p^{\text{N}}_{b,u}\left(d_\iota, z_u\right)^{\left(\tilde{I}_{d_\iota} - i_{d_\iota}\right)} \frac{\tau^{\hat{m}-1} \exp\left(-\frac{\tau}{\hat{\theta}}\right)}{\hat{\theta}^{\hat{m}} \Gamma\left(\hat{m}\right)} \right]. \end{aligned}$$

where $H^{(i_\iota)} = \sum_{\forall \iota} H^{(i_{d_\iota})}$. The CDF of the generalized aggregated ICI can then be approximated as:

$$\begin{aligned} & F_{I_{\text{tot}}}\left(\tau, \tilde{I}_{d_1}, \ldots, \tilde{I}_{d_{\bar{I}}}, p^{\text{L}}_{b,u}\left(d_1, z_u\right), \ldots, p^{\text{L}}_{b,u}\left(d_{\bar{I}}, z_u\right)\right) \\ \approx & \sum_{\forall i_\iota \in \mathcal{L}} \mathbb{P}\left(\tilde{L}_{d_1} = i_{d_1}, \ldots, \tilde{L}_{d_{\bar{I}}} = i_{d_{\bar{I}}}\right) F_{H^{(i_\iota)}}\left(\tau, \hat{m}, \hat{\theta}\right) \\ = & \sum_{\forall i_\iota \in \mathcal{L}} \left[\prod_{\tilde{L}_{d_\iota} = i_{d_\iota}, \forall \iota} \binom{\tilde{I}_{d_\iota}}{i_{d_\iota}} p^{\text{L}}_{b,u}\left(d_\iota, z_u\right)^{i_{d_\iota}} \times \right. \\ & \left. p^{\text{N}}_{b,u}\left(d_\iota, z_u\right)^{\left(\tilde{I}_{d_\iota} - i_{d_\iota}\right)} \int_0^\tau \frac{\tau'^{\hat{m}-1} \exp\left(-\frac{\tau'}{\hat{\theta}}\right)}{\hat{\theta}^{\hat{m}} \Gamma\left(\hat{m}\right)} d\tau' \right]. \end{aligned}$$

REFERENCES

[1] W. K. New, C. Y. Leow, K. Navaie, and Z. Ding, "Network NOMA for co-existence of aerial and terrestrial users," in *2020 IEEE 92nd Vehicular Technology Conference (VTC2020-Fall)*, pp. 1–5, IEEE.

[2] S. Hayat, E. Yanmaz, and R. Muzaffar, "Survey on Unmanned Aerial Vehicle Networks for Civil Applications: A Communications Viewpoint," *IEEE Communications Surveys Tutorials*, vol. 18, pp. 2624–2661, Fourthquarter 2016.

[3] Y. Zeng, J. Lyu, and R. Zhang, "Cellular-Connected UAV: Potential, Challenges, and Promising Technologies," *IEEE Wireless Communications*, vol. 26, pp. 120–127, February 2019.

[4] Y. Zeng, Q. Wu, and R. Zhang, "Accessing from the sky: A tutorial on UAV communications for 5G and beyond," *Proceedings of the IEEE*, vol. 107, pp. 2327–2375, Dec 2019.

[5] X. Lin, R. Wiren, S. Euler, A. Sadam, H.-L. Maattanen, S. Muruganathan, S. Gao, Y.-P. E. Wang, J. Kauppi, Z. Zou, and V. Yajnanarayana, "Mobile network-connected drones: Field trials, simulations, and design insights," *IEEE Vehicular Technology Magazine*, vol. 14, no. 3, pp. 115–125, 2019.

[6] A. Garcia-Rodriguez, G. Geraci, D. Lopez-Perez, L. G. Giordano, M. Ding, and E. Bjornson, "The essential guide to realizing 5G-connected UAVs with massive MIMO," *IEEE Communications Magazine*, vol. 57, no. 12, pp. 84–90, 2019.

[7] "3GPP Technical Report 36.777-Enhanced LTE Support for Aerial Vehicles," tech. rep., 3rd Generation Partnership Project, 2017.

[8] Q. Technologies, "LTE unmanned aircraft systems: Trial report v1.0.1," tech. rep., May 2017.

[9] X. Lin, V. Yajnanarayana, S. D. Muruganathan, S. Gao, H. Asplund, H. Maattanen, M. Bergstrom, S. Euler, and Y. E. Wang, "The sky is not the limit: LTE for unmanned aerial vehicles," *IEEE Communications Magazine*, vol. 56, pp. 204–210, Apr. 2018.

[10] J. Stanczak, I. Z. Kovacs, D. Koziol, J. Wigard, R. Amorim, and H. Nguyen, "Mobility Challenges for Unmanned Aerial Vehicles Connected to Cellular LTE Networks," in *2018 IEEE 87th Vehicular Technology Conference (VTC Spring)*, pp. 1–5, June 2018.

[11] I. Kovacs, R. Amorim, H. C. Nguyen, J. Wigard, and P. Mogensen, "Interference analysis for UAV connectivity over LTE using aerial radio measurements," in *Proc. 2017 IEEE 86th Vehicular Technology Conference (VTC-Fall)*, pp. 1–6, Sept 2017.

[12] H. C. Nguyen and R. Amorim and J. Wigard and I. Z. Kovács and T. B. Sørensen and P. E. Mogensen, "How to Ensure Reliable Connectivity for Aerial Vehicles Over Cellular Networks," *IEEE Access*, vol. 6, pp. 12304–12317, 2018.

[13] V. Yajnanarayana, Y. Eric Wang, S. Gao, S. Muruganathan, and X. Lin Ericsson, "Interference mitigation methods for unmanned aerial vehicles served by cellular networks," in *2018 IEEE 5G World Forum (5GWF)*, pp. 118–122, July 2018.

[14] S. Euler, H. Maattanen, X. Lin, Z. Zou, M. Bergstrom, and J. Sedin, "Mobility support for cellular connected unmanned aerial vehicles: Performance and analysis," in *2019 IEEE Wireless Communications and Networking Conference (WCNC)*, pp. 1–6, April 2019.

[15] M. M. Azari, F. Rosas, and S. Pollin, "Cellular connectivity for UAVs: Network modeling, performance analysis, and design guidelines," *IEEE Transactions on Wireless Communications*, vol. 18, pp. 3366–3381, July 2019.

[16] W. Mei and R. Zhang, "Cooperative downlink interference transmission and cancellation for cellular-connected UAV: A divide-and-conquer approach," *IEEE Transactions on Communications*, vol. 68, no. 2, pp. 1297–1311, 2020.

[17] W. Mei and R. Zhang, "Aerial-ground interference mitigation for cellular-connected UAV," *IEEE Wireless Communications*, vol. 28, no. 1, pp. 167–173, 2021.

[18] B. Makki, K. Chitti, A. Behravan, and M. S. Alouini, "A Survey of NOMA: Current Status and Open Research Challenges," *IEEE Open Journal of the Communications Society*, vol. 1, pp. 179–189, 2020.

[19] Y. Liu, Z. Qin, M. Elkashlan, Z. Ding, A. Nallanathan, and L. Hanzo, "Nonorthogonal Multiple Access for 5G and Beyond," *Proceedings of the IEEE*, vol. 105, no. 12, pp. 2347–2381, 2017.

[20] Z. Ding, X. Lei, G. K. Karagiannidis, R. Schober, J. Yuan, and V. K. Bhargava, "A Survey on Non-Orthogonal Multiple Access for 5G Networks: Research Challenges and Future Trends," *IEEE Journal on Selected Areas in Communications*, vol. 35, pp. 2181–2195, Oct 2017.

[21] Z. Yang, C. Pan, W. Xu, Y. Pan, M. Chen, and M. Elkashlan, "Power Control for Multi-Cell Networks With Non-Orthogonal Multiple Access," *IEEE Transactions on Wireless Communications*, vol. 17, pp. 927–942, Feb 2018.

[22] W. Shin, M. Vaezi, B. Lee, D. J. Love, J. Lee, and H. V. Poor, "Non-Orthogonal Multiple Access in Multi-Cell Networks: Theory, Performance, and Practical Challenges," *IEEE Communications Magazine*, vol. 55, pp. 176–183, Oct 2017.

[23] A. Beylerian and T. Ohtsuki, "Coordinated Non-Orthogonal Multiple Access (CO-NOMA)," in *2016 IEEE Global Communications Conference (GLOBECOM)*, pp. 1–5, Dec 2016.

[24] J. Choi, "Non-Orthogonal Multiple Access in Downlink Coordinated Two-Point Systems," *IEEE Communications Letters*, vol. 18, pp. 313–316, February 2014.

[25] X. Sun, N. Yang, S. Yan, Z. Ding, D. W. K. Ng, C. Shen, and Z. Zhong, "Joint Beamforming and Power Allocation in Downlink NOMA Multiuser MIMO Networks," *IEEE Transactions on Wireless Communications*, vol. 17, pp. 5367–5381, Aug 2018.

[26] V. Nguyen, H. D. Tuan, T. Q. Duong, H. V. Poor, and O. Shin, "Precoder Design for Signal Superposition in MIMO-NOMA Multicell Networks," *IEEE Journal on Selected Areas in Communications*, vol. 35, pp. 2681–2695, Dec 2017.

[27] M. S. Ali, E. Hossain, and D. I. Kim, "Coordinated Multipoint Transmission in Downlink Multi-Cell NOMA Systems: Models and Spectral Efficiency Performance," *IEEE Wireless Communications*, vol. 25, pp. 24–31, April 2018.

[28] Y. Sun, Z. Ding, X. Dai, and G. K. Karagiannidis, "A Feasibility Study on Network NOMA," *IEEE Transactions on Communications*, vol. 66, pp. 4303–4317, Sep. 2018.

[29] M. S. Ali, E. Hossain, A. Al-Dweik, and D. I. Kim, "Downlink Power Allocation for CoMP-NOMA in Multi-Cell Networks," *IEEE Transactions on Communications*, vol. 66, pp. 3982–3998, Sep. 2018.

[30] Y. Tian, A. R. Nix, and M. Beach, "On the Performance of Opportunistic NOMA in Downlink CoMP Networks," *IEEE Communications Letters*, vol. 20, pp. 998–1001, May 2016.

[31] M. F. Sohail, C. Y. Leow, and S. Won, "Non-orthogonal multiple access for unmanned aerial vehicle assisted communication," *IEEE Access*, vol. 6, pp. 22716–22727, 2018.

[32] M. F. Sohail, C. Y. Leow, and S. Won, "Energy-efficient non-orthogonal multiple access for UAV communication system," *IEEE Transactions on Vehicular Technology*, vol. 68, no. 11, pp. 10834–10845, 2019.

[33] N. Rupasinghe, Y. Yapici, I. Guvenc, and Y. Kakishima, "Non-orthogonal multiple access for mmWave drone networks with limited feedback," *IEEE Transactions on Communications*, vol. 67, pp. 762–777, Jan 2019.

[34] T. Hou, Y. Liu, Z. Song, X. Sun, and Y. Chen, "Exploiting NOMA for UAV communications in large-scale cellular networks," *IEEE Transactions on Communications*, vol. 67, pp. 6897–6911, Oct 2019.

[35] W. K. New, C. Y. Leow, K. Navaie, and Z. Ding, "Robust non-orthogonal multiple access for aerial and ground users," *IEEE Transactions on Wireless Communications*, vol. 19, no. 7, pp. 4793–4805, 2020.

[36] T. Z. H. Ernest, A. S. Madhukumar, R. P. Sirigina, and A. K. Krishna, "NOMA-aided UAV communications over correlated Rician shadowed fading channels," *IEEE Transactions on Signal Processing*, vol. 68, pp. 3103–3116, 2020.

[37] X. Mu, Y. Liu, L. Guo, and J. Lin, "Non-orthogonal multiple access for air-to-ground communication," *IEEE Transactions on Communications*, vol. 68, no. 5, pp. 2934–2949, 2020.

[38] W. K. New, C. Y. Leow, K. Navaie, Y. Sun, and Z. Ding, "Application of NOMA for cellular-connected UAVs: Opportunities and challenges," *Information Sciences*, vol. 64, no. 140302, pp. 1–140302, 2021.

[39] X. Xu and Y. Zeng, "Cellular-Connected UAV: Performance Analysis with 3D Antenna Modelling," in *2019 IEEE International Conference on Communications Workshops (ICC Workshops)*, pp. 1–6, May 2019.

[40] M. M. Azari, F. Rosas, and S. Pollin, "Reshaping cellular networks for the sky: Major factors and feasibility," in *2018 IEEE International Conference on Communications (ICC)*, pp. 1–7, May 2018.

[41] R. Amer, W. Saad, and N. Marchetti, "Toward a Connected Sky: Performance of Beamforming With Down-Tilted Antennas for Ground and UAV User Co-Existence," *IEEE Communications Letters*, vol. 23, pp. 1840–1844, Oct 2019.

[42] W. K. New, C. Y. Leow, K. Navaie, Y. Sun, and Z. Ding, "Interference-aware NOMA for cellular-connected UAVs: Stochastic geometry analysis," *IEEE Journal on Selected Areas in Communications*, pp. 1–1, 2021.

[43] H. He, S. Zhang, Y. Zeng, and R. Zhang, "Joint altitude and beamwidth optimization for UAV-enabled multiuser communications," *IEEE Communications Letters*, vol. 22, pp. 344–347, Feb 2018.

[44] Z. Yang, C. Pan, M. Shikh-Bahaei, W. Xu, M. Chen, M. Elkashlan, and A. Nallanathan, "Joint altitude, beamwidth, location, and bandwidth optimization for UAV-enabled communications," *IEEE Communications Letters*, vol. 22, pp. 1716–1719, Aug 2018.

[45] A. Khidre, F. Yang, and A. Z. Elsherbeni, "Reconfigurable Microstrip Antenna with Tunable Radiation Beamwidth," in *2013 IEEE Antennas and Propagation Society International Symposium (APSURSI)*, pp. 1444–1445, July 2013.

[46] T. Debogovic, J. Perruisseau-Carrier, and J. Bartolic, "Partially Reflective Surface Antenna With Dynamic Beamwidth Control," *IEEE Antennas and Wireless Propagation Letters*, vol. 9, pp. 1157–1160, 2010.

[47] M. Elhattab, M.-A. Arfaoui, C. Assi, and A. Ghrayeb, "Reconfigurable intelligent surface assisted coordinated multipoint in downlink NOMA networks," *IEEE Communications Letters*, vol. 25, no. 2, pp. 632–636, 2021.

[48] R. Lei and D. Xu, "On the outage performance of JT-CoMP-CNOMA Networks with SWIPT," *IEEE Communications Letters*, vol. 25, no. 2, pp. 432–436, 2021.

[49] W. Mei and R. Zhang, "Uplink cooperative NOMA for cellular-connected UAV," *IEEE Journal of Selected Topics in Signal Processing*, pp. 1–1, 2019.

[50] N. Cherif, M. Alzenad, H. Yanikomeroglu, and A. Yongacoglu, "Downlink coverage and rate analysis of an aerial user in vertical heterogeneous networks (VHetNets)," *IEEE Transactions on Wireless Communications*, vol. 20, no. 3, pp. 1501–1516, 2021.

[51] C. A. Balanis, *Antenna Theory: Analysis and Design, 3rd Edition*. John wiley & sons, 2005.

[52] S. Boyd, S. P. Boyd, and L. Vandenberghe, *Convex Optimization*. Cambridge university press, 2004.

[53] P. Moscuoroums, "The Distribution of The Sum of Independent Gamma Random Variables," *Ann. Inst. Statist. Math*, vol. 37, no. Part A, pp. 541–544, 1985.

[54] S. Covo and A. Elalouf, "A Novel Single-Gamma Approximation to The Sum of Independent Gamma Variables, And A Generalization to Infinitely Divisible Distributions," *Electronic Journal of Statistics*, vol. 8, no. 1, pp. 894–926, 2014.

Aerial-Terrestrial Network NOMA for Cellular-Connected UAVs

Wee Kiat New, *Student Member*, IEEE, Chee Yen Leow, *Member*, IEEE, Keivan Navaie, *Senior Member*, IEEE, and Zhiguo Ding, *Fellow*, IEEE.

Abstract

Efficient connectivity in cellular-connected unmanned aerial vehicles (UAV)s is limited by scarcity of the radio spectrum and strong inter-cell interference (ICI). To address these issues, we propose an aerial-terrestrial network non-orthogonal multiple access (ATN-NOMA) scheme. In this proposed scheme, we pair the aerial user (AU) and terrestrial user (TU) in a NOMA setting to leverage their asymmetric channel gains and rate demands in downlink communications. In ATN-NOMA, the strong ICI issue at the AU receiver is further managed by an elevation-angle based user association, equipping the AU with an adjustable beamwidth directional antenna, and forming a beamforming among the coordinated terrestrial base stations (BS)s. We then obtain the optimal beamwidth and power allocation so that the TUs' sum-rate is maximized subject to the AU's Quality-of-Service (QoS) requirement. The corresponding optimization problem is non-convex in which we exploit the structure of the problem and apply successive convex approximation (SCA) to obtain a local optimal solution. We then derive the statistical properties, which consequently enable us to estimate the aggregated ICI. In cases where no interfering BSs have the same elevation angle as the coordinated BSs, we further approximate the AU's outage probability. We then compare the TUs' sum-rate and the outage probability of the ATN-NOMA with multiple existing schemes. Extensive simulation results show that our proposed ATN-NOMA scheme outperforms existing schemes by 52-91% in terms of the sum-rate, and its analytical

This work was supported in part by the Ministry of Higher Education Malaysia and Universiti Teknologi Malaysia under Grant 4J416, Grant 08G83, Grant 19H58, and Grant 04G37, Grant 09G15, and Grant 00L27. Part of this paper has been presented in IEEE VTC2020-Fall [1]. Wee Kiat New (email: weekiat@graduate.utm.my) and Chee Yen Leow (email: bruceleow@fke.utm.my) are with the Wireless Communication Centre, School of Electrical Engineering, Faculty of Engineering, Universiti Teknologi Malaysia, 81310 Skudai, Johor, Malaysia; Keivan Navaie (e-mail: k.navaie@lancaster.ac.uk) is with the School of Computing and Communications, Lancaster University, Lancaster, LA1 4WA, United Kingdom; Zhiguo Ding (e-mail: zhiguo.ding@manchester.ac.uk) is with the School of Electrical and Electronic Engineering, the University of Manchester, Manchester, M13 9PL, United Kingdom.

outage probability can be as low as the order of 10^{-17}. Furthermore, we show that the pairing of AU and TU in multi-cell networks remains beneficial, subject to effective mitigation of ICI.

Index Terms

Non-Orthogonal Multiple Access, Cellular-Connected UAV, Coordinated Multi-Point Transmission, Inter-cell Interference

I. Introduction

Unmanned aerial vehicles (UAV)s have emerged as promising tools in civil applications such as agriculture, construction, delivery, inspection, and surveillance [2]. Serving UAVs as aerial users (AU)s in the existing cellular networks enables beyond visual line-of-sight operation. Such idea is referred to as cellular-connected UAVs [3], [4]. Field trials and simulation studies have been conducted to verify the feasibility of cellular-connected UAVs in 4th generation (4G) [5] and 5th generation (5G) cellular networks [6]. Preliminary results show that the idea is feasible.

Co-existence of AUs and terrestrial users (TU)s, however, introduces new challenges to the operation of cellular networks. One of the key issues is strong inter-cell interference (ICI) at the AUs. In general, AUs that are hovering at a high altitude establish line-of-sight (LOS) links with their associated terrestrial base stations (BS)s. Nevertheless, as analyzed in [7]–[10], AUs also establish LOS links with other terrestrial BSs. This causes strong ICI at the AUs, where other terrestrial BSs transmit to their associated users via the same resource block (RB). Due to high altitudes and LOS links, the ICI at the AUs is much stronger than that of the TUs located at the cell-edge.

To address this issue, [11], [12] have examined the applications of the conventional interference mitigation techniques, such as antenna beam selection and coordinated multi-point (CoMP) transmission. To ensure a reliable cell-acquisition for the AUs, [13] exploits the coverage extension feature of long-term evolution networks, which can achieve a higher maximum coupling loss and alleviate the ICI. Similarly, [14] shows that the coverage extension feature can better support the mobility of the AUs. Nevertheless, severe ICI issue remains unsolved by these conventional techniques.

In [15], the use of a tilted directional antenna with a fixed beamwidth is explored, and furthermore [16] proposes a new cooperative beamforming and interference cancellation (CB-ITC) technique. Nevertheless, the use of a tilted antenna with fixed beamwidth is only beneficial

for a low or intermediate network density [15]. Moreover, CB-ITC can only be employed for low user density [16]. Different types of aerial-ground interference mitigation techniques are also compared in [17] for evaluation purpose. Many works (e.g., [7]–[17]) focus on orthogonal multiple access (OMA) to support both AUs and TUs. Although OMA avoids multi-user interference in a single-cell network, its spectral efficiency and number of concurrent connections are fundamentally limited as each orthogonal RB can only be assigned to a single user.

To overcome these limitations, non-orthogonal multiple access (NOMA) has been proposed for beyond 5th generation cellular networks [18]–[20]. By leveraging superposition coding (SC) at the transmitter and successive interference cancellation (SIC) at the receiver, NOMA allows multiple users to share the same RB. With the same amount of radio resources, NOMA enhances the spectral efficiency and enables massive connectivity. Nevertheless, using NOMA in multi-cell networks is also challenged by the ICI problem, i.e., mainly for the cell-edge users. There are several promising solutions to this problem. For instance, [21] proposes an optimal coefficient and power allocation in a multi-cell NOMA system. It is further shown in [21] that utilization of power control technique is sufficient to reduce the ICI level resulting in outperforming an equivalent OMA system.

Several efficient coordinated multi-point (CoMP) techniques have also been proposed to enhance the NOMA performance in multi-cell networks [22]. For example, [23], [24] have proposed coordinated scheduling (CS)-NOMA to mitigate the ICI of the cell-edge users. To further improve the spectral efficiency, [25], [26] have proposed coordinated beamforming (CB)-NOMA to eliminate the ICI of the cell-edge users via precoding. CB-NOMA is, however, not applicable to all scenarios because the dimension of the user channels may be different, e.g., the cell-edge user experiences multiple channels from neighboring cell while a cell-center user experiences a single channel from its serving cell [27].

To address this issue, joint transmission (JT)-NOMA, also known as network NOMA [28], has been proposed. In network NOMA, each coordinated BS pairs a non-CoMP user and a CoMP user over the same RB. The non-CoMP user is referred to as a user who is independently served by its associated BS and the CoMP user is referred to as a user who is jointly served by a set of coordinated BSs [27], [29]. In [28], the analytical outage probability of network NOMA with fixed power allocation is derived and in [29], a distributed power allocation that maximizes the users' sum-rate is investigated. Later, an opportunistic network NOMA is proposed, where some users are served by network NOMA and some are served by basic NOMA [30]. Nevertheless,

[21]–[30] do not consider the co-existence of AUs and TUs, and, therefore, strong ICI issue at the AUs in the multi-cell NOMA networks remains to be addressed.

Some existing studies on NOMA-enabled UAV communications have been conducted in recent years. On the one hand, existing works (e.g., [31]–[34]) have considered the applications of aerial base stations. On the other hand, existing works have focused on the applications of AUs. Pertaining to the latter, [35] has proposed a robust NOMA scheme to serve AUs and TUs for control and data links, respectively, and [36] has derived the outage probability and finite SINR diversity gain where multiple AUs are served by a terrestrial BS. Nevertheless, the ICI issue at the AUs is not considered in [35], [36]. Besides, [37] has proposed an optimal trajectory and user association that minimizes the AU's mission completion time. In [37], the ICI of AU is considered but no ICI mitigation technique is proposed.

Mitigating strong ICI of the AUs is a very challenging problem [38]. Several mechanisms need to be carefully designed. In particular, [39] shows that the AUs' user association plays an important role in determining the AUs' performance. [40] shows that using directional antenna with fixed beamwidth at the AUs leads to a tradeoff between the coverage and the ICI level. Also, [41] shows that the use of beamforming improves the performance of the AUs. Besides, [42] verifies that efficient usage of NOMA for aerial-terrestrial multi-cell networks requires a combination of an appropriate user association, receive antenna, and interference mitigation technique.

Due to the aforementioned motivations, we propose an aerial-terrestrial network NOMA (ATN-NOMA) scheme. In this scheme, we propose an elevation-angle based user association for the AUs. Specifically, the AUs are associated to a set of coordinated BSs that have the largest elevation angle to the AUs. This enables the AUs to have a higher probability of experiencing LOS to the coordinated BSs, and a lower probability of LOS with the interfering BSs. Inspired by [43], [44], we then propose the use of a directional antenna with adjustable beamwidth at the AU receivers. The use of a directional antenna with adjustable beamwidth has been applied in various applications such as satellite communication and remote sensing. There are at least two antenna designs to enable adjustable beamwidth such as the re-configurable parasitic element [45] or switchable partially reflective surface [46] that are placed in the vicinity of a single antenna source. In addition, we propose employing network NOMA, so that beamforming can be used as an extra tool to tackle the severe ICI at the AUs. As shown later in this paper, these combinations can result in zero ICI of the AUs with limited number of coordinated BSs.

In this paper, we consider the downlink multi-cell networks with the co-existence of an AU and TUs. We assume that the coordinated BSs are simultaneously serving the AU as well as their own associated TUs via NOMA. The objective of the proposed ATN-NOMA scheme is subject to efficient TUs' sum-rate and while AU's reliable connectivity is emphasized. Since the control link is directly related to the safe operation of the UAV, a corresponding QoS requirement is imposed. We then investigate the maximum sum-rate of the TUs subject to AU's QoS requirement. The major contributions of this paper are summarized as follows.

- We propose a novel ATN-NOMA scheme for the co-existence of AUs and TUs. Specifically, we pair the AU and TU in a NOMA setting to leverage their asymmetric channel and rate demand characteristics. In our proposed scheme, we employ the elevation-angle based user association, the use of a directional antenna with adjustable beamwidth at the AU, and network NOMA to address the strong ICI issue at the AU.
- We then formulate an optimization problem to maximize the sum-rate of the TUs by optimal beamwidth and power allocation subject to the AU's QoS requirement. A local optimal solution is also obtained for the non-convex optimization problem by exploiting the structure of the problem and applying successive convex approximation (SCA).
- By leveraging the unique properties of the proposed scheme and the statistical channel state information (CSI), we derive the probability density function (pdf) and cumulative distribution function (CDF) of the aggregated ICI experienced at the AU. Deriving the statistical properties is a challenging task because the aggregated ICI is generally the sum of independent non-identical gamma random variables conditioned by the number of LOS/NLOS links. Utilizing the derived statistical properties, the aggregated ICI at the AU can be estimated reliably.
- Based on the techniques we have developed, we further outline a criterion where AU experiences zero ICI. Specifically, AU experiences zero ICI when there are no interfering BSs having the same elevation angle as the coordinated BSs. In such cases, we further approximate the AU's outage probability. This analytical result helps to verify the superiority of the proposed ATN-NOMA scheme in terms of outage probability, and confirms that the proposed ATN-NOMA scheme is able to support reliable communications for the AU's links.
- Extensive simulation results with different network parameters and settings are presented.

Our simulation results provide quantitative insights on the effects of AU's interference, and also reveal the key factors that determine the performance of our proposed scheme at a fundamental level.

We note that this paper is a substantial extension of our previous work [1]. In this paper, we further consider the ICI of the TUs. By exploiting the structure of the problem and applying SCA, we also obtain a local optimal solution of the corresponding non-convex optimization problem. Besides, this paper considers an elevation-angle based user association, which subsequently allows us to outline the criterion where AU experiences zero ICI. Furthermore, the statistical properties of the aggregated ICI are derived and the AU's outage probability is approximated. Extensive simulation results over various network parameters and settings are also presented. In addition, in this paper, we demonstrate that the pairing of AU and TU in multi-cell networks remains beneficial as compared to the pairing of TU and TU, subject to effective mitigation of ICI.

The rest of the paper is organized as follows: Section II details the system model and the proposed scheme, and Section III presents the solution to maximize the sum-rate of the TUs subject to the AU's QoS requirement. Section IV then presents the statistical properties of the aggregated ICI in the proposed scheme as well as the analytical outage probability. The simulation results are provided in Section V followed by the conclusion drawn in Section VI.

Notations: In this paper, scalar parameters/variables are denoted by italic letters (e.g., c), vectors are denoted by boldface letters (e.g., $\boldsymbol{c}$), and card(C) denotes the cardinality of set C. Besides, $c \sim \text{Gamma}(m, \theta)$ denotes that c is a gamma distributed random variable with rate, m, and scale, θ, while $c \sim \text{Bino}(n, p)$ denotes that c is a binomial distributed random variable with n trials and probability of p. Furthermore, $\|\cdot\|$ denotes Euclidean norm, $\log(\cdot)$ denotes logarithm with base 2, $(\cdot)^T$ denotes transpose, and $(\cdot)^H$ denotes conjugate transpose.

II. System Model and The Proposed Scheme

As shown in Fig. 1, we consider a downlink wireless communication system with multiple terrestrial BSs in a subregion, $\mathcal{A}$. In this paper, we focus on the performance of a set of non-CoMP users and a CoMP user over an orthogonal RB as in [27], [28], [47], [48]. In our proposed scheme, the non-CoMP users are the cell-center TUs who are not significantly affected by ICI, and the CoMP user is the AU who suffers strong ICI. No cell-edge TU is considered in our proposed scheme.

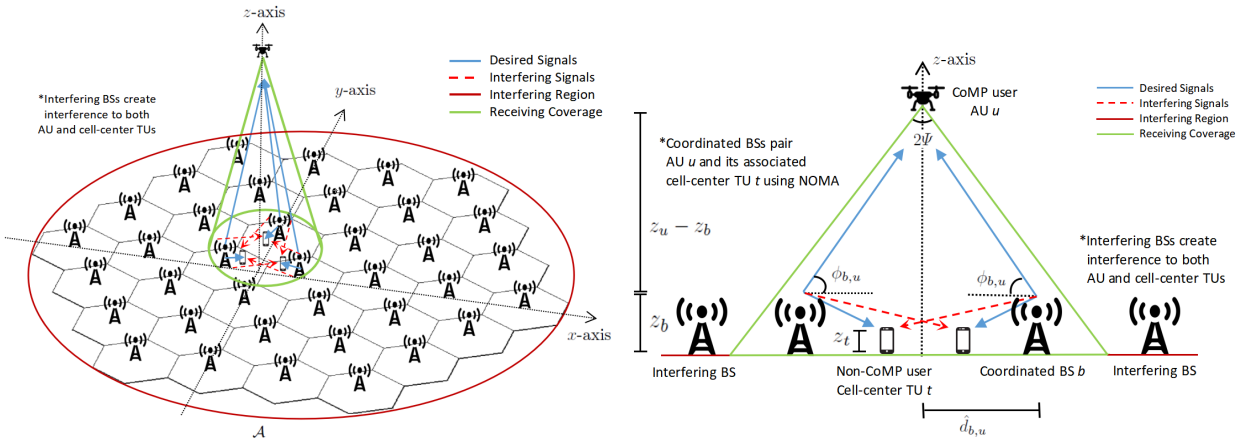

Figure 1: A schematic of downlink multi-cell networks with AU and TUs: (a) 3-dimensional; (b) 2-dimensional.

Similar to existing network NOMA schemes, our proposed scheme can be used to serve multiple CoMP users (e.g., AUs) and non-CoMP users (e.g., cell-center TUs) by using a multi-carrier NOMA system. Specifically, a CoMP user and multiple non-CoMP users can be paired over a single orthogonal RB. Different pairs of CoMP users and non-CoMP users can then be served by using different orthogonal RBs.

We denote the subscript, u, as the AU, $t \in \mathcal{T} = \{1, \ldots, T\}$, as the associated cell-center TUs, $b \in \mathcal{B} = \{1, \ldots, B\}$, as the coordinated terrestrial BSs with $T = B > 1$, and $\mathcal{I} = \{B+1, B+2, \ldots, I\}$, as the set of interfering terrestrial BSs. The cell-centered TUs are TUs not located near to the cell-edge, and the interfering BSs are non-coordinated terrestrial BSs that transmit to their own users via the same RB. For brevity, we assume a fixed card$(\mathcal{B})$.

According to [16], [49], we assume that the locations of the terrestrial BSs are distributed according to the hexagonal cellular structure with a radius of r_0 and a height of z_b within a subregion $\mathcal{A}$. The locations of the associated cell-center TUs are uniformly distributed around their associated BS with a maximum distance of $\frac{r_0}{2}$ and a fixed height of z_t.

Without loss of generality, we assume that the cell-center TU, $t \in \mathcal{T}$, is associated to the BS, $b \in \mathcal{B}$, if $t = b$, and the cell-center TU, $t \in \mathcal{T}$, is not associated to the BS, $b \in \mathcal{B}$, if $t \neq b$. We denote $\boldsymbol{w}^{\text{AU}} = [x_u, y_u, z_u]^T$, $\boldsymbol{w}_t^{\text{TU}} = [x_t^{\text{TU}}, y_t^{\text{TU}}, z_t^{\text{TU}}]^T$, and $\boldsymbol{w}_b^{\text{BS}} = \left[x_b^{\text{BS}}, y_b^{\text{BS}}, z_b^{\text{BS}}\right]^T$ as the 3D location of the AU, TU t, and BS b, respectively. The Euclidean distance between TU t and BS

b is:

$$d_{b,t} = \left\| \boldsymbol{w}_t^{\mathrm{TU}} - \boldsymbol{w}_b^{\mathrm{BS}} \right\|, \tag{1}$$

and the Euclidean distance between the AU and BS b is:

$$d_{b,u} = \left\| \boldsymbol{w}^{\mathrm{AU}} - \boldsymbol{w}_b^{\mathrm{BS}} \right\|. \tag{2}$$

Let $\hat{\boldsymbol{w}}_b^{\mathrm{BS}} \triangleq \left[x_b^{\mathrm{BS}}, y_b^{\mathrm{BS}}\right]^T$ and $\hat{\boldsymbol{w}}^{\mathrm{AU}} \triangleq [x_u, y_u]^T$ be the 2D coordinates of the BS b and AU, respectively. We then denote the horizontal distance between AU and BS b as $\hat{d}_{b,u} = \left\| \hat{\boldsymbol{w}}^{\mathrm{AU}} - \hat{\boldsymbol{w}}_b^{\mathrm{BS}} \right\|$.

A. Aerial-Terrestrial Channel Model

According to [15], [50], the aerial communication link between the AU and the BS b follows the probabilistic LOS/NLOS model. Denote $\upsilon \in \{\mathrm{L},\ \mathrm{N}\}$ as the types of links, where, L, and, N, represent the LOS and NLOS links, respectively. The probability of LOS between the AU and BS b is:

$$p_{b,u}^{\mathrm{L}}\left(\hat{d}_{b,u}, z_u\right) = -\varphi \cdot \exp\left(-\xi \cdot \phi_{b,u}\right) + \zeta, \tag{3}$$

where $\phi_{b,u}$ is the elevation angle between the AU and BS b. In (3), φ, ξ, and ζ are constant coefficients related to the communication environment [50]. The probability of NLOS between the AU and BS b is $p_{b,u}^{\mathrm{N}}\left(\hat{d}_{b,u}, z_u\right) = 1 - p_{b,u}^{\mathrm{L}}\left(\hat{d}_{b,u}, z_u\right)$.

Given link type, υ, the channel gain between the AU and BS b is:

$$\left|h_{b,u}^{\upsilon}(\Psi)\right|^2 = \Xi_{b,u}^{\upsilon}(\Psi)\left|\Omega_{b,u}^{\upsilon}\right|^2, \upsilon \in \{\mathrm{L},\ \mathrm{N}\}, \tag{4}$$

where $\Xi_{b,u}^{\upsilon}(\Psi) \triangleq \frac{E_u F G_u^{\mathrm{rx}}(\Psi)}{{d_{b,u}}^{\alpha_\upsilon}}$, and $\left|\Omega_{b,u}^{\upsilon}\right|^2$ are the large and small-scale fading effects, respectively. In large-scale fading, $\Xi_{b,u}^{\upsilon}(\Psi)$, E_u is the BS's side lobe antenna gain, $F = \left(\frac{4\pi f_{\mathrm{c}}}{c}\right)^{-2}$ is the attenuation loss at the operating frequency f_{c}, $G_u^{\mathrm{rx}}(\Psi)$ is the receiving antenna gain at the AU with a beamwidth Ψ, and α_υ denotes the aerial pathloss exponents. In (4), $\left|\Omega_{b,u}^{\upsilon}\right|^2 \sim$ Gamma $(m_u^{\upsilon}, \theta_u^{\upsilon})$.

The channel gain between the TU t and BS b is:

$$|h_{b,t}|^2 = \Xi_{b,t}\left|\Omega_{b,t}\right|^2. \tag{5}$$

In (5), $\Xi_{b,t} \triangleq \frac{E_t F G_t^{\mathrm{rx}}}{{d_{b,t}}^{\alpha}}$, and $|\Omega_{b,t}|^2$ are the large and small-scale fading effects, respectively. In the large-scale fading effect, $\Xi_{b,t}$, E_t is the BS's main lobe antenna gain, G_t^{rx} is the receiving antenna gain at the TU t, and α is the terrestrial pathloss exponent. Moreover, $|\Omega_{b,t}|^2 \sim$ Gamma $(m_{\mathrm{t}}, \theta_{\mathrm{t}})$. We assume that the TUs are equipped with omni-directional antenna and thus $G_t^{\mathrm{rx}} = 1, \forall t$. In practice, we have $\alpha \geq \alpha_{\mathrm{N}} \geq \alpha_{\mathrm{L}}$, and $m_u^{\mathrm{L}} \geq m_u^{\mathrm{N}} \geq m_t$.

B. ATN-NOMA: Elevation-Angle Based User Association

The proposed ATN-NOMA scheme consists of three mechanisms: user association, receiving, and transmitting strategies. To enable AU to have a higher probability of LOS with the coordinated BSs, $b \in \mathcal{B}$, and a lower probability of LOS with the interfering BSs, $b \in \mathcal{I}$, we propose an elevation-angle based user association. The elevation angle between the AU and BS b is $\phi_{b,u} = \tan^{-1}\left(\frac{z_u - z_b}{\hat{d}_{\mathrm{b,u}}}\right)$. In the elevation-angle based user association, the AU is served by the terrestrial BSs that have the B largest elevation-angle, so that:

$$\phi_{b,u} \geq \phi_{b'',u}\,, \quad \forall b \in \mathcal{B}, \forall b'' \in \mathcal{I}. \tag{6}$$

As seen later in this paper, the property in (6) is very useful in characterizing the ICI.

C. ATN-NOMA: Transmitting and Receiving Strategies

Based on the unique characteristics of the aerial-terrestrial networks, we design efficient receiving and transmitting strategies. In this scheme, a single directional antenna with adjustable beamwidth is implemented at the AU. The antenna is pointing directly below the AU (i.e., $\hat{\boldsymbol{w}}^{\mathrm{AU}}$). We denote ψ_u^{a} and ψ_u^{e} as the azimuth and elevation angles at the AU, respectively. The azimuth and elevation half-power beamwidth are assumed equal and they are denoted by 2Ψ, where $\Psi \in \left(0, \frac{\pi}{2}\right)$. According to [51], (eq. 2.2-2.51), the antenna gain in the direction of $(\psi_u^{\mathrm{a}}, \psi_u^{\mathrm{e}})$ is:

$$G_u^{\mathrm{rx}}(\Psi) = \begin{cases} \frac{G_{\mathrm{ref}}}{\Psi^2}, & \text{if } 0 \leq \psi_u^{\mathrm{a}} \leq \Psi, 0 \leq \psi_u^{\mathrm{e}} \leq \Psi, \\ G_0 \approx 0, & \text{otherwise}, \end{cases} \tag{7}$$

where $G_{\mathrm{ref}} \approx 2.2856$, and G_0 denotes the antenna gain outside the beamwidth of the directional antenna[1]. For any given $\boldsymbol{w}^{\mathrm{AU}}$, the receiving coverage of the AU is:

$$\mathcal{K}(\Psi) = \left\{ \boldsymbol{w}_k \;\middle|\; \begin{array}{c} x = (z_u - c_u)\tan\Psi\cos\psi, \\ y = (z_u - c_u)\tan\Psi\sin\psi, \\ z = c_u\,,\; c_u \in [0, z_u]\,, \psi \in [0, 2\pi)\,, \end{array} \right\}, \tag{8}$$

where $\boldsymbol{w}_k = [x + x_u, y + y_u, z]^T$, $\mathcal{K}(\Psi)$ is a cone, $\boldsymbol{w}^{\mathrm{AU}}$ is the apex of the cone, $z_u \tan\Psi$ is the radius of the cone base, and z_u is the height of the cone (see, Fig. 2).

[1]Similar to [15], [42]–[44], for brevity, we assume $G_o = 0$.

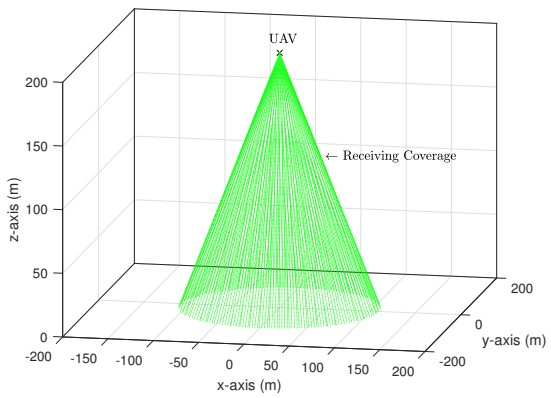

Figure 2: The AU receiving coverage, for $\boldsymbol{w}^{\text{AU}} = [0, 0, 200]^T$, $\Psi = 0.5$.

In addition, we adopt network NOMA that is promising to the pairing of cell-center TUs and AU. In the context of ATN-NOMA, each coordinated BS, $b \in \mathcal{B}$, pairs its associated cell-center TU t (i.e., the non-CoMP user) and the AU (i.e., the CoMP user) over the same RB. In each cell, the pairing consists of only two users to ensure low co-channel interference, hardware complexity, and processing delay [35]. Due to the high-altitude, the AU is a common user among the coordinated BSs. Hence, each coordinated terrestrial BS, $b \in \mathcal{B}$, transmits the following signal to jointly form maximum ratio transmission (MRT) beamforming to the AU[2]:

$$\tilde{S}_b = \frac{h^v_{b,u}(\Psi)}{\left\|\boldsymbol{h}^{\boldsymbol{v}}_{\boldsymbol{b,u}}(\boldsymbol{\Psi})\right\|}\sqrt{\rho_{b,u}P_{\text{tx}}}s_u + \frac{h^v_{b,u}(\Psi)}{\left\|\boldsymbol{h}^{\boldsymbol{v}}_{\boldsymbol{b,u}}(\boldsymbol{\Psi})\right\|}\sqrt{\rho_b P_{\text{tx}}}s_b, \tag{9}$$

where $\boldsymbol{h}^{\boldsymbol{v}}_{\boldsymbol{b,u}}(\boldsymbol{\Psi}) = \left[h^v_{1,u}(\Psi), \ldots, h^v_{B,u}(\Psi)\right]$ is the complex channel vector among the coordinated BS $b \in \mathcal{B}$, $h^v_{b,u}(\Psi)$ is the complex channel tap between BS b and the AU, $\frac{h^v_{b,u}(\Psi)}{\left\|\boldsymbol{h}^{\boldsymbol{v}}_{\boldsymbol{b,u}}(\boldsymbol{\Psi})\right\|}$ is the beamforming phase from the BS b to the AU and P_{tx} is the total transmit power at the BS. Note that, the cell-center TU t is associated to the BS b if $t = b$. Furthermore, s_u and s_b are random signals intended for AU and the associated cell-center TU b, respectively, with $\mathbb{E}\left[|s_u|^2\right] = \mathbb{E}\left[|s_b|^2\right] = 1$. Besides, $\rho_{b,u}$ and ρ_b are the power coefficients assigned to AU and the associated cell-center TU b, respectively, where $\rho_{b,u} + \rho_b \leq 1$.

Unlike terrestrial cell-edge user, AU experiences strong ICI from other BSs due to its high altitude. The received signal at the AU is:

[2]The MRT beamforming is suboptimal in a multi-cell setting, however, we choose this beamforming because its closed-form expression allows us to characterize the AU's outage probability.

$$y_u^{\mathrm{rx}} = \sum_{\forall b \in \mathcal{B}} h_{b,u}^{v}(\Psi)^H \tilde{S}_b + \underbrace{\sum_{\forall b'' \in \mathcal{I}} h_{b'',u}^{v}(\Psi)^H \tilde{S}_{b''}}_{\text{ICI term}} + \sigma_{\mathrm{u}}, \tag{10}$$

where $\sigma_u \sim \mathcal{CN}(0, \sigma_{\mathrm{n}}^2)$ is the additive white Gaussian noise (AWGN) observed at the AU and σ_{n}^2 is the noise power level. In order to decode its own signal, AU has to treat $s_b, \forall b \in \mathcal{B}$, and $\tilde{S}_{b''}, \forall b'' \in \mathcal{I}$, as noise [3]. Hence, the signal-to-interference-plus-noise ratio (SINR) at the AU is:

$$\mathrm{SINR}_u = \frac{\sum\limits_{\forall b \in \mathcal{B}} \rho_{b,u} N \left| h_{b,u}^{v}(\Psi) \right|^2}{\sum\limits_{\forall b \in \mathcal{B}} \rho_b N \left| h_{b,u}^{v}(\Psi) \right|^2 + \sum\limits_{\forall b'' \in \mathcal{I}} N \left| h_{b'',u}^{v}(\Psi) \right|^2 + 1}, \tag{11}$$

where $N = \frac{P_{\mathrm{tx}}}{B_{\mathrm{w}} \cdot \sigma_{\mathrm{n}}^2}$ is the normalized transmit signal-to-noise ratio (SNR) and B_{w} is the system bandwidth. The achievable rate of AU is therefore:

$$R_u = B_{\mathrm{w}} \log\left(1 + \mathrm{SINR}_u\right). \tag{12}$$

At the terrestrial platform, the signal observed by the cell-center TU t is:

$$y_t^{\mathrm{rx}} = \tilde{h}_{b,t}^H \tilde{S}_b + \sum_{\forall b' \in \mathcal{B} \setminus b} \tilde{h}_{b',t}^H \tilde{S}_{b'} + \sum_{\forall b'' \in \mathcal{I}} \tilde{h}_{b'',t}^H \tilde{S}_{b''} + \sigma_t, \tag{13}$$

where $\tilde{h}_{b,t}$ is the complex channel tap from its associated BS b to the cell-center TU t such that $b = t$, $\tilde{h}_{b',t}$ and $\tilde{h}_{b'',t}$ are the complex channel tap from non-associated BS b' and b'', respectively, to the cell-center TU t such that $b' \neq t$ and $b'' \neq t$, and $\sigma_t \sim \mathcal{CN}(0, \sigma_{\mathrm{n}}^2)$ is the AWGN observed at t. We denote $h_{b,t} = \frac{\tilde{h}_{b,t}^H h_{b,u}^{v}(\Psi)}{\left\| \boldsymbol{h}_{\boldsymbol{b,u}}^{\boldsymbol{v}}(\boldsymbol{\Psi}) \right\|}$. To decode its own message, the associated cell-center TU t carries out SIC by first removing the message to AU, where:

$$\mathrm{SINR}_t^{(u)} = \frac{\sum\limits_{\forall b \in \mathcal{B}} \rho_{b,u} N \left| h_{b,t} \right|^2}{\sum\limits_{\forall b \in \mathcal{B}} \rho_b N \left| h_{b,t} \right|^2 + \sum\limits_{\forall b'' \in \mathcal{I}} N \left| h_{b'',t} \right|^2 + 1}. \tag{14}$$

Following the principle of NOMA, the associated cell-center TU t decodes its own message with the following SINR:

$$\mathrm{SINR}_t = \frac{\rho_b N \left| h_{b,t} \right|^2}{\sum\limits_{\forall b' \in \mathcal{B} \setminus b} \rho_{b'} N \left| h_{b',t} \right|^2 + \sum\limits_{\forall b'' \in \mathcal{I}} N \left| h_{b'',t} \right|^2 + 1}. \tag{15}$$

The achievable rate of TU t is therefore:

$$R_t = B_{\mathrm{w}} \log\left(1 + \mathrm{SINR}_t\right). \tag{16}$$

[3]The reverse SIC order, where the AU performs SIC and cell-center TUs treat AU's message as noise, has been considered. Nevertheless, such a SIC order is not promising in ATN-NOMA because the SIC at the AU might fail due to strong ICI. To ensure reliable communications to the AU, we assume the AU treats cell-center TUs' messages as noise and the cell-center TUs perform SIC.

III. Optimal Beamwidth and Power Allocation

The objective of ATN-NOMA is to efficiently serve the TUs' link and reliably support the AU's link. For this reason, we maximize the sum-rate of the cell-center TUs by optimal beamwidth and power allocation subject to the AU's QoS requirement (i.e., reliability). The optimization problem can be formulated as follows:

$$\max_{\Psi,\, \boldsymbol{\rho_{b,u}},\, \boldsymbol{\rho_b}} \quad \sum_{\forall b \in \mathcal{B}} R_b, \tag{17a}$$

$$\text{s.t.} \quad R_u \geq R_{\min}, \tag{17b}$$

$$B_{\mathrm{w}} \log(1 + \mathrm{SINR}_b^{(u)}) \geq R_{\min}, \forall b \in \mathcal{B}, \tag{17c}$$

$$0 \leq \rho_b\,,\ 0 \leq \rho_{b,u}, \forall b \in \mathcal{B}, \tag{17d}$$

$$\rho_b + \rho_{b,u} \leq 1, \forall b \in \mathcal{B}, \tag{17e}$$

$$\boldsymbol{w}_b^{\mathrm{BS}} \subseteq \mathcal{K}\left(\Psi\right), \forall b \in \mathcal{B}, \tag{17f}$$

where $\boldsymbol{\rho_{b,u}} = [\rho_{1,u}, \ldots, \rho_{B,u}]^T$ and $\boldsymbol{\rho_b} = [\rho_1, \ldots, \rho_B]^T$. (17a) is the sum-rate of the cell-center TUs, constraint (17b) ensures the AU's QoS requirement is satisfied, and (17c) ensures that each associated cell-center TU can decode the AU information successfully. In addition, (17d) ensures the power coefficients are non-negative, (17e) ensures the power allocation is feasible, and (17f) ensures the coordinated BSs are within the receiving coverage of the AU so that the ATN-NOMA can be performed. Note that, the formulation in (17) is expressed using the fact that the cell-center TU $t \in \mathcal{T}$ is associated to the BS $b \in \mathcal{B}$ if $t = b$.

Problem (17) is a non-convex optimization problem due to (17a), (17b), and (17c). Furthermore, the optimization variables are mutually coupled. To find the optimal solution, we exploit the structure of the problem (17). Note that (17a), (17c), (17d) and (17e) are independent of Ψ. To obtain the optimal beamwidth, we use the following propositions:

Proposition 1. *R_u is a non-increasing function of Ψ.*

Proof: Substituting (4) and (7) into (12), yields

$$R_u = B_{\mathrm{w}} \log \left(1 + \frac{\sum\limits_{\forall b \in \mathcal{B}} \frac{\Upsilon_b^{\upsilon} \rho_{b,u}}{\Psi^2}}{\sum\limits_{\forall b \in \mathcal{B}} \frac{\Upsilon_b^{\upsilon} \rho_b}{\Psi^2} + \sum\limits_{\forall b \in \mathcal{I}} \frac{\Upsilon_b^{\upsilon}}{\Psi^2} + 1} \right). \tag{18}$$

where $\Upsilon_b^{\upsilon} = \frac{NE_uFG_{ref}|\Omega_{u,\upsilon}|^2}{{d_{b,u}}^{\alpha_\upsilon}}$. Taking the derivative of R_u w.r.t. Ψ, yields:

$$\frac{\partial R_u}{\partial \Psi} = \frac{-2B_{\mathrm{w}}\Psi \sum\limits_{\forall b\in\mathcal{B}} \Upsilon_b^{\upsilon}\rho_{b,u}}{\ln(2)\, c_1 \cdot c_2} \leq 0, \tag{19}$$

where $c_1 = \left(\Psi^2 + \sum\limits_{\forall b\in\mathcal{B}} \Upsilon_b^{\upsilon}\left(\rho_b + \rho_{b,u}\right) + \sum\limits_{\forall b\in\mathcal{I}} \Upsilon_b^{\upsilon}\right)$ and $c_2 = \left(\Psi^2 + \sum\limits_{\forall b\in\mathcal{B}} \Upsilon_b^{\upsilon}\rho_b + \sum\limits_{\forall b\in\mathcal{I}} \Upsilon_b^{\upsilon}\right)$. ■

Interestingly, this suggests that the desired signal of the AU always increases more than the ICI level if the beamwidth is reduced and it is independent of the number of coordinated BSs and interfering BSs.

Proposition 2. *The optimal bandwidth Ψ^* in* (17) *is* $\Psi^* = \tan^{-1}\left(\arg\max\limits_{b\in\mathcal{B}} \frac{\left\|\hat{\boldsymbol{w}}_b^{BS} - \hat{\boldsymbol{w}}^{AU}\right\|}{(z_u - z_b)}\right)$.

Proof: Since (17a), (17c), (17d) and (17e) are independent of Ψ, and according to proposition 1, R_u is a non-increasing function of Ψ, the optimal bandwidth Ψ in (17) can be equivalently obtained by solving the following convex optimization problem:

$$\min_{\Psi} \qquad \Psi, \tag{20a}$$

$$\text{s.t.} \qquad \hat{d}_{b,u} \leq (z_u - z_b)\tan\Psi, \qquad \forall b \in \mathcal{B}. \tag{20b}$$

To obtain the closed form solution in (20), we denote $b' = \left\{b \,|\, \arg\max\limits_{b\in\mathcal{B}} \frac{\left\|\hat{\boldsymbol{w}}_b^{\mathrm{BS}} - \hat{\boldsymbol{w}}^{\mathrm{AU}}\right\|}{(z_u - z_b)}\right\}$. The 3D location of the coordinated BS b' is $\boldsymbol{w}_{b'}^{\mathrm{BS}} = [x_{b'}, y_{b'}, z_{b'}]^T$. For $\boldsymbol{w}_{b'}^{\mathrm{BS}} \subseteq \mathcal{K}(\Psi)$, we must have $\boldsymbol{w}_{b'}^{\mathrm{BS}} \subseteq \mathcal{K}'(\Psi) \subseteq \mathcal{K}(\Psi)$, where $\mathcal{K}'(\Psi) = \{\boldsymbol{w}_{k'} | x = r'\cos\psi, y = r'\sin\psi, z = z_{b'}, r' = (z_u - z_{b'})\tan\Psi\}$. This implies that $\boldsymbol{w}_{b'}^{\mathrm{BS}} \subseteq \mathcal{K}'(\Psi) \iff [x_{b'}, y_{b'}, z_{b'}]^T \subseteq [x + x_u, y + y_u, z_{b'}]^T$. By the rule of translation, we conclude that $[x_{b'} - x_u, y_{b'} - y_u, z_{b'}]^T \subseteq [r'\cos\psi, r'\sin\psi, z_{b'}]^T$. We then use Euclidean norm, and write:

$$\sqrt{(x_{b'} - x_u)^2 + (y_{b'} - y_u)^2} = \left\|\hat{\boldsymbol{w}}_{b'}^{\mathrm{BS}} - \hat{\boldsymbol{w}}^{\mathrm{AU}}\right\| = \hat{d}_{b',u}, \tag{21}$$

and

$$\sqrt{(r'\cos\psi)^2 + (r'\sin\psi)^2} = r' = (z_u - z_{b'})\tan\Psi. \tag{22}$$

Thus, $[x_{b'} - x_u, y_{b'} - y_u, z_{b'}]^T \subseteq [r'\cos\psi, r'\sin\psi, z_{b'}]^T$, implies that:

$$\hat{d}_{b',u} \leq (z_u - z_{b'})\tan\Psi. \tag{23}$$

According to proposition 1, Ψ should be minimized such that (23) is satisfied. Therefore, the closed-form solution is $\Psi^* = \tan^{-1}\left(\arg\max\limits_{b\in\mathcal{B}} \frac{\left\|\hat{\boldsymbol{w}}_b^{\mathrm{BS}} - \hat{\boldsymbol{w}}^{\mathrm{AU}}\right\|}{(z_u - z_b)}\right)$. ■

This suggests that the optimal beamwidth in (17) is unique and it is the smallest beamwidth that covers all the coordinated BSs. Using proposition 2, (17) is then reduced to the following problem:

$$\max_{\boldsymbol{\rho_{b,u}},\,\boldsymbol{\rho_b}} \sum_{\forall b\in\mathcal{B}} B_{\mathrm{w}} \log\left(1+\frac{\rho_b N\left|h_{b,b}\right|^2}{\sum\limits_{\forall b'\in\mathcal{B}\setminus b}\rho_{b'}N\left|h_{b,b}\right|^2+I_{\mathrm{tot}}^{(b)}+1}\right), \tag{24a}$$

$$\text{s.t.} \quad B_{\mathrm{w}} \log\left(1+\frac{\boldsymbol{\rho_{b,u}}^T \boldsymbol{h}_u\left(\Psi^*\right)}{\boldsymbol{\rho_b}^T \boldsymbol{h}_u\left(\Psi^*\right)+I_{\mathrm{tot}}^{(u)}+1}\right) \geq R_{\min}, \tag{24b}$$

$$B_{\mathrm{w}} \log\left(1+\frac{\boldsymbol{\rho_{b,u}}^T \boldsymbol{h}_b}{\boldsymbol{\rho_b}^T \boldsymbol{h}_b+I_{\mathrm{tot}}^{(b)}+1}\right) \geq R_{\min}, \forall b\in\mathcal{B}, \tag{24c}$$

$$0\leq \boldsymbol{\rho_b},\, 0\leq \boldsymbol{\rho_{b,u}},\, \boldsymbol{\rho_b}+\boldsymbol{\rho_{b,u}}\leq 1, \tag{24d}$$

where $\boldsymbol{h}_u\left(\Psi^*\right)=N\left[\left|h_{1,u}^v\left(\Psi^*\right)\right|^2,\ldots\left|h_{B,u}^v\left(\Psi^*\right)\right|^2\right]^T$ and $\boldsymbol{h}_b=N\left[\left|h_{1,b}\right|^2,\ldots,\left|h_{B,b}\right|^2\right]^T$. Besides, $I_{\mathrm{tot}}^{(u)}=N\sum\limits_{\forall b''\in\mathcal{I}}\left|h_{b'',u}^v\left(\Psi^*\right)\right|^2$ and $I_{\mathrm{tot}}^{(b)}=N\sum\limits_{\forall b''\in\mathcal{I}}\left|h_{b'',b}\right|^2$ are the aggregated ICI at the AU u and TU $t=b$, respectively.

The optimization problem in (24) is still a non-convex optimization problem. To address this issue, we introduce an auxiliary variable $\boldsymbol{q_b}=[q_1,\ldots,q_B]$, which can be interpreted as the SINR of the TUs. By rearranging the term, (24) is reformulated as follows:

$$\max_{\boldsymbol{q_b},\,\boldsymbol{\rho_{b,u}},\,\boldsymbol{\rho_b}} \sum_{\forall b\in\mathcal{B}} B_{\mathrm{w}}\log\left(1+q_b\right), \tag{25a}$$

$$\text{s.t.} \quad \frac{\rho_b N\left|h_{b,b}\right|^2}{\sum\limits_{\forall b'\in\mathcal{B}\setminus b}\rho_{b'}N\left|h_{b',b}\right|^2+I_{\mathrm{tot}}^{(b)}+1}\geq q_b, \forall b\in\mathcal{B}, \tag{25b}$$

$$\boldsymbol{\rho_{b,u}}^T \boldsymbol{h}_u\left(\Psi^*\right)\geq r\left(\boldsymbol{\rho_b}^T \boldsymbol{h}_u\left(\Psi^*\right)+I_{\mathrm{tot}}^{(u)}+1\right), \tag{25c}$$

$$\boldsymbol{\rho_{b,u}}^T \boldsymbol{h_b}\geq r\left(\boldsymbol{\rho_b}^T \boldsymbol{h_b}+I_{\mathrm{tot}}^{(b)}+1\right), \tag{25d}$$

$$(24d),$$

where $r=\left(2^{\frac{R_{\min}}{B_{\mathrm{w}}}}-1\right)$.

In (25), only (25b) remains to be non-convex[4]. To address the non-convexity challenge, we employ SCA. Rearranging the term and applying first order Taylor approximation to (25b), (25) can be successively solved via the following convex optimization problem:

[4]Note that if the ICI of cell-center TUs is negligible, (25) can be reformulated as a convex optimization problem.

$$\max_{\boldsymbol{q_b},\,\boldsymbol{\rho_{b,u}},\,\boldsymbol{\rho_b}} \quad \sum_{\forall b\in\mathcal{B}} B_{\mathrm{w}} \log\left(1+q_b\right), \tag{26a}$$

$$\text{s.t.} \quad \rho_b N\left|h_{b,b}\right|^2 \geq q_b^{(n)}\Big(\sum_{\forall b'\in\mathcal{B}\setminus b}\rho_{b'}^{(n)} N\left|h_{b',b}\right|^2 + I_{\mathrm{tot}}^{(b)} + 1\Big) \tag{26b}$$

$$+\left(q_b - q_b^{(n)}\right)\Big(\sum_{\forall b'\in\mathcal{B}\setminus b}\rho_{b'}^{(n)} N\left|h_{b',b}\right|^2 + I_{\mathrm{tot}}^{(b)} + 1\Big)$$

$$+\left(\rho_{b'} - \rho_{b'}^{(n)}\right)\sum_{\forall b'\in\mathcal{B}\setminus b} q_b^{(n)} N\left|h_{b',b}\right|^2, \forall b\in\mathcal{B},$$

$$(25c), (25d), (24d),$$

where $q_b^{(n)}$ and $\rho_b^{(n)}$ are the optimal values of q_b and ρ_b, respectively, in the $(n-1)$th iterations. Note that, the initial values of $\rho_b^{(0)}, \forall b$, can be randomly initialized between $[0,1]$ while the initial values of $q_b^{(0)}, \forall b$, can be initialized by setting (25b) with equality. Since (26) is a convex optimization problem, it can be solved efficiently [52].

IV. Inter-Cell Interference and AU's Outage Probability

In this section, we estimate the aggregated ICI by leveraging the unique properties of the proposed ATN-NOMA scheme and the statistical CSI. Then, we use the derived statistical properties to approximate the AU's outage probability in cases where no interfering BSs have the same elevation angle as the coordinated BSs. To estimate the aggregated ICI, we utilize the following proposition and corollary:

Proposition 3. *The interfering BSs $b\in\mathcal{I}$ that impose ICI have the same elevation-angle as the coordinated BS b'.*

Proof: Let $b^{'} = \left\{b \,|\, \arg\max_{b\in\mathcal{B}} \frac{\left\|\boldsymbol{w}_b^{\mathrm{BS}} - \boldsymbol{w}^{\mathrm{AU}}\right\|}{(z_u - z_{\mathrm{b}})}\right\}$ and $\Psi^* = \tan^{-1}\left(\frac{\left\|\hat{\boldsymbol{w}}_{b'}^{\mathrm{BS}} - \hat{\boldsymbol{w}}^{\mathrm{AU}}\right\|}{(z_u - z_{b'})}\right)$. Then, (6) ensures that $\phi_{b',u} \geq \phi_{b'',u}$ for $\forall b''\in\mathcal{I}$. Define $\Psi_{b''} = \tan^{-1}\left(\frac{\left\|\hat{\boldsymbol{w}}_{b''}^{\mathrm{BS}} - \hat{\boldsymbol{w}}^{\mathrm{AU}}\right\|}{(z_u - z_{b''})}\right)$ for $\forall b''\in\mathcal{I}$. It is then observed that $\Psi^* \leq \Psi_{b''}$ for $\forall b''\in\mathcal{I}$ since $\Psi_b + \phi_{b,u} = \frac{\pi}{2}$. Let $\mathcal{I}_0 = \left\{b'' \,|\, \Psi^* = \Psi_{b''}, \forall b''\in\mathcal{I}\right\}$, and $\mathcal{I}_1 = \left\{b'' \,|\, \Psi^* < \Psi_{b''}, \forall b''\in\mathcal{I}\right\}$. According to (4), (7) and Proposition 2, $\left|h_{b'',u}\left(\Psi^*\right)\right|^2 = 0$ for $\forall b''\in\mathcal{I}_1$. Since $\Psi^* = \Psi_b \Longleftrightarrow \phi_{b',u} = \phi_{b,u}$, $\forall b\in\mathcal{I}_0$, the interfering BSs $b\in\mathcal{I}_0$ that causes ICI (e.g., $\left|h_{b,u}\left(\Psi^*\right)\right|^2 \neq 0$) have the same elevation-angle as the coordinated BS b'. ■

Corollary 1. *If no interfering BSs $b \in \mathcal{I}$ have the same elevation-angle as the coordinated BS b', the AU experiences zero ICI*[5].

Proof: When no interfering BSs $b \in \mathcal{I}$ have the same elevation-angle as the coordinated BS b', $\mathcal{I}_0 = \emptyset$. Thus, the AU experiences zero ICI. ■

Using (4), the aggregated ICI, $I_{\text{tot}} = \sum_{\forall b \in \mathcal{I}} N \left| h^{\upsilon}_{b,u}(\Psi^*) \right|^2$, is then written as:

$$I_{\text{tot}} = \sum_{\forall b \in \mathcal{I}} N \Xi^{\upsilon}_{b,u}(\Psi^*) \left| \Omega^{\upsilon}_{b,u} \right|^2. \tag{27}$$

Using proposition 3, the interfering BSs $b \in \mathcal{I}_0$ that impose the ICI have the same elevation-angle as the coordinated BS b'. For ease of exposition, we assume the interfering BSs have the same height here, and thus the same probability of LOS. In Appendix A, we generalize our analysis to cases where the interfering BSs have different heights. Let $\tilde{I} = \text{card}(\mathcal{I}_0)$ and $\tilde{L}$ be the number of LOS links among these $\tilde{I}$ interfering links. Further define $\mathcal{I}^{\text{L}}$ as the set of interfering BSs that establishes LOS links to the AU, i.e., $\tilde{L} = \text{card}(\mathcal{I}^{\text{L}})$, and $\mathcal{I}^{\text{N}}$ as the set of interfering BSs that establishes NLOS links to the AU, such that $\mathcal{I} = \mathcal{I}^{\text{L}} \cup \mathcal{I}^{\text{N}}$ and $\mathcal{I}^{\text{L}} \cap \mathcal{I}^{\text{N}} = \emptyset$.

Given above definitions, it is straightforward to see that $\tilde{L}$ is a binomial random variable with $\tilde{I}$ interfering links, and probability of $p^{\text{L}}_{b,u}\left(\hat{d}_{b,u}, z_u\right)$, i.e., $\tilde{L} \sim \text{Bino}\left(\tilde{I}, p^{\text{L}}_{b,u}\left(\hat{d}_{b,u}, z_u\right)\right)$. Therefore, its probability mass function (pmf) is:

$$f\left(i, \tilde{I}, p^{\text{L}}_{b,u}\left(\hat{d}_{b,u}, z_u\right)\right) = \binom{\tilde{I}}{i} p^{\text{L}}_{b,u}\left(\hat{d}_{b,u}, z_u\right)^{i} p^{\text{N}}_{b,u}\left(\hat{d}_{b,u}, z_u\right)^{(\tilde{I}-i)}. \tag{28}$$

More concretely, (28) is the probability of getting exactly i LOS links and $\tilde{I} - i$ NLOS links with $\tilde{I}$ interfering links. Suppose there are i LOS links among $\tilde{I}$ interfering links, then $I^{(i)}_{\text{tot}}$ is:

$$\begin{aligned} I^{(i)}_{\text{tot}} &= \sum_{\forall b \in \mathcal{I}_0} N \Xi^{\upsilon}_{b,u}(\Psi^*) \left| \Omega^{\upsilon}_{b,u} \right|^2, \\ &= \sum_{\forall b \in \mathcal{I}^L} N \Xi^{\text{L}}_{b,u}(\Psi^*) \left| \Omega^{\text{L}}_{b,u} \right|^2 + \sum_{\forall b \in \mathcal{I}^N} N \Xi^{\text{N}}_{b,u}(\Psi^*) \left| \Omega^{\text{N}}_{b,u} \right|^2, \\ &= H^{\text{L}}_{i} + H^{\text{N}}_{(\tilde{I}-i)}. \end{aligned} \tag{29}$$

Given the number of LOS links, H^{L}_{i} and $H^{\text{N}}_{(\tilde{I}-i)}$ are gamma distributed random variables. Suppose $H \sim \text{gamma}(m, \theta)$. The pdf of the gamma random variable H is given as:

$$f_H(h, m, \theta) = \frac{h^{m-1} \exp\left(-\frac{h}{\theta}\right)}{\theta^m \Gamma(m)}, h > 0, \tag{30}$$

[5]Corollary 1 suggests that in irregular cellular networks the AU in our proposed scheme is likely to experience zero ICI. This is because it is difficult to find multiple BSs having the same elevation angle to the AU in such settings.

where $\Gamma(\cdot)$ is the gamma function. The CDF of the gamma random variable is:

$$F_H\left(\bar{h}, m, \theta\right) = \int_0^{\bar{h}} \frac{h^{m-1}\exp\left(-\frac{h}{\theta}\right)}{\theta^m \Gamma(m)} dh, \bar{h} > 0. \tag{31}$$

In the gamma distribution, there exists summation and scaling properties. That is, if $H_i \sim$ gamma(m_i, θ), then $\sum_{\forall i} H_i \sim$ gamma $\left(\sum_{\forall i} m_i, \theta\right)$. If $H \sim$ gamma (m, θ), then $c{\cdot}H \sim$ gamma $(m, c\theta)$. Thus, if $i = 0$, then $I_{\text{tot}}^{(0)} = H_{\tilde{I}}^{\text{N}} \sim$ gamma$\left(\tilde{I} m_u^{\text{N}}, N\Xi_{b,u}^{\text{N}}\left(\Psi^*\right)\theta_u^{\text{N}}\right)$, and if $i = \tilde{I}$, then $I_{\text{tot}}^{(\tilde{I})} = H_{\tilde{I}}^{\text{L}} \sim$ gamma$\left(\tilde{I} m_u^{\text{L}}, N\Xi_{b,u}^{\text{L}}\left(\Psi^*\right)\theta_u^{\text{L}}\right)$.

According to [53], if $0 < i < \tilde{I}$, then $I_{\text{tot}}^{(i)}$ is the summation of independent non-identical distributed (i.n.i.d.) gamma random variables, where $H_i^{\text{L}} \sim$ gamma$\left(i m_u^{\text{L}}, N\Xi_{b,u}^{\text{L}}\left(\Psi^*\right)\theta_u^{\text{L}}\right)$ and $H_{\left(\tilde{I}-i\right)}^{\text{N}} \sim$ gamma$\left(\left(\tilde{I}-i\right) m_u^{\text{N}}, N\Xi_{b,u}^{\text{N}}\left(\Psi^*\right)\theta_u^{\text{N}}\right)$. The exact pdf is:

$$f_{I_{\text{tot}}^{(i)}}(h) = C\sum_{j=0}^{\infty} \frac{\delta_j h^{k+j-1}\exp\left(-\frac{h}{\theta_{\min}}\right)}{\Gamma(k+j)\,\theta_{\min}^{k+j}}, \qquad h > 0, \tag{32}$$

where $\theta_{\min} = \arg\min_{\upsilon\in\{\text{L,N}\}}\left\{N\Xi_{b,u}^{\upsilon}\left(\Psi^*\right)\theta_u^{\upsilon}\right\}$, $k = i m_u^{\text{L}} + \left(\tilde{I}-i\right) m_u^{\text{N}}$, $\delta_{j+1} = \frac{1}{j+1}\sum_{l=1}^{j+1} l\gamma_l \delta_{j+1-l}$ with $\delta_0 = 1$,

$$\gamma_j = \frac{i m_u^{\text{L}}\left(1 - \frac{\theta_{\min}}{N\Xi_{b,u}^{\text{L}}(\Psi^*)\theta_u^{\text{L}}}\right)^j}{j} + \frac{\left(\tilde{I}-i\right) m_u^{\text{N}}\left(1 - \frac{\theta_{\min}}{N\Xi_{b,u}^{\text{N}}(\Psi^*)\theta_u^{\text{N}}}\right)^j}{j},$$

and

$$C = \left(\frac{\theta_{\min}}{N\Xi_{b,u}^{\text{L}}\left(\Psi^*\right)\theta_u^{\text{L}}}\right)^{i m_u^{\text{L}}} \times \left(\frac{\theta_{\min}}{N\Xi_{b,u}^{\text{N}}\left(\Psi^*\right)\theta_u^{\text{N}}}\right)^{\left(\tilde{I}-i\right)m_u^{\text{N}}}.$$

The CDF is therefore:

$$F_{I_{\text{tot}}^{(i)}}\left(\bar{h}\right) = C\sum_{j=0}^{\infty}\delta_j \int_0^{\bar{h}} \left[\frac{h^{k+j-1}\exp\left(-\frac{h}{\theta_{\min}}\right)}{\Gamma(k+j)\,\theta_{\min}^{k+j}}\right] dh. \tag{33}$$

The exact pdf and CDF respectively shown in (32) and (33) are in fact theoretically important. However, they are not very useful in this application. This is because, although the infinite series in the expressions can be truncated to a finite series with a bounded error, the numerical value of $\theta_{\min}^{k+j}$ in the denominator of (32) and (33) may be zero due to the magnitude of the large-scale fading effect. Hence, an approximation is required for our purpose.

According to [54], $I_{\text{tot}}^{(i)}$ for $0 < i < \tilde{I}$, can be approximated by $H^{(i)} \sim$ gamma$\left(\hat{m}, \hat{\theta}\right)$, where

$$\hat{m} = \frac{\mu^2}{\hat{m}_L \vartheta_L^2 + \hat{m}_N \vartheta_N^2}, \tag{34}$$

$$\hat{\theta} = \frac{\hat{m}_L \vartheta_L^2 + \hat{m}_N \vartheta_N^2}{\mu}, \tag{35}$$

In (34) and (35), $\hat{m}_L = i m_u^{\mathrm{L}}$, $\vartheta_L = N \Xi_{b,u}^{\mathrm{L}} (\Psi^*) \theta_u^{\mathrm{L}}$, $\hat{m}_N = \left(\tilde{I} - i\right) m_u^{\mathrm{N}}$, $\vartheta_N = N \Xi_{b,u}^{\mathrm{N}} (\Psi^*) \theta_u^{\mathrm{N}}$, and $\mu = \hat{m}_L \vartheta_L + \hat{m}_N \vartheta_N$. Based on the above, we present the following:

Proposition 4. *The pdf of the aggregated ICI, I_{tot}, in ATN-NOMA is approximated as:*

$$\begin{aligned} & f_{I_{tot}} \left(\tau, \tilde{I}, p_{b,u}^L \left(\hat{d}_{b,u}, z_u\right), \hat{m}, \hat{\theta}\right) \\ \approx & \sum_{0 \le i \le \tilde{I}} f\left(i, \tilde{I}, p_{b,u}^L \left(\hat{d}_{b,u}, z_u\right)\right) f_{H^{(i)}} \left(\tau, \hat{m}, \hat{\theta}\right), \tau > 0 \\ = & \sum_{0 \le i \le \tilde{I}} \left[\binom{\tilde{I}}{i} p_{b,u}^L \left(\hat{d}_{b,u}, z_u\right)^i p_{b,u}^N \left(\hat{d}_{b,u}, z_u\right)^{(\tilde{I}-i)} \frac{\tau^{\hat{m}-1} \exp\left(-\frac{\tau}{\hat{\theta}}\right)}{\hat{\theta}^{\hat{m}} \Gamma(\hat{m})} \right]. \end{aligned} \tag{36}$$

The CDF of the aggregated ICI, I_{tot}, in ATN-NOMA is approximated as:

$$\begin{aligned} & F_{I_{tot}} \left(\tau, \tilde{I}, p_{b,u}^L \left(\hat{d}_{b,u}, z_u\right), \hat{m}, \hat{\theta}\right) \\ \approx & \sum_{0 \le i \le \tilde{I}} f\left(i, \tilde{I}, p_{b,u}^L \left(\hat{d}_{b,u}, z_u\right)\right) F_{H^{(i)}} \left(\tau, \hat{m}, \hat{\theta}\right), \tau > 0 \\ = & \sum_{0 \le i \le \tilde{I}} \left[\binom{\tilde{I}}{i} p_{b,u}^L \left(\hat{d}_{b,u}, z_u\right)^i p_{b,u}^N \left(\hat{d}_{b,u}, z_u\right)^{(\tilde{I}-i)} \int_0^\tau \frac{\tau'^{\hat{m}-1} \exp\left(-\frac{\tau'}{\hat{\theta}}\right)}{\hat{\theta}^{\hat{m}} \Gamma(\hat{m})} d\tau' \right]. \end{aligned} \tag{37}$$

Proof: $f_{I_{\mathrm{tot}}}$ and $F_{I_{\mathrm{tot}}}$ in (36) and (37), respectively, follow immediately noting that I_{tot} is the sum of i.n.i.d. gamma random variables conditioned by the number of LOS/NLOS links. ■

In proposition 4, it is observed that I_{tot} follows exactly a gamma distribution in cases where the probabilities of LOS/NLOS are one. Using proposition 4, we can now estimate the aggregated ICI, I_{tot}, with $\hat{I}_{\mathrm{tot}}$ for a given probability δ, as follows:

$$\mathbb{P}\left(I_{\mathrm{tot}} \le \hat{I}_{tot}\right) = \delta, \tag{38}$$

where $\hat{I}_{\mathrm{tot}}$ must satisfy the following equality:

$$F_{I_{\mathrm{tot}}} \left(\hat{I}_{\mathrm{tot}}, \tilde{I}, p_{b,u}^{\mathrm{L}} \left(\hat{d}_{b,u}, z_u\right), \hat{m}, \hat{\theta}\right) = \delta. \tag{39}$$

Note that using (38), the proposed scheme only requires the CSI of the coordinated BSs to perform ATN-NOMA.

Due to zero ICI and low data rate requirement, the AU's outage probability is extremely low. Thus, it is useful to approximate the AU's outage probability if there are no interfering BSs having the same elevation-angle as the coordinated BS b'. Specifically, the outage probability can be written as follows:

$$P^{\mathrm{out}} = \mathbb{P}\left\{R_u < R_{\min}\right\}. \tag{40}$$

Proposition 5. *If no interfering BSs $b \in \mathcal{I}$ have the same elevation-angle as the coordinated BS b', the AU's outage probability is approximately:*

$$P^{out} \approx F_{\beta_{tot}}\left(r, \tilde{B}_{d_1}, \ldots, \tilde{B}_{d_{\bar{\beta}}}, p^{L}_{b,u}\left(d_1, z_u\right), \ldots, p^{L}_{b,u}\left(d_{\bar{\beta}}, z_u\right)\right), \tag{41}$$

$$= \sum_{\forall b_d \in \mathcal{L}} \left[\prod_{\tilde{L}_{d_\beta} = b_{d_\beta}, \forall \beta} \binom{\tilde{B}_{d_\beta}}{b_{d_\beta}} p^{L}_{b,u}\left(d_\beta, z_u\right)^{b_{d_\beta}} \times \right.$$

$$\left. p^{N}_{b,u}\left(d_\beta, z_u\right)^{\left(\tilde{B}_{d_\beta} - b_{d_\beta}\right)} \int_0^r \frac{\tau'^{\hat{m}-1} \exp\left(-\frac{\tau'}{\hat{\theta}}\right)}{\hat{\theta}^{\hat{m}} \Gamma\left(\hat{m}\right)} d\tau' \right].$$

Proof: Using Corollary 1 and maximizing R_u, (40) is reduced to:

$$P^{\text{out}} = \mathbb{P}\left\{ \sum_{\forall b \in \mathcal{B}} N \left| h^{v}_{b,u}\left(\Psi^*\right) \right|^2 < 2^{\frac{R_{\min}}{B_w}} - 1 \right\}. \tag{42}$$

Denote $\beta_{\text{tot}} = \sum_{\forall b \in \mathcal{B}} N \left| h^{v}_{b,u}\left(\Psi^*\right) \right|^2$. Note that β_{tot} is the sum of i.n.i.d. gamma random variables conditioned by the number of LOS/NLOS links. Define $\mathcal{D} = \left\{d_1, \ldots, d_{\bar{\beta}}\right\}$ as the set of *distinctive* horizontal distance between the AU and the coordinated BS, $b \in \mathcal{B}$, where $\bar{\beta} \leq B$, and $\mathcal{B}_{d_\beta} = \left\{ b \,|\, \hat{d}_{b,u} = d_\beta, \forall b \in \mathcal{B} \right\}$ as the set of coordinated BSs with horizontal distance d_β from the AU. Let $\tilde{B}_{d_\beta} = \text{card}\left(\mathcal{B}_{d_\beta}\right)$ and $\tilde{L}_{d_\beta}$ be the number of LOS links among these $\tilde{B}_{d_\beta}$ connected links. Further define $\mathcal{L} = \left\{ \left(\tilde{L}_{d_1}, \ldots, \tilde{L}_{d_{\bar{\beta}}}\right) | 0 \leq \tilde{L}_{d_\beta} \leq \tilde{B}_{d_\beta}, \beta = 1, \ldots, \bar{\beta} \right\}$, and $b_d = \left(b_{d_1}, \ldots, b_{d_{\bar{\beta}}}\right)$. Note that, $\tilde{L}_{d_\beta} \sim \text{Bino}\left(\tilde{B}_{d_\beta}, p^{\text{L}}_{b,u}\left(d_\beta, z_u\right)\right)$. Since $\tilde{L}_{d_\beta}$ is independent of $\tilde{L}_{d_{\beta'}}$ for $\beta \neq \beta'$, we have:

$$\begin{aligned} &\mathbb{P}\left(\tilde{L}_{d_1} = b_{d_1}, \ldots, \tilde{L}_{d_{\bar{\beta}}} = b_{d_{\bar{\beta}}}\right) \\ &= \prod_{\tilde{L}_{d_\beta} = b_{d_\beta}, \forall \beta} f_{\tilde{L}_{d_\beta}}\left(b_{d_\beta}, \tilde{B}_{d_\beta}, p^{\text{L}}_{b,u}\left(d_\beta, z_u\right)\right). \end{aligned} \tag{43}$$

Denote $H^{(b_d)} = \sum_{\forall \beta} H^{\left(b_{d_\beta}\right)}$, and $r = 2^{\frac{R_{\min}}{B_w}} - 1$. The CDF of the β_{tot} is approximated as:

$$\begin{aligned} &F_{\beta_{\text{tot}}}\left(r, \tilde{B}_{d_1}, \ldots, \tilde{B}_{d_{\bar{\beta}}}, p^{\text{L}}_{b,u}\left(d_1, z_u\right), \ldots, p^{\text{L}}_{b,u}\left(d_{\bar{\beta}}, z_u\right)\right) \\ \approx\ & \sum_{\forall b_d \in \mathcal{L}} \mathbb{P}\left(\tilde{L}_{d_1} = b_{d_1}, \ldots, \tilde{L}_{d_{\bar{\beta}}} = b_{d_{\bar{\beta}}}\right) F_{H^{(b_d)}}\left(r, \hat{m}, \hat{\theta}\right) \\ =\ & \sum_{\forall b_d \in \mathcal{L}} \left[\prod_{\tilde{L}_{d_\beta} = b_{d_\beta}, \forall \beta} \binom{\tilde{B}_{d_\beta}}{b_{d_\beta}} p^{\text{L}}_{b,u}\left(d_\beta, z_u\right)^{b_{d_\beta}} \times \right. \\ & \left. p^{\text{N}}_{b,u}\left(d_\beta, z_u\right)^{\left(\tilde{B}_{d_\beta} - b_{d_\beta}\right)} \int_0^r \frac{\tau'^{\hat{m}-1} \exp\left(-\frac{\tau'}{\hat{\theta}}\right)}{\hat{\theta}^{\hat{m}} \Gamma\left(\hat{m}\right)} d\tau' \right]. \end{aligned} \tag{44}$$

■

We note that the outage probability of CoMP-OMA with optimal beamwidth, and network NOMA with fixed power allocation and optimal beamwidth can similarly be obtained using (41) by replacing r with $r_{\text{OMA}} = 2\left(2^{\frac{2R_{\min}}{B_{\text{w}}}} - 1\right)$ and $r_{\text{FNOMA}} = \frac{r}{\left[\rho_{b,u} - \rho_b r\right]^+}$, respectively. Furthermore, in cases where card $(\mathcal{D}) = 1$ and the probabilities of LOS/NLOS are one, the outage probability can be approximated using a gamma distribution.

V. Simulation Results

In this section, we provide the simulation results to evaluate the performance of our proposed ATN-NOMA scheme. Since multiple techniques are jointly employed in the proposed scheme, the contributions of each technique are unclear. Thus, we consider multiple schemes based on different combinations to identify their corresponding gains and effects at a fundamental level. In this paper, we consider the following schemes:

- CoMP-OMA [11] with fixed beamwidth (FB-OMA),
- CoMP-OMA [11] with optimal beamwidth (OB-OMA),
- Network NOMA with fixed power allocation [28] and fixed beamwidth (FB-FNOMA),
- Network NOMA with fixed power allocation [28] and optimal beamwidth (OB-FNOMA),
- Network NOMA with fixed beamwidth and optimal power allocation (FB-NOMA),
- The proposed ATN-NOMA with optimal beamwidth, power allocation, and statistical CSI (ATN-NOMA-S),
- The proposed ATN-NOMA with optimal beamwidth, power allocation, and perfect CSI (ATN-NOMA-P).

For CoMP-OMA, we consider FDMA with equal bandwidth allocation to the AU and TUs. For fixed beamwidth, we set $\Psi_f = \tan\left(\frac{2r_o}{81}\right)$ to ensure card $(\mathcal{B}) = 3$. For network NOMA with fixed power allocation, we set $\rho_{b,\text{u}} = 0.9$ and $\rho_b = 0.1$ to compensate the ICI at the AU. For the proposed ATN-NOMA-S scheme, we set $\delta = 0.999$ to guarantee reliable communications to the AU. Unless stated otherwise, the parameters used in the simulation are as shown in Table I.

A. Statistical Properties of Aggregated ICI

Fig. 3 shows the statistical properties of the aggregated ICI in the proposed ATN-NOMA scheme, where we consider the AU at the origin. We also consider two altitudes: 100m and 500m. Fig. 3(a) and Fig. 3(b) show the pdf and CDF of the aggregated ICI, respectively. As observed, the numerical results match the analytical results given in (36) and (37). Hence, by

Table I: Parameter Settings

Parameter	Value	Parameter	Value
P_{tx}	26 dBm	f_{c}	2 GHz
B_{w}	180 KHz	r_0	500 m
σ_{n}^2	-174 dBm/Hz	(E_u, E_t)	(-3, 10) dB
R_{min}	100 Kbps	(φ, ξ, ζ)	(1, .151, 1)
card $(\mathcal{B} \cup \mathcal{I}) \subseteq \mathcal{A}$	37	$(\alpha_{\text{L}}, \alpha_{\text{N}}, \alpha)$	(2.1, 3.7, 4)
card $(\mathcal{B})$	3	$\left(m_u^{\text{L}}, m_u^{\text{N}}, m_t\right)$	(3, 2, 1)
z_b, z_t	(19, 1.5) m	$\left(\theta_u^{\text{L}}, \theta_u^{\text{N}}, \theta_t\right)$	$(\frac{1}{3}, \frac{1}{2}, 1)$

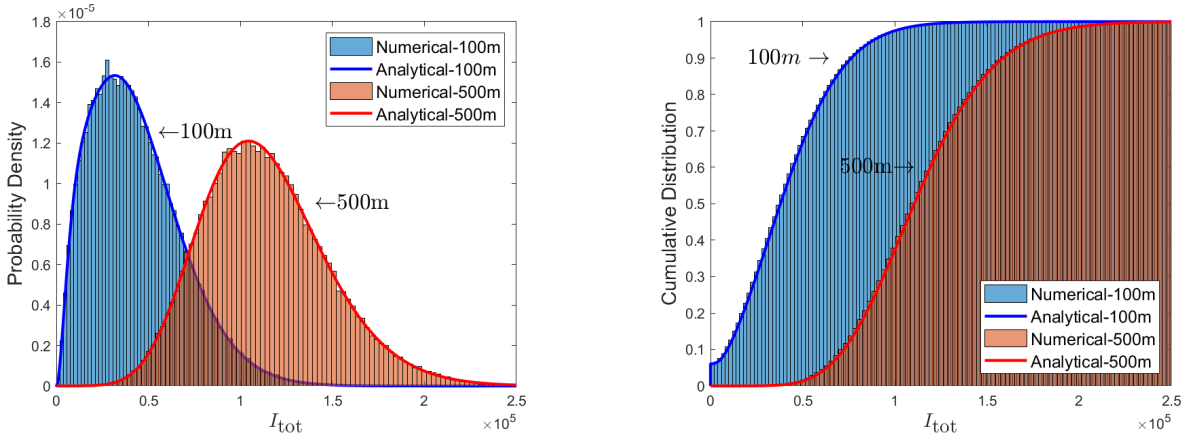

(a) (b)

Figure 3: The statistical properties of the aggregated ICI: (a) pdf; (b) CDF.

leveraging the derived statistical properties, the aggregated ICI in the proposed ATN-NOMA scheme can be reliably estimated for any given δ.

B. Accuracy of the Analytical Outage Probability

In cases where the data rate requirement is low and the AU experiences zero ICI, the outage probabilities of OB-OMA, OB-FNOMA, and ATN-NOMA are extremely low. In such cases, an exorbitant number of samples might be required to accurately observe the numerical outage probability (e.g., 10^{20} samples are required if $R_{\text{min}} = 100$ Kbps). This is computationally challenging. Thus, as an alternative, we examine the analytical outage probability. Fig. 4 compares the numerical and analytical outage probabilities of OB-OMA, OB-FNOMA, and ATN-NOMA schemes. As seen in Fig. 4(a)-(c), the numerical results closely match the analytical results given

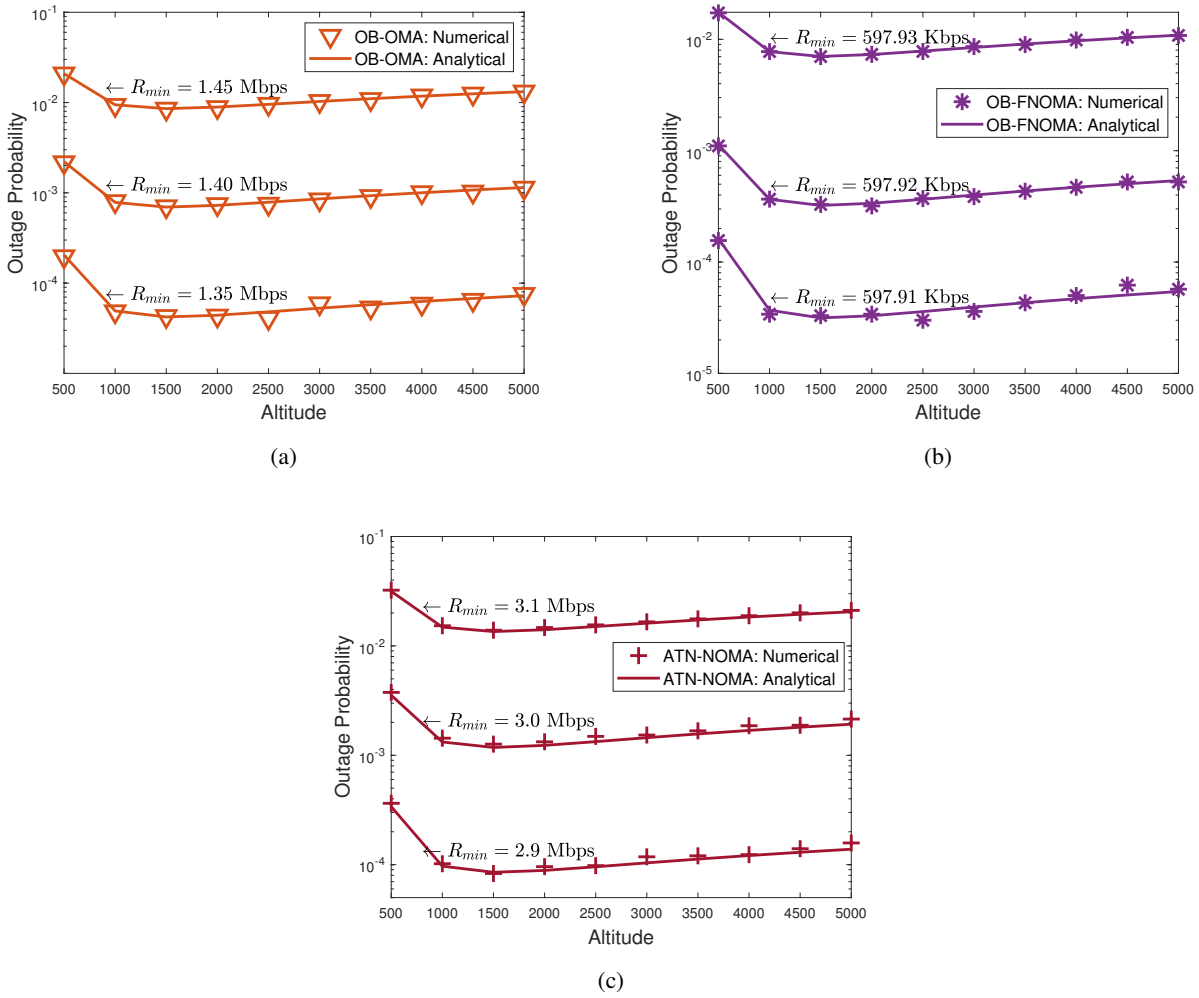

Figure 4: Numerical outage probability vs. analytical outage probability: (a) OB-OMA; (b) OB-FNOMA; (c) ATN-NOMA.

in (41). This suggests that we may efficiently measure the analytical outage probability of OB-OMA, OB-FNOMA, and ATN-NOMA using (41) in cases where the AU experiences zero ICI and the data rate requirement is low. Furthermore, in cases where the AU experiences zero ICI, we notice that the outage probability first decreases as the AU's altitude increases. This is due to the LOS gain. After the LOS gain is substantially obtained at a certain altitude, the outage probability then increases due to higher path loss.

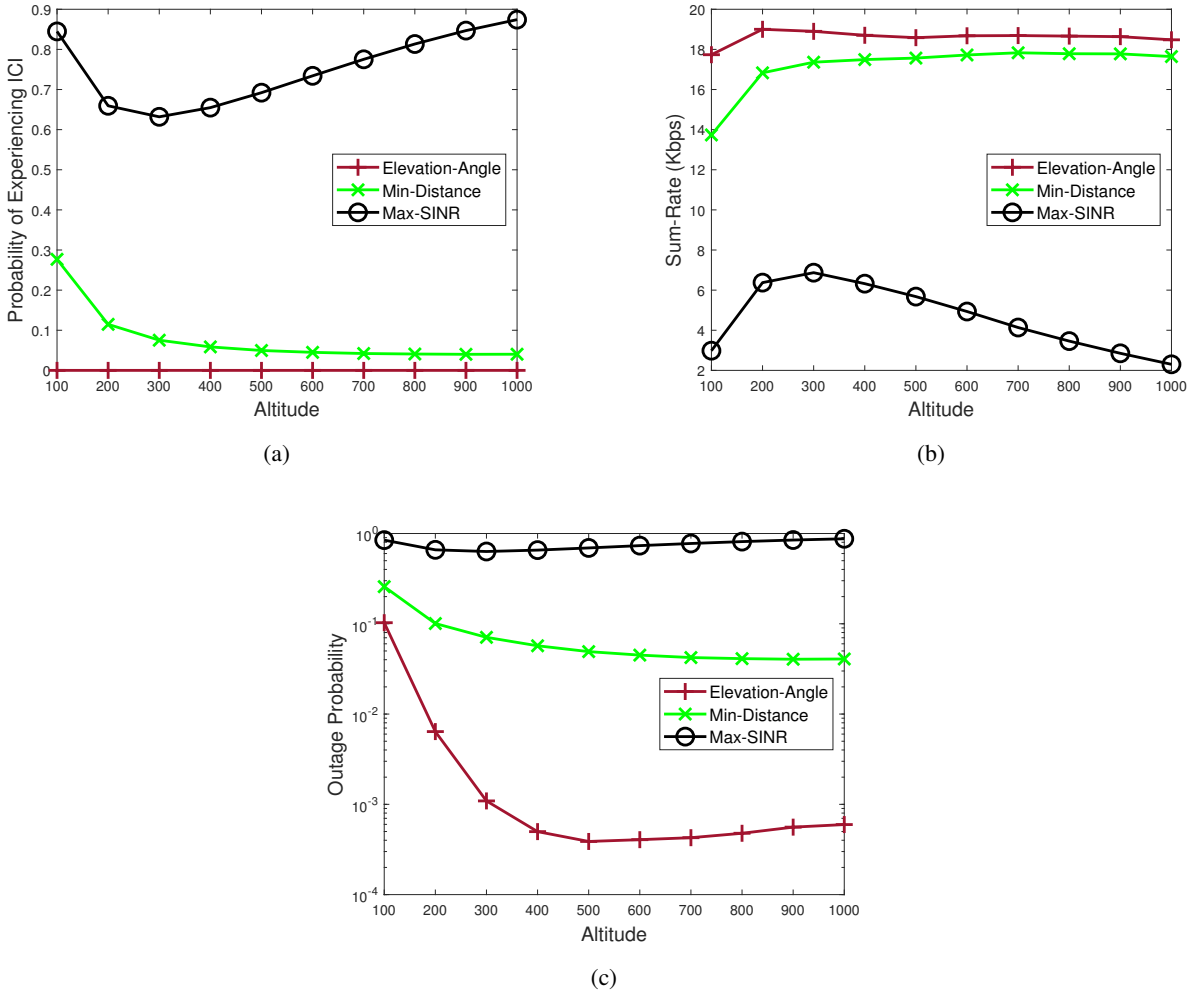

Figure 5: Performance of different user association policies: (a) probability of experiencing ICI; (b) sum-rate; (c) outage probability.

C. *Types of User Association Policies*

Fig. 5 compares the performance of the proposed elevation-angle based user association, minimum-distance based user association, and maximum-SINR based user association along with adjustable beamwidth directional antenna and network NOMA. Here, the AU is randomly located inside a disk centered at the origin with a radius of 500m, the BSs' height are uniformly distributed between 15m and 45m, and $R_{\min} = 2.8$ Mbps. As shown in Fig. 5(a), the minimum-distance and maximum-SINR based user associations are more likely to experience ICI. In the minimum-distance based user association, the nearest BSs might have a smaller elevation-angle

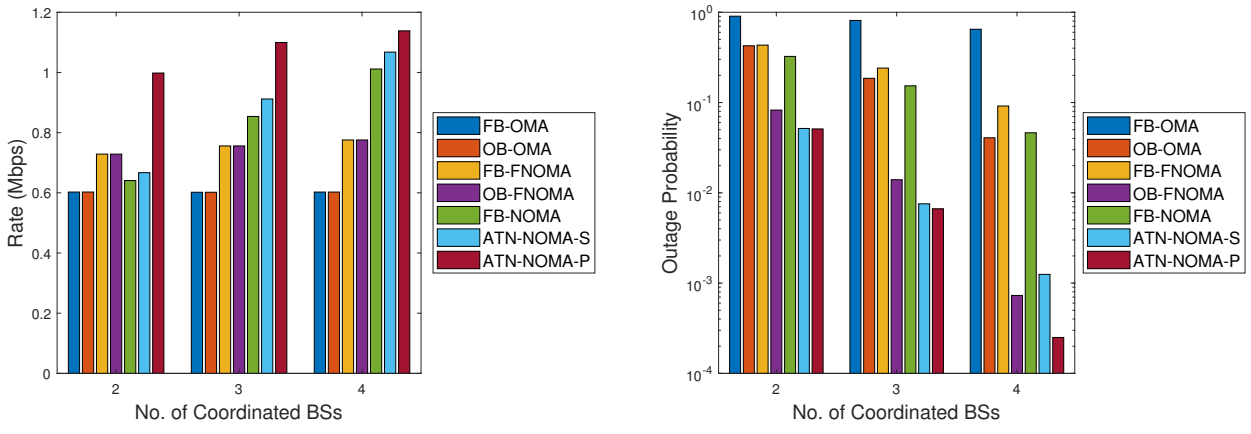

(a) (b)

Figure 6: The effect on the number of coordinated BSs: (a) average TU rate; (b) outage probability.

to the AU. In the maximum-SINR based user association, the strongest BSs might be located farther away from the AU. In both cases, the optimal beamwidth might need to cover a larger area inclusive of the interfering BSs. This leads to a performance degradation in terms of sum-rate and outage probability as shown in Fig. 5(b) and Fig. 5(c), respectively. Nevertheless, if the proposed elevation-angle based user association is employed, the AU is more likely to experience zero ICI. This is because the optimal beamwidth typically covers a smaller area exclusive of the interfering BSs. Furthermore, using the smaller beamwidth increases the channel gain between the AU and the coordinated BSs. As a result, the proposed elevation-angle based user association outperforms existing user associations in both sum-rate and outage probability.

D. Transmitting Strategy: Effects on the Number of Coordinated BSs

Fig. 6 depicts the effects of increasing the number of coordinated BSs, i.e., card $(\mathcal{B})$. Here, the AU is located at the origin with an altitude of 500m. As seen in Fig. 6(a), the average TU rate of the proposed ATN-NOMA schemes improves by increasing the number of coordinated BSs. The outage probability of the AU also decreases as shown in Fig. 6(b).

These improvements are contributed by two factors. Firstly, the increase number of coordinated BSs leads to an increase in the beamforming gain. We note that the beamforming gain is only obtained if optimal power allocation is used. Secondly, an increase in the number of coordinated

BSs reduces the number of interfering BSs and hence the aggregated ICI experienced at the AU is reduced. Due to the latter factor, the performance of the ATN-NOMA-S also approaches the ATN-NOMA-P by increasing the number of coordinated BSs.

Due to the ICI estimation, the outage probabilities of ATN-NOMA-S is bounded by $(1-\delta)$. However, if there are no interfering BSs having the same elevation-angle as the coordinated BSs, the bound vanishes and ATN-NOMA-S would achieve the same performance as ATN-NOMA-P. To fully mitigate the ICI of the AU, these results also suggest that increasing the number of coordinated BSs is the only solution.

In Fig. 6(a), it is observed that the average TU rates of FB-FNOMA and OB-FNOMA outperform FB-NOMA and ATN-NOMA-S, where card $(\mathcal{B}) = 2$. This is because a fixed power is allocated to the TUs in FNOMA regardless of the AU's QoS requirement. Without prioritizing the AU's QoS requirement, the outage probabilities of FB-FNOMA and OB-FNOMA are higher than that of the FB-NOMA and ATN-NOMA-S, respectively. Moreover, schemes based on NOMA generally outperform schemes based on OMA in terms of the average TU rate and outage probability, thanks to the spectrum sharing technique.

In addition, FB-OMA and OB-OMA achieve the same TU rate because fixed resource allocation is given to the TUs regardless of the AU's performance. For the same reason, FB-FNOMA and OB-FNOMA achieve the same TU rate. Nevertheless, the benefit of optimal beamwidth (OB) over fixed beamwidth (FB) can be observed in Fig. 6(b). Specifically, schemes based on OB have a lower outage probability than that of schemes based on FB as the ICI of the AU is minimized.

E. Receiving Strategy: Effects on the AU's Position

Fig. 7 presents the effects of the AU's position. As shown in Fig. 7(a), we investigate three important locations to understand the effects of AU's position. These locations are: (A) on top of one of the coordinated BSs, (B) on the cell-edge of two coordinated BSs, and (C) on the cell-edge of three coordinated BSs. In these locations, we assume that the AU is hovering at an altitude of 500m.

Since card $(\mathcal{B}) = 3$, both the sum-rate and outage probability perform the best where the AU is located at position C (i.e., the cell-edge of the three coordinated BSs). This is anticipated because position C is the central region of the three coordinated BSs. Therefore, a higher level of macro diversity can be obtained at this location. With *optimal beamwidth*, the AU also experiences zero

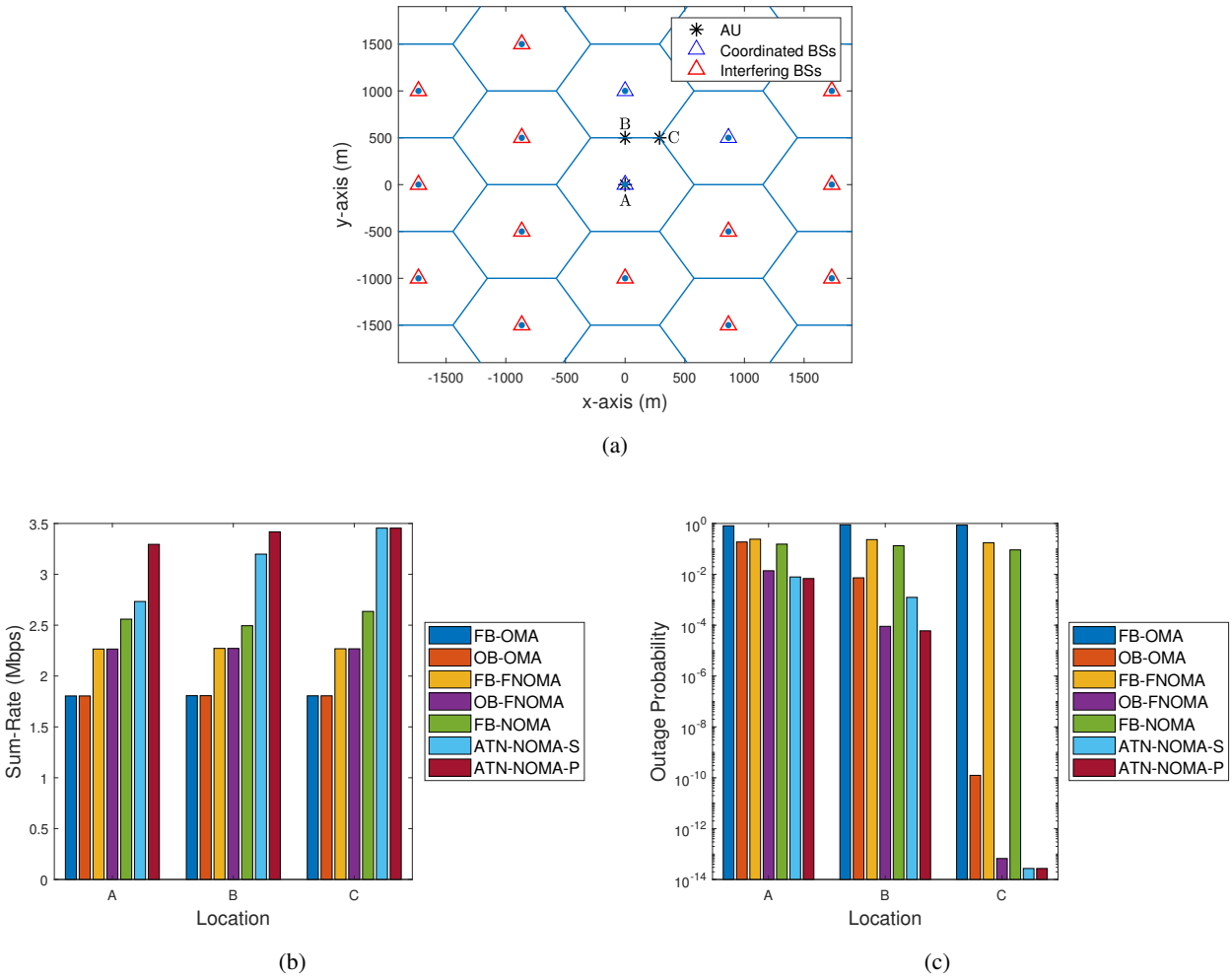

(a) (b) (c)

Figure 7: The effect on the 3D location of the AU: (a) locations of the AU; (b) sum-rate of the TUs; (c) outage probability.

ICI at this position, as guaranteed by Corollary 1, because the receiving coverage only covers the coordinated BS and there are no interfering BSs in the receiving coverage.

In cases where the AU is located at position A and B, it experiences ICI from interfering BSs. The performance degradation in terms of outage probability is enormous, see Fig. 7(c). Specifically, the AU's outage probability may increase from the order of 10^{-14} to 10^{-2}. Nevertheless, the ICI issue can be addressed by designing an opportunistic ATN-NOMA scheme, where card $(\mathcal{B})$ is adaptively varied. When card $(\mathcal{B})$ is adaptive, the AU can still experience zero ICI (see, section V-D and Corollary 1).

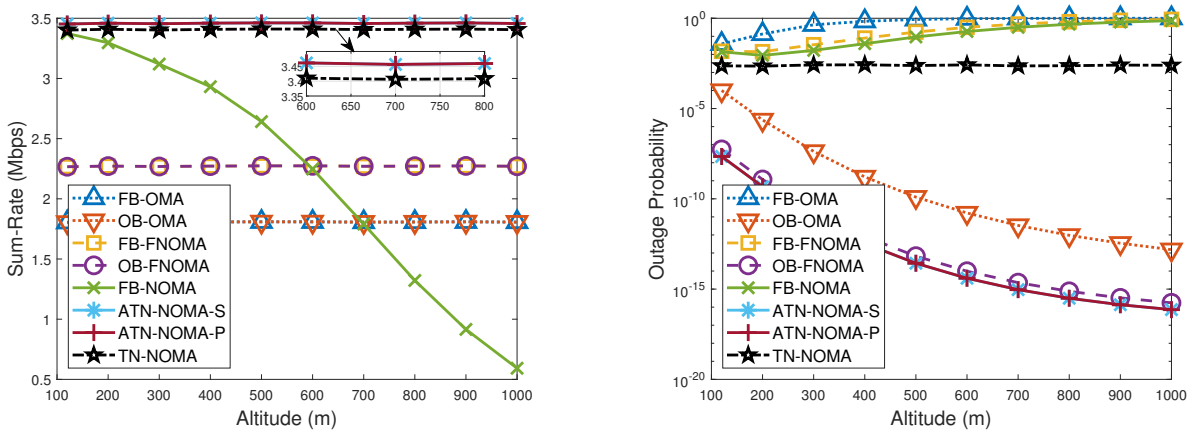

(a) (b)

Figure 8: The performance of different pairing schemes versus AU's altitude: (a) sum-rate of the TUs; (b) outage probability.

F. AU/TUs vs. TU/TUs Pairing

The above results have shown that each of the proposed techniques is important in achieving an outstanding performance. However, it remains unclear whether the pairing of AU and TU in multi-cell networks remains beneficial as compared to the pairing of TU and TU. Thus, Fig. 8 further compares the performance of two different pairing schemes. On the one hand, we consider the pairing of the AU and the cell-center TUs (ATN-NOMA). On the other hand, we consider the pairing of the cell-edge TU and the cell-center TUs, also referred as TN-NOMA. We assume the AU and the cell-edge TU are located at position C while only the AU can vary its altitude.

Figs. 8(a) and 8(b) show that, among all of the considered schemes, only the newly proposed ATN-NOMA schemes outperform TN-NOMA in both sum-rate and outage probability. In particular, the proposed ATN-NOMA scheme achieves an average of 91% and 52% sum-rate improvement as compared to schemes based on OMA and FNOMA, respectively. As compared to TN-NOMA, the sum-rate improvement is marginal although the AU gain is 30-60 dB higher than the cell-edge TU. This phenomenon occurs because the beamforming is performed on the AU and the cell-edge TU, while the objective of the schemes is to maximize the sum-rate of the cell-center TUs subject to the minimum rate requirement of the AU or the cell-edge TU. Thus, the advantage of the beamforming actually lies on the outage probability rather than the

sum-rate of the cell-center TUs.

Specifically, the outage probability of TN-NOMA is 2.5×10^{-3} whereas the outage probability of the proposed ATN-NOMA scheme is 6.25×10^{-8} to 7.3×10^{-17}. Such an outstanding performance is anticipated because aerial links are stronger. This suggests that the proposed ATN-NOMA scheme is able to support reliable communications for the AU links. Furthermore, the pairing of AU and TU in multi-cell networks remains beneficial, subject to effective mitigation of ICI.

VI. Conclusion

In this paper, we considered the downlink multi-cell networks with the co-existence of an AU and TUs. To ensure high spectral efficiency and massive connectivity, we proposed the ATN-NOMA scheme to support both AU and TUs for control and data links, respectively. In the proposed ATN-NOMA scheme, an elevation-angle based user association was employed, a directional antenna with adjustable beamwidth was implemented at the AU, and beamforming was performed by the coordinated BSs to mitigate the strong ICI issue at the AU. To guarantee the optimality of the proposed ATN-NOMA scheme, we maximized the sum-rate of the TUs by optimal beamwidth and power allocation subject to the AU's QoS requirement. The optimal beamwidth was then obtained in closed-form expression while the optimal power allocation was obtained via SCA. Furthermore, we derived the pdf, CDF, and consequently estimated the aggregated ICI in the proposed ATN-NOMA scheme. In cases where there are no interfering BSs having the same elevation-angle as the coordinated BSs, the AU experiences zero ICI, and, in such cases, we approximated the AU's outage probability analytically. Our simulation results showed that the proposed ATN-NOMA scheme significantly outperforms existing schemes in terms of the TUs' sum-rate and the AU's outage probability. When compared to the pairing of the cell-edge TU and the cell-center TUs, the proposed ATN-NOMA scheme also provided a much lower outage probability and some improvements in the sum-rate of the TUs.

Appendix A: Inter-Cell Interference with Different Interfering BS Heights

If the interfering BSs have different heights, we can approximate I_{tot} using the same method as approximating β_{tot}. Specifically, define $\mathcal{D} = \{d_1, \ldots, d_{\bar{I}}\}$ as the set of *distinctive* horizontal distance between AU and interfering BSs, and $\mathcal{I}_{d_\iota} = \left\{b \,|\, \hat{d}_{b,u} = d_\iota, \forall b \in \mathcal{I}\right\}$ as the set of

interfering BSs with horizontal distance d_ι from the AU. Let $\tilde{I}_{d_\iota} = \text{card}(\mathcal{I}_{d_\iota})$ and $\tilde{L}_{d_\iota}$ be the number of LOS links among these $\tilde{I}_{d_\iota}$ interfering links. Also, define

$$\mathcal{L} = \left\{ \left(\tilde{L}_{d_1}, \ldots, \tilde{L}_{d_{\bar{I}}} \right) | 0 \leq \tilde{L}_{d_\iota} \leq \tilde{I}_{d_\iota}, \iota = 1, \ldots, \bar{I} \right\}$$

and $i_\iota = \left(i_{d_1}, \ldots, i_{d_{\bar{I}}} \right)$.

As discussed, $\tilde{L}_{d_\iota} \sim \text{Bino}\left(\tilde{I}_{d_\iota}, p^{\text{L}}_{b,u}\left(d_\iota, z_u\right) \right)$. Since $\tilde{L}_{d_\iota}$ is independent of $\tilde{L}_{d_{\iota'}}$ for $\iota \neq \iota'$, we have:

$$\mathbb{P}\left(\tilde{L}_{d_1} = i_{d_1}, \ldots, \tilde{L}_{d_{\bar{\iota}}} = i_{d_{\bar{\iota}}} \right) = \prod_{\tilde{L}_{d_\iota} = i_{d_\iota}, \forall \iota} f_{\tilde{L}_{d_\iota}} \left(i_{d_\iota}, \tilde{I}_{d_\iota}, p^{\text{L}}_{b,u}\left(d_\iota, z_u\right) \right).$$

Following the same line of argument in Section IV, the pdf of the generalized aggregated ICI can be approximated as:

$$\begin{aligned} & f_{I_{\text{tot}}} \left(\tau, \tilde{I}_{d_1}, \ldots, \tilde{I}_{d_{\bar{I}}}, p^{\text{L}}_{b,u}\left(d_1, z_u\right), \ldots, p^{\text{L}}_{b,u}\left(d_{\bar{I}}, z_u\right) \right) \\ \approx & \sum_{\forall i_\iota \in \mathcal{L}} \mathbb{P}\left(\tilde{L}_{d_1} = i_{d_1}, \ldots, \tilde{L}_{d_{\bar{I}}} = i_{d_{\bar{I}}} \right) f_{H^{(i_\iota)}}\left(\tau, \hat{m}, \hat{\theta} \right) \\ = & \sum_{\forall i_\iota \in \mathcal{L}} \left[\prod_{\tilde{L}_{d_\iota} = i_{d_\iota}, \forall \iota} \binom{\tilde{I}_{d_\iota}}{i_{d_\iota}} p^{\text{L}}_{b,u}\left(d_\iota, z_u\right)^{i_{d_\iota}} p^{\text{N}}_{b,u}\left(d_\iota, z_u\right)^{\left(\tilde{I}_{d_\iota} - i_{d_\iota}\right)} \frac{\tau^{\hat{m}-1} \exp\left(-\frac{\tau}{\hat{\theta}}\right)}{\hat{\theta}^{\hat{m}} \Gamma\left(\hat{m}\right)} \right]. \end{aligned}$$

where $H^{(i_\iota)} = \sum_{\forall \iota} H^{(i_{d_\iota})}$. The CDF of the generalized aggregated ICI can then be approximated as:

$$\begin{aligned} & F_{I_{\text{tot}}} \left(\tau, \tilde{I}_{d_1}, \ldots, \tilde{I}_{d_{\bar{I}}}, p^{\text{L}}_{b,u}\left(d_1, z_u\right), \ldots, p^{\text{L}}_{b,u}\left(d_{\bar{I}}, z_u\right) \right) \\ \approx & \sum_{\forall i_\iota \in \mathcal{L}} \mathbb{P}\left(\tilde{L}_{d_1} = i_{d_1}, \ldots, \tilde{L}_{d_{\bar{I}}} = i_{d_{\bar{I}}} \right) F_{H^{(i_\iota)}}\left(\tau, \hat{m}, \hat{\theta} \right) \\ = & \sum_{\forall i_\iota \in \mathcal{L}} \left[\prod_{\tilde{L}_{d_\iota} = i_{d_\iota}, \forall \iota} \binom{\tilde{I}_{d_\iota}}{i_{d_\iota}} p^{\text{L}}_{b,u}\left(d_\iota, z_u\right)^{i_{d_\iota}} p^{\text{N}}_{b,u}\left(d_\iota, z_u\right)^{\left(\tilde{I}_{d_\iota} - i_{d_\iota}\right)} \int_0^\tau \frac{\tau'^{\hat{m}-1} \exp\left(-\frac{\tau'}{\hat{\theta}}\right)}{\hat{\theta}^{\hat{m}} \Gamma\left(\hat{m}\right)} d\tau' \right]. \end{aligned}$$

REFERENCES

[1] W. K. New, C. Y. Leow, K. Navaie, and Z. Ding, "Network NOMA for co-existence of aerial and terrestrial users," in *2020 IEEE 92nd Vehicular Technology Conference (VTC2020-Fall)*, pp. 1–5, IEEE.

[2] S. Hayat, E. Yanmaz, and R. Muzaffar, "Survey on Unmanned Aerial Vehicle Networks for Civil Applications: A Communications Viewpoint," *IEEE Communications Surveys Tutorials*, vol. 18, pp. 2624–2661, Fourthquarter 2016.

[3] Y. Zeng, J. Lyu, and R. Zhang, "Cellular-Connected UAV: Potential, Challenges, and Promising Technologies," *IEEE Wireless Communications*, vol. 26, pp. 120–127, February 2019.

[4] Y. Zeng, Q. Wu, and R. Zhang, "Accessing from the sky: A tutorial on UAV communications for 5G and beyond," *Proceedings of the IEEE*, vol. 107, pp. 2327–2375, Dec 2019.

[5] X. Lin, R. Wiren, S. Euler, A. Sadam, H.-L. Maattanen, S. Muruganathan, S. Gao, Y.-P. E. Wang, J. Kauppi, Z. Zou, and V. Yajnanarayana, "Mobile network-connected drones: Field trials, simulations, and design insights," *IEEE Vehicular Technology Magazine*, vol. 14, no. 3, pp. 115–125, 2019.

[6] A. Garcia-Rodriguez, G. Geraci, D. Lopez-Perez, L. G. Giordano, M. Ding, and E. Bjornson, "The essential guide to realizing 5G-connected UAVs with massive MIMO," *IEEE Communications Magazine*, vol. 57, no. 12, pp. 84–90, 2019.

[7] "3GPP Technical Report 36.777-Enhanced LTE Support for Aerial Vehicles," tech. rep., 3rd Generation Partnership Project, 2017.

[8] Q. Technologies, "LTE unmanned aircraft systems: Trial report v1.0.1," tech. rep., May 2017.

[9] X. Lin, V. Yajnanarayana, S. D. Muruganathan, S. Gao, H. Asplund, H. Maattanen, M. Bergstrom, S. Euler, and Y. E. Wang, "The sky is not the limit: LTE for unmanned aerial vehicles," *IEEE Communications Magazine*, vol. 56, pp. 204–210, Apr. 2018.

[10] J. Stanczak, I. Z. Kovacs, D. Koziol, J. Wigard, R. Amorim, and H. Nguyen, "Mobility Challenges for Unmanned Aerial Vehicles Connected to Cellular LTE Networks," in *2018 IEEE 87th Vehicular Technology Conference (VTC Spring)*, pp. 1–5, June 2018.

[11] I. Kovacs, R. Amorim, H. C. Nguyen, J. Wigard, and P. Mogensen, "Interference analysis for UAV connectivity over LTE using aerial radio measurements," in *Proc. 2017 IEEE 86th Vehicular Technology Conference (VTC-Fall)*, pp. 1–6, Sept 2017.

[12] H. C. Nguyen and R. Amorim and J. Wigard and I. Z. Kovács and T. B. Sørensen and P. E. Mogensen, "How to Ensure Reliable Connectivity for Aerial Vehicles Over Cellular Networks," *IEEE Access*, vol. 6, pp. 12304–12317, 2018.

[13] V. Yajnanarayana, Y. Eric Wang, S. Gao, S. Muruganathan, and X. Lin Ericsson, "Interference mitigation methods for unmanned aerial vehicles served by cellular networks," in *2018 IEEE 5G World Forum (5GWF)*, pp. 118–122, July 2018.

[14] S. Euler, H. Maattanen, X. Lin, Z. Zou, M. Bergstrom, and J. Sedin, "Mobility support for cellular connected unmanned aerial vehicles: Performance and analysis," in *2019 IEEE Wireless Communications and Networking Conference (WCNC)*, pp. 1–6, April 2019.

[15] M. M. Azari, F. Rosas, and S. Pollin, "Cellular connectivity for UAVs: Network modeling, performance analysis, and design guidelines," *IEEE Transactions on Wireless Communications*, vol. 18, pp. 3366–3381, July 2019.

[16] W. Mei and R. Zhang, "Cooperative downlink interference transmission and cancellation for cellular-connected UAV: A divide-and-conquer approach," *IEEE Transactions on Communications*, vol. 68, no. 2, pp. 1297–1311, 2020.

[17] W. Mei and R. Zhang, "Aerial-ground interference mitigation for cellular-connected UAV," *IEEE Wireless Communications*, vol. 28, no. 1, pp. 167–173, 2021.

[18] B. Makki, K. Chitti, A. Behravan, and M. S. Alouini, "A Survey of NOMA: Current Status and Open Research Challenges," *IEEE Open Journal of the Communications Society*, vol. 1, pp. 179–189, 2020.

[19] Y. Liu, Z. Qin, M. Elkashlan, Z. Ding, A. Nallanathan, and L. Hanzo, "Nonorthogonal Multiple Access for 5G and Beyond," *Proceedings of the IEEE*, vol. 105, no. 12, pp. 2347–2381, 2017.

[20] Z. Ding, X. Lei, G. K. Karagiannidis, R. Schober, J. Yuan, and V. K. Bhargava, "A Survey on Non-Orthogonal Multiple Access for 5G Networks: Research Challenges and Future Trends," *IEEE Journal on Selected Areas in Communications*, vol. 35, pp. 2181–2195, Oct 2017.

[21] Z. Yang, C. Pan, W. Xu, Y. Pan, M. Chen, and M. Elkashlan, "Power Control for Multi-Cell Networks With Non-Orthogonal Multiple Access," *IEEE Transactions on Wireless Communications*, vol. 17, pp. 927–942, Feb 2018.

[22] W. Shin, M. Vaezi, B. Lee, D. J. Love, J. Lee, and H. V. Poor, "Non-Orthogonal Multiple Access in Multi-Cell Networks: Theory, Performance, and Practical Challenges," *IEEE Communications Magazine*, vol. 55, pp. 176–183, Oct 2017.

[23] A. Beylerian and T. Ohtsuki, "Coordinated Non-Orthogonal Multiple Access (CO-NOMA)," in *2016 IEEE Global Communications Conference (GLOBECOM)*, pp. 1–5, Dec 2016.

[24] J. Choi, "Non-Orthogonal Multiple Access in Downlink Coordinated Two-Point Systems," *IEEE Communications Letters*, vol. 18, pp. 313–316, February 2014.

[25] X. Sun, N. Yang, S. Yan, Z. Ding, D. W. K. Ng, C. Shen, and Z. Zhong, "Joint Beamforming and Power Allocation in Downlink NOMA Multiuser MIMO Networks," *IEEE Transactions on Wireless Communications*, vol. 17, pp. 5367–5381, Aug 2018.

[26] V. Nguyen, H. D. Tuan, T. Q. Duong, H. V. Poor, and O. Shin, "Precoder Design for Signal Superposition in MIMO-NOMA Multicell Networks," *IEEE Journal on Selected Areas in Communications*, vol. 35, pp. 2681–2695, Dec 2017.

[27] M. S. Ali, E. Hossain, and D. I. Kim, "Coordinated Multipoint Transmission in Downlink Multi-Cell NOMA Systems: Models and Spectral Efficiency Performance," *IEEE Wireless Communications*, vol. 25, pp. 24–31, April 2018.

[28] Y. Sun, Z. Ding, X. Dai, and G. K. Karagiannidis, "A Feasibility Study on Network NOMA," *IEEE Transactions on Communications*, vol. 66, pp. 4303–4317, Sep. 2018.

[29] M. S. Ali, E. Hossain, A. Al-Dweik, and D. I. Kim, "Downlink Power Allocation for CoMP-NOMA in Multi-Cell Networks," *IEEE Transactions on Communications*, vol. 66, pp. 3982–3998, Sep. 2018.

[30] Y. Tian, A. R. Nix, and M. Beach, "On the Performance of Opportunistic NOMA in Downlink CoMP Networks," *IEEE Communications Letters*, vol. 20, pp. 998–1001, May 2016.

[31] M. F. Sohail, C. Y. Leow, and S. Won, "Non-orthogonal multiple access for unmanned aerial vehicle assisted communication," *IEEE Access*, vol. 6, pp. 22716–22727, 2018.

[32] M. F. Sohail, C. Y. Leow, and S. Won, "Energy-efficient non-orthogonal multiple access for UAV communication system," *IEEE Transactions on Vehicular Technology*, vol. 68, no. 11, pp. 10834–10845, 2019.

[33] N. Rupasinghe, Y. Yapici, I. Guvenc, and Y. Kakishima, "Non-orthogonal multiple access for mmWave drone networks with limited feedback," *IEEE Transactions on Communications*, vol. 67, pp. 762–777, Jan 2019.

[34] T. Hou, Y. Liu, Z. Song, X. Sun, and Y. Chen, "Exploiting NOMA for UAV communications in large-scale cellular networks," *IEEE Transactions on Communications*, vol. 67, pp. 6897–6911, Oct 2019.

[35] W. K. New, C. Y. Leow, K. Navaie, and Z. Ding, "Robust non-orthogonal multiple access for aerial and ground users," *IEEE Transactions on Wireless Communications*, vol. 19, no. 7, pp. 4793–4805, 2020.

[36] T. Z. H. Ernest, A. S. Madhukumar, R. P. Sirigina, and A. K. Krishna, "NOMA-aided UAV communications over correlated Rician shadowed fading channels," *IEEE Transactions on Signal Processing*, vol. 68, pp. 3103–3116, 2020.

[37] X. Mu, Y. Liu, L. Guo, and J. Lin, "Non-orthogonal multiple access for air-to-ground communication," *IEEE Transactions on Communications*, vol. 68, no. 5, pp. 2934–2949, 2020.

[38] W. K. New, C. Y. Leow, K. Navaie, Y. Sun, and Z. Ding, "Application of NOMA for cellular-connected UAVs: Opportunities and challenges," *Information Sciences*, vol. 64, no. 140302, pp. 1–140302, 2021.

[39] X. Xu and Y. Zeng, "Cellular-Connected UAV: Performance Analysis with 3D Antenna Modelling," in *2019 IEEE International Conference on Communications Workshops (ICC Workshops)*, pp. 1–6, May 2019.

[40] M. M. Azari, F. Rosas, and S. Pollin, "Reshaping cellular networks for the sky: Major factors and feasibility," in *2018 IEEE International Conference on Communications (ICC)*, pp. 1–7, May 2018.

[41] R. Amer, W. Saad, and N. Marchetti, "Toward a Connected Sky: Performance of Beamforming With Down-Tilted Antennas for Ground and UAV User Co-Existence," *IEEE Communications Letters*, vol. 23, pp. 1840–1844, Oct 2019.

[42] W. K. New, C. Y. Leow, K. Navaie, Y. Sun, and Z. Ding, "Interference-aware NOMA for cellular-connected UAVs: Stochastic geometry analysis," *IEEE Journal on Selected Areas in Communications*, pp. 1–1, 2021.

[43] H. He, S. Zhang, Y. Zeng, and R. Zhang, "Joint altitude and beamwidth optimization for UAV-enabled multiuser communications," *IEEE Communications Letters*, vol. 22, pp. 344–347, Feb 2018.

[44] Z. Yang, C. Pan, M. Shikh-Bahaei, W. Xu, M. Chen, M. Elkashlan, and A. Nallanathan, "Joint altitude, beamwidth, location, and bandwidth optimization for UAV-enabled communications," *IEEE Communications Letters*, vol. 22, pp. 1716–1719, Aug 2018.

[45] A. Khidre, F. Yang, and A. Z. Elsherbeni, "Reconfigurable Microstrip Antenna with Tunable Radiation Beamwidth," in *2013 IEEE Antennas and Propagation Society International Symposium (APSURSI)*, pp. 1444–1445, July 2013.

[46] T. Debogovic, J. Perruisseau-Carrier, and J. Bartolic, "Partially Reflective Surface Antenna With Dynamic Beamwidth Control," *IEEE Antennas and Wireless Propagation Letters*, vol. 9, pp. 1157–1160, 2010.

[47] M. Elhattab, M.-A. Arfaoui, C. Assi, and A. Ghrayeb, "Reconfigurable intelligent surface assisted coordinated multipoint in downlink NOMA networks," *IEEE Communications Letters*, vol. 25, no. 2, pp. 632–636, 2021.

[48] R. Lei and D. Xu, "On the outage performance of JT-CoMP-CNOMA Networks with SWIPT," *IEEE Communications Letters*, vol. 25, no. 2, pp. 432–436, 2021.

[49] W. Mei and R. Zhang, "Uplink cooperative NOMA for cellular-connected UAV," *IEEE Journal of Selected Topics in Signal Processing*, pp. 1–1, 2019.

[50] N. Cherif, M. Alzenad, H. Yanikomeroglu, and A. Yongacoglu, "Downlink coverage and rate analysis of an aerial user in vertical heterogeneous networks (VHetNets)," *IEEE Transactions on Wireless Communications*, vol. 20, no. 3, pp. 1501–1516, 2021.

[51] C. A. Balanis, *Antenna Theory: Analysis and Design, 3rd Edition*. John wiley & sons, 2005.

[52] S. Boyd, S. P. Boyd, and L. Vandenberghe, *Convex Optimization*. Cambridge university press, 2004.

[53] P. Moscuoroums, "The Distribution of The Sum of Independent Gamma Random Variables," *Ann. Inst. Statist. Math*, vol. 37, no. Part A, pp. 541–544, 1985.

[54] S. Covo and A. Elalouf, "A Novel Single-Gamma Approximation to The Sum of Independent Gamma Variables, And A Generalization to Infinitely Divisible Distributions," *Electronic Journal of Statistics*, vol. 8, no. 1, pp. 894–926, 2014.